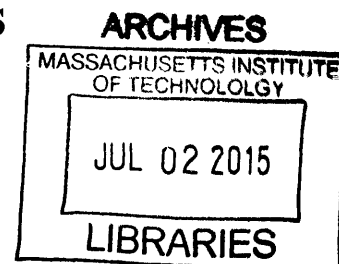# Formation and Evolution of Atmospheric Organic Matter from Radical Intermediates

by

Anthony Joseph Carrasquillo

A.B. in Chemistry and Environmental Studies, Bowdoin College, 2007

Submitted to the Department of Civil and Environmental Engineering
in partial fulfillment of the requirements for the degree of

Doctor of Philosophy in Environmental Chemistry

at the

MASSACHUSETTS INSTITUTE OF TECHNOLOGY

June 2015

Author . . . .

Signature redacted

Department of Civil and Environmental Engineering
February 27, 2015

Certified by . . . .

Signature redacted

Jesse H. Kroll
Associate Professor of Civil, Environmental, and Chemical Engineering
Thesis Supervisor

Accepted by. . . . .

Signature redacted

Heidi M. Nepf
Donald and Martha Harleman Professor of Civil and Environmental Engineering
Chair, Graduate Program Committee

Formation and Evolution of Atmospheric Organic Matter from Radical Intermediates

by

Anthony Joseph Carrasquillo

Submitted to the Department of Civil and Environmental Engineering
on February 27, 2015, in partial fulfillment of the
requirements for the degree of
Doctor of Philosophy in Environmental Chemistry

Abstract

Atmospheric particulate matter (or "aerosol") has important implications for public health, climate change, and visibility. Our ability to predict its formation and fate is hindered by uncertainties associated with one type in particular, organic aerosol (OA). The study of the chemistry underlying OA formation is complicated by the large number of reaction pathways and oxidation generations for a given precursor species. This thesis describes a series of experiments in which the chemistry is simplified to that of a single alkoxy radical (RO) isomer generated from the direct photolysis of alkyl nitrites (RONO). First, OA was generated from eleven different C_{10} RO isomers to determine the role of radical molecular structure in the formation of low-volatility species. Here, measured aerosol yields and chemical composition were explained by two major effects: (1) the relative importance of isomerization and fragmentation pathways, which control the distribution of products, and (2) differences in saturation vapor pressure of individual isomers. Next, we developed a method to investigate the reactivity of alkoxy radicals in the condensed phase. The long chain C_{20} RO radical was generated in hexane solvent to identify possible intermolecular (bimolecular) reactions with the condensed-phase. The lack of formation of the C_{20} alcohol, the expected product of the bimolecular reaction of RO with hexane indicates that these intermolecular reactions are unable to compete with available unimolecular isomerization processes. Finally, a molecular-level study of this same condensed-phase system with a soft ionization technique permitted the observation of molecular ions that are assigned to specific oxidation products. This approach enables the determination of the extent of branching for another important intermediate, the alkylperoxy radical. The results from this thesis highlight the role of radical structure in the formation of low-volatility products in the atmosphere, in addition to identifying the major reaction pathways responsible for particle-phase oxidative processing.

Thesis Supervisor: Jesse H. Kroll
Title: Associate Professor of Civil, Environmental, and Chemical Engineering

Acknowledgements

Simply stated: **Graduate school has been both the most challenging and rewarding experience of my life.** I have a distinct memory of a particular prompt from an undisclosed standardized test that said "you should make your vocation your vacation". and while I tend to immediately push the details of testing out of my head, this stuck with me. To me, a career in science is my vacation. While I may complain and get frustrated at times, this is similar to the effects of losing luggage or waiting in line for the next roller coaster on the overall *vacation* experience. My graduate school experience was the same way – I didn't love every single minute of it, but the highs or "ups" that I experienced certainly outweighed the "downs". Is this my way of saying that I would rather be in grad school vs. the beach?- Not necessarily. I don't think that anyone can say that, but I simply can't imagine doing anything else that I would enjoy more...

Much of why grad school was such a great experience as a graduate student is because of the people involved in my everyday life and in particular my advisor Jesse Kroll. I was initially hesitant to join Jesse's group because, at the time, I was more interested in pursuing a research program focused on aqueous chemistry and honestly thought that the atmosphere seemed like it involved too much p-chem for my liking – vapor pressures? what? After my first meeting with Jesse I decided to go with my gut and it was the best choice that I could have possibly made. I have exactly **_zero_** regrets in doing so. I have had the opportunity to work in a number of labs and have met a lot of scientists, but have yet to

meet anyone like Jesse. His never-ending supply of support and encouragement, even when things truly were not working, really helped me solve some difficult problems and kept me constantly motivated. This will be the third time that I have said this, but "if I could be even 1% of the scientist that he is, I would be happy". The remarkable piece here is that he does this while remaining so grounded and personable - qualities that everyone appreciates. My only qualm with Jesse is that he has terrible taste in movies and music, although now that he owns several of the most important films in cinema history, all that could change. Its been a great experience working and learning from him and I will sincerely miss being an active member of his group.

I started grad school at the same time as Kelly Daumit and James Hunter, and amazingly we all defended within a month of each other- coming full circle together. We struggled through a kinetics course that we didn't have the pre-req for, aquatic chemistry problem sets that took 20+ hours per week, and spent thousands of hours in the lab together. Working with them in the lab is amazing because we know each other so well that we can actually predict what the other person is going to do or say before they do it. This is the sign of a true *team*. It is difficult (impossible at the moment) to imagine how not constantly interacting with them is going to impact my day-to-day life, but I know that we will always be colleagues and remain in touch. I thank them for that. They are the Ron and Hermoine to my Harry.

Even the simplest of experiments in atmospheric chemistry often require several sets of hands, and as a result I have had the opportunity to work closely with every member of the Kroll Group (past and present). Each and every experiment bears some resemblance to that final car chase scene at the end of (each installment) my favorite movie

series where Vin Diesel, Paul Walker, and Michelle Rodriguez work together to bring down some crafty cartel. Our research really is *that* exciting sometimes, minus the villain and the car chases, but instead including a 7.5 m^3 teflon chamber. Kelsey, Chris, Sean, Jon, David, Ellie, and Eben – thank you for being my partners in crime. I have learned more from you guys than you can ever possibly imagine.

I have been blessed throughout my grad school time to have many *unofficial advisors*. My thesis committee, Phil Gschwend, Colette Heald, and Dan Cziczo, have pushed me to think beyond my individual experiments and how they fit into the big picture. For that I am ever grateful. For part of my thesis work I ventured to Berkeley to collaborate with Kevin Wilson, Lance Lee, and Theo Nah, and I thank them for their time, effort, and giving me the chance to work together to do some awesome science! The entire Summons Lab at MIT, including Roger and Carolyn – you have both provided me with a never-ending supply of support (and solvents), and I am very appreciative. Professor Dharni Vasudevan or "Boss" – its been seven years since I graduated and I still email you once a week for advice on something. Thanks for putting up with me!

Then there is the Parsons Community (past and present). A special thank you to Vicki Murphy, Sheila Frankel, Jim Long, and Jackie Foster- without you guys, Parsons would be in serious trouble! And, as the ever-wise Vin Diesel once said "I don't have friends, I got family." Parsons is just that, a family. Some of my best friends in the world (live?) and work(ed) here. In particular, I need to acknowledge Sara Lincoln (half-time Parosnite/Summons Labber), Kyle Peet, Dave Whittleston, Thomas Petersen, and Mason Stahl – five of the best friends and colleagues that I could ask for. We have been through a lot together over the past few years and you each had a special part in my completing this

thesis. Similarly, I have met some other amazing people here that I would feel terrible for not mentioning: Fatima, Nisha, Jared, Jen (both nice and mean), the Parsons Unihoc team, Gaj, Mitul, Jeff, Knox, Candice, Kaighin, Dave, Ben, Robin, Alex, Dave, Will, Elizabeth, Erin, Patricia, Gabe, etc. etc. etc. etc. etc. You are all awesome! Thanks!

Lastly (but certainly not least), I need to thank my non-MIT family and friends, without which I would not have been able to get to this point. My mother has been very supportive of me throughout all of my endeavors. My grandmother, while unable to make it to my defense, is still one of the most important people in my life. She was my best friend growing up, and I cant thank her enough for all that she has done for me. As for siblings, I am definitely the *younger brother*, and my sister is more than tolerant when it comes to my antics. Thank you for always being there for me. Similarly to my brother, brother in law and nephews (including Salem)- thanks for keeping me grounded and (mostly) sane throughout this process. To my aunts and uncles, particularly Aunt Marie and Uncle Kenny who drive me back and forth between Cambridge and Revere every Sunday evening and gave me a place to live in between Bowdoin and MIT, thank you! I also need to acknowledge my extended family, the Malones who have been there for me throughout my entire life, thank you. Anthony- I cant believe that you put up with me and my grad school madness for so long.. And to my best friends from home, Jenn and Jen – we have been best friends for 25 years… enough said.

If you are reading this and think that you should be here, and I forgot to acknowledge you, let me know so we can discuss. If I agree that it was truly an oversight I will pay for lunch.

-This is Anthony, over and out.

Table of Contents

Chapter 1

Introduction

Atmospheric particulate matter or *aerosol* particles have important implications for human health, global climate change, and visibility.[1] The health risks associated with exposure to aerosols, such as increased risks of cardiopulmonary disease and lung cancer, are well documented.[2] Dockery et. al. have shown a strong relationship between air pollution and mortality rates, with fine particulates having the strongest correlation, highlighting their negative impact on human health.[3] In addition, aerosols represent the single largest uncertainty in global radiative forcing, and thus have large implications for our understanding of global climate change.[4] Aerosol particles can impact climate directly by absorption or scattering of incoming solar radiation (relative to the less intense terrestrial derived long-wave radiation), resulting in heating or cooling, or indirectly by enhancing the brightness and lifetime of clouds.[5] Unfortunately, even the most sophisticated, state-of-the-art models for predicting aerosol formation and properties, based on the results of controlled laboratory chamber experiments are unable to accurately predict aerosol yields and lifetimes in the ambient atmosphere. In many cases there is a strong under-prediction of aerosol loading, often of an order of magnitude or greater, which appears to be associated with one class of aerosol in particular, organic aerosol (OA).[6,7]

OA is primary (POA), emitted directly as a particle, or secondary (SOA), formed by the gas-phase oxidation of volatile organic compounds (VOCs), producing low-volatility organic species, which condense into the particle phase.[8,9] Once in the particle phase, organic species

will continue "aging," or reacting with gas-phase oxidants to form new products (Figure 1). It is this formation of SOA and its chemical evolution that drive most of the uncertainty discussed above. In order to accurately predict SOA loadings, a detailed understanding of the underlying chemical oxidation pathways forming low volatility organics from VOCs is necessary.
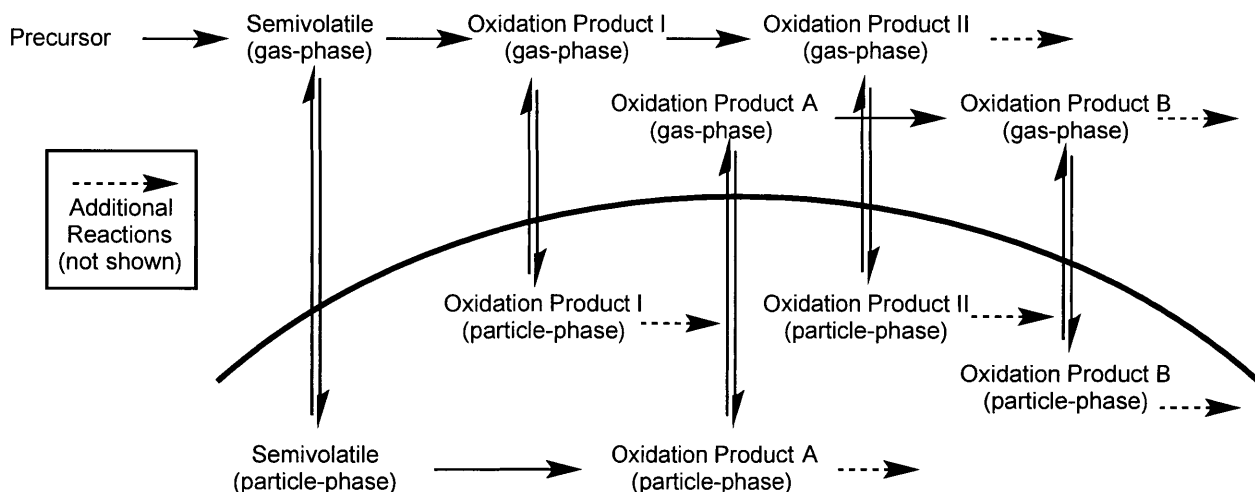
Figure 1. A highly generalized schematic of the complexity associated with VOC oxidation. The precursor VOC is oxidized with OH, followed by the subsequent gas/particle partitioning and chemical processing of individual oxidation products.

Three major problems confound the identification of individual products and pathways: (1) there are a large number of reaction pathways and products that form, making the measurement of every individual compound unrealistic (Figure 1), (2) products of the first oxidation reaction can also be oxidized leading to several "generations" of oxidation, often existing simultaneously and (3) it is often difficult to reproduce atmospheric conditions in laboratory studies. It is the goal of this thesis work to add to the current understanding of the formation and evolution of OA and help close the gap between predicted aerosol loadings and measured loadings.

Figure 2 (adapted from Lim and Ziemann, 2009) shows a highly generalized atmospheric hydrocarbon oxidation scheme for a simple hydrocarbon (RH), highlighting the number of

potential reaction pathways.[10] Initiation occurs via hydrogen abstraction by an OH radical yielding an alkyl radical (R). As any hydrogen atom can be abstracted, the number of possible alkyl radicals produced in the initiation step scales with the number of carbon atoms present in the molecule. The alkyl radical rapidly reacts with molecular oxygen to form the alkylperoxy radical (RO_2), which can react by one of many channels, including: (i) reaction with NO to form the alkoxy radical (RO), (ii) self-reaction with another RO_2 to form a carbonyl species and an
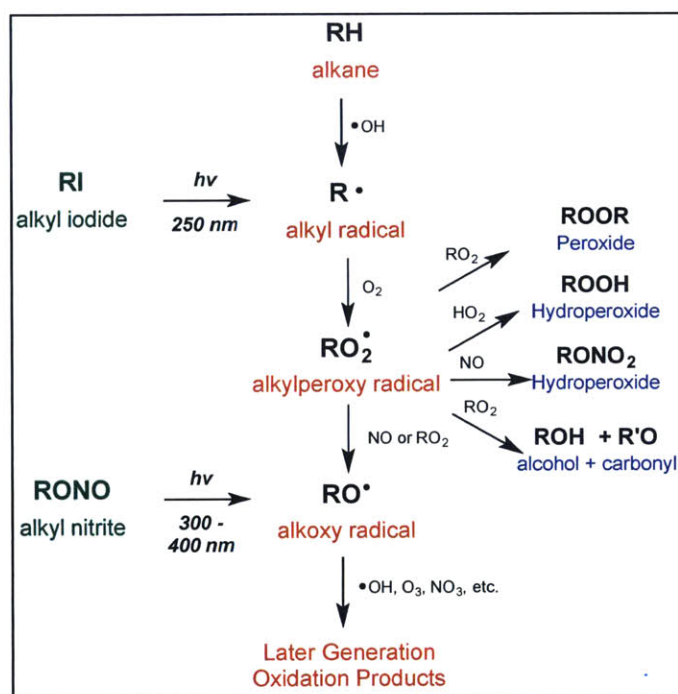
Figure 2. Simplified mechanism of hydrocarbon oxidation shown here for an alkane (RH). Species involved in chain-propagating reactions are shown in red, while chain-terminating reactions are in blue and photolytic precursors in green.

alcohol (R'O and ROH), a peroxide (ROOR), or two RO radicals, (iii) react with HO_2 to form a hydroperoxide (ROOH). The RO generated from RO_2 reaction with NO or RO_2 will further react to form the chain terminating alkyl nitrate ($RONO_2$) or carbonyl (R'O), or a new chain propagating RO_2 radical. Such branch points have the potential to produce a wide range of

intermediates and products (shown in the figure), thereby increasing the chemical complexity of the system hindering our ability to predict SOA yields and composition. Further complicating this problem, the chain-terminating products formed may also react with oxidants (OH, O_3, or NO_3) and initiate a new radical chain mechanism. The measurement of products from the simple oxidation of a single model compound thus contains a mixture of products from multiple "generations" of oxidation.[10]

Reproducing atmospheric conditions that facilitate SOA formation and evolution in the laboratory is difficult for a number of reasons. Both the oxidation of VOCs to SOA and the heterogeneous aging of OA typically occur over a week or two in the atmosphere, while experimental constraints typically limit smog chamber studies to a few days at most. Laboratory aging studies assume that oxidation kinetics are first order with respect to oxidant concentration, and therefore by exposing a VOC to elevated concentrations of oxidant, the most oxidized products can be formed over much shorter timescales (a week of oxidation in the atmosphere can be attained in several hours in the chamber). A complicating factor is that product formation is not necessarily linear with respect to oxidant concentration.[11] As a result elevated oxidant concentrations, can complicate the interpretation of the underlying chemistry, as multiple generation products can be present simultaneously. Furthermore, the higher concentrations of intermediates in these studies can facilitate radical-radical intermediates that are likely not atmospherically relevant.

In this work I extend a novel approach that was recently demonstrated by our group for studying the detailed chemical mechanisms underlying SOA formation and evolution, by the direct photolytic generation of organic radical species.[12] Previously, alkyl iodides (RI) were photolyzed with 254 nm light, to generate alkyl radicals and initiate the radical chain mechanism,

14

leading to the formation of SOA in the absence of an oxidant (Figure 2). This method has the advantages of (1) constraining the RO_2 intermediate to one specific isomer and therefore simplifying the number of products and (2) limiting oxidation to a single generation and thereby allowing the major reaction pathways to be determined. The aerosol generated from newly formed condensed products was measured and characterized using an Aerodyne High-Resolution Time of Flight Aerosol Mass Spectrometer (HR-ToF-AMS). A major drawback to this approach is the necessity of the 254 nm light for the initiation step, introducing the potential for photochemistry that may not be atmospherically relevant. In addition, the iodide radical is assumed to be inert, however, some inorganic iodine species were detected in the particles, suggesting that the iodine may influence the aerosol formation chemistry. In this thesis I will use a similar approach to study the reactivity of RO radicals, the photolysis of alkyl nitrite (RONO) species. This approach has the advantage of occurring more atmospherically relevant conditions, and without the production of a reactive photofragment.

Alkyl nitrite photolysis has long served as a means for studying the reactivity and kinetics of alkoxy radicals in the physical organic chemistry literature.[13,14] However, much of this work has been done with small ($C_1 - C_5$) RONO compounds under conditions that are not atmospherically relevant (i.e. O_2 free conditions or at excessively high concentrations ~ 1 – 10%). The absorption of alkyl nitrites in the 300 – 450 nm is believed to occur from the electronic transition (n $\rightarrow$ π^*) of a lone-pair electron on the nitrogen atom. The result is a cleavage of the RO-NO bond and the formation of the corresponding RO and NO radicals in equation 1:

$$RONO + h\nu \rightarrow RO + NO \qquad\qquad (1)$$

Unlike RI photolysis, the wavelength range over which this reaction occurs overlaps nicely with

the solar spectrum and the output from traditional black lights (Figure 3), thus implying its relevance to atmospheric wavelengths. Note that the intensity from the UV lamp may not be identical to that from the solar spectrum, however, we use the same lights for all experiments and thus the data obtained here should be unaffected, but caution should be applied for direct application of photolysis rate constants to the atmosphere. Furthermore, NO is a common and important radical in urban atmospheres and unlike the iodide radical and thus its production is not an unreasonable addition to the experiment. Quantum yields for this reaction with small (< C_5) RONO have been reported and are ~1 when conducted at standard temperature and pressure, implying that collisional deactivation of any excited state RO by a bath gas (i.e. N_2 or O_2) is both fast and efficient.[13]
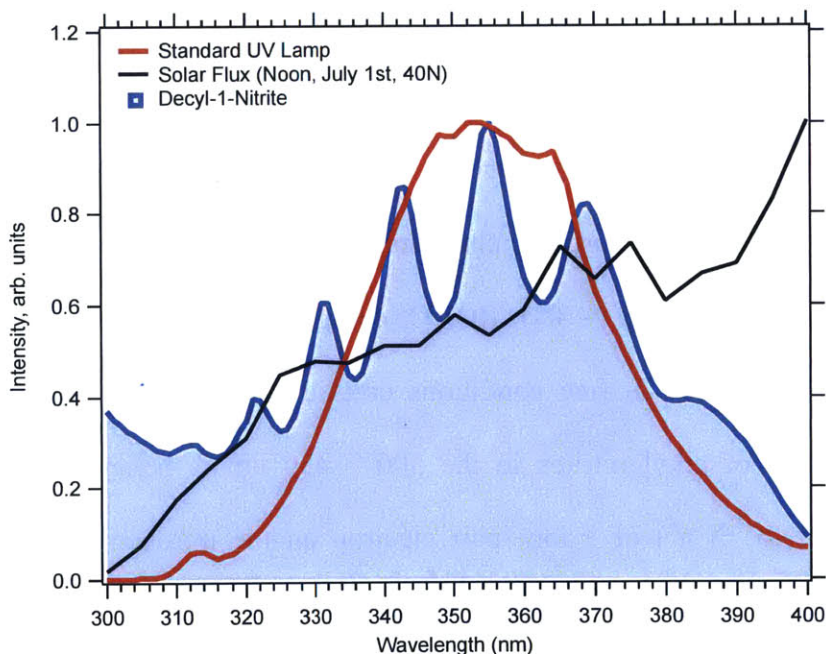
Figure 3. UV-Vis spectrum from 300 – 400 nm of decyl-1-nitrite (blue) overlaid with the output of a standard UV lamp (red) and the solar flux (black). Absorption intensity is normalized to the maximum absorption over this wavelength range. The maximum absorption for RONO species is between 315-380 nm, which overlaps nicely with the absorption from a standard UV-lamp (centered around 350 nm).

16

In this thesis I use this technique to generate radical species that then react to form products that we measure analytically; an approach that will be useful for constraining the major reactive pathways for radical intermediates. This work focuses specifically on addressing the following three questions:

(1) What is the role of alkoxy radical structure on its reactivity as it pertains to the formation of low volatility organic species?

(2) How does the phase of the alkoxy radical, gas or aerosol (condensed) impact its reactivity?

(3) What are the major pathways and products of condensed phase alkoxy and alkylperoxy radicals?

To address these questions a series of experiments were conducted that are detailed explicitly in the following chapters:

Chapter 2. The role of alkoxy radical structure on the formation of low volatility species was investigated by measuring the yields and composition of SOA that formed from the photolysis of eleven $C_{10}H_{21}ONO$ isomers. The isomers include those that would form from decane oxidation, one primary and four secondary, as well as a number of branched species with the location of the radical center relative to the branch varied (i.e. the substituent is α, β, γ, or δ to the radical center). Comparison of the yields and elemental composition (O/C, H/C, and N/C) for the SOA that forms from each isomer permits the explicit identification of the relative roles of fragmentation and isomerization reactions.

Chapter 3. The molecular environment of an alkoxy radical is believed to have a defining role in determining the reactions that are accessible. For example, in the condensed liquid phase, the reaction of alkoxy radicals with neighboring organic compounds is possible given their closer proximity than in the gas-phase.[e.g.14,15] To examine this further, in this chapter I developed a method to monitor the products of condensed phase radical reactivity using nebulization of the mixture and measurements with the AMS. Results from real-time (*on-line*) and off-line analysis are presented to highlight the relative importance of the common pathways discussed above, unimolecular and bimolecular with inorganic species and with the surrounding organic aerosol solution.

Chapter 4. The major pathways for condensed phase RO and RO_2 radicals are identified using the setup developed in Chapter 3. Here, instead of the AMS, we use a sensitive chemical ionization technique to identify individual products formed from the photolysis of large RONO precursors and identify the likely mechanisms leading to their formation.

The results from this thesis will be useful for better constraining the role of radical reactions in the fate of organic compounds in the atmosphere. They will add to the current body of knowledge for how organic compounds evolve physically (i.e. partitioning between gas and particle phases) and chemically in the atmosphere- information which is crucial to better assessing the potential impacts on human health, climate, and visibility. Specifically, the size and loadings of aerosol particles directly impact their health effects, while an improved understanding the chemical pathways presents a means to estimate the potential for the production of toxic products. Furthermore, the effects of organic aerosol on the global climate

system are dependent on the extent to which a given aerosol either scatters or absorbs incoming

solar radiation; processes that are related to their size, concentration, and chemical composition.

References

(1)   Kanakidou, M.; Seinfeld, J. H.; Pandis, S. N.; Barnes, I.; Dentener, F. J.; Facchini, M. C.; Van Dingenen, R.; Ervens, B.; Nenes, A.; Nielsen, C. J.; et al. Organic Aerosol and Global Climate Modelling: A Review. *Atmos. Chem. Phys.* **2005**, *5*, 1053–1123.

(2)   Pope, C. A.; Muhlestein, J. B.; May, H. T.; Renlund, D. G.; Anderson, J. L.; Horne, B. D. Ischemic Heart Disease Events Triggered by Short-Term Exposure to Fine Particulate Air Pollution. *Circulation* **2006**, *114*, 2443–2448.

(3)   Dockery, D. W.; Pope, C. A.; Xu, X.; Spengler, J. D.; Ware, J. H.; Fay, M. E.; Ferris, B. G.; Speizer, F. E. An Association between Air Pollution and Mortality in Six U.S. Cities. *N. Engl. J. Med.* **1993**, *329*, 1753–1759.

(4)   IPCC Working Group 1, I.; Stocker, T. F.; Qin, D.; Plattner, G.-K.; Tignor, M.; Allen, S. K.; Boschung, J.; Nauels, A.; Xia, Y.; Bex, V.; et al. IPCC, 2013: Climate Change 2013: The Physical Science Basis. Contribution of Working Group I to the Fifth Assessment Report of the Intergovernmental Panel on Climate Change. *IPCC* **2013**, *AR5*, 1535.

(5)   Lamb, D.; Verlinde, J. *Physics and Chemistry of Clouds*; Cambridge University Press: New York, 2011; p. 584.

(6)   Volkamer, R.; Jimenez, J. L.; San Martini, F.; Dzepina, K.; Zhang, Q.; Salcedo, D.; Molina, L. T.; Worsnop, D. R.; Molina, M. J. Secondary Organic Aerosol Formation from Anthropogenic Air Pollution: Rapid and Higher than Expected. *Geophys. Res. Lett.* **2006**, *33*, L17811.

(7)   Heald, C. L. A Large Organic Aerosol Source in the Free Troposphere Missing from Current Models. *Geophys. Res. Lett.* **2005**, *32*, L18809.

(8)   Kroll, J. H.; Seinfeld, J. H. Chemistry of Secondary Organic Aerosol: Formation and Evolution of Low-Volatility Organics in the Atmosphere. *Atmos. Environ.* **2008**, *42*, 3593–3624.

(9)   Hallquist, M.; Wenger, J. C.; Baltensperger, U.; Rudich, Y.; Simpson, D.; Claeys, M.; Dommen, J.; Donahue, N. M.; George, C.; Goldstein, A. H.; et al. The Formation, Properties and Impact of Secondary Organic Aerosol: Current and Emerging Issues. *Atmos. Chem. Phys.* **2009**, *9*, 5155–5236.

(10) Lim, Y. Bin; Ziemann, P. J. Chemistry of Secondary Organic Aerosol Formation from OH Radical-Initiated Reactions of Linear, Branched, and Cyclic Alkanes in the Presence of NOx. *Aerosol Sci. Technol.* **2009**, *43*, 604–619.

(11) Presto, A. A.; Donahue, N. M. Investigation of Alpha-Pinene + Ozone Secondary Organic Aerosol Formation at Low Total Aerosol Mass. *Environ. Sci. Technol.* **2006**, *40*, 3536–3543.

(12) Kessler, S. H.; Nah, T.; Carrasquillo, A. J.; Jayne, J. T.; Worsnop, D. R.; Wilson, K. R.; Kroll, J. H. Formation of Secondary Organic Aerosol from the Direct Photolytic Generation of Organic Radicals. *J. Phys. Chem. Lett.* **2011**, *2*, 1295–1300.

(13) Heicklen, J. The Decomposition of Alkyl Nitrites and the Reaction of Alkoxy Radicals. *Adv. Photochem.* **1988**, *14*, 177–272.

(14) Gray, P.; Williams, A. The Thermochemistry And Reactivity Of Alkoxyl Radicals. *Chem. Rev.* **1959**, *59*, 239–328.

(15) Liu, C.-L.; Smith, J. D.; Che, D. L.; Ahmed, M.; Leone, S. R.; Wilson, K. R. The Direct Observation of Secondary Radical Chain Chemistry in the Heterogeneous Reaction of Chlorine Atoms with Submicron Squalane Droplets. *Phys. Chem. Chem. Phys.* **2011**, *13*, 8993–9007.

Chapter 2

Secondary Organic Aerosol Formation from the Isolation of Individual Reactive Pathways: Role of Alkoxy Radical Structure

Adapted from: Carrasquillo, A. J.; Hunter, J. F.; Daumit, K. E.; Kroll, J. H. Secondary Organic Aerosol Formation via the Isolation of Individual Reactive Intermediates: Role of Alkoxy Radical Structure. *J. Phys. Chem. A* **2014**, *118*, 8807–8816.

2.1 Introduction

Organic aerosol (OA) particles have important implications for human health, visibility, and climate; however our ability to accurately predict ambient OA loadings, chemical composition, and properties is limited.[1-3] Particularly uncertain is the chemistry associated with secondary organic aerosol (SOA), formed from the oxidation of gas-phase VOCs and the subsequent condensation of low-volatility products. SOA formation is immensely complex, involving a large number of chemical species, and reaction pathways, and oxidation generations.[3,4] This chemical complexity poses major challenges in understanding the detailed chemistry and specific reaction pathways that govern SOA formation and evolution, particularly when the reaction of a single oxidant with a single VOC can lead to the formation of a multitude of products.

Figure 1 illustrates the large number of reaction pathways and intermediates possible for even a very simple reaction system, the oxidation of an *n*-alkane by the OH radical. The reaction is initiated by H-abstraction by OH at one of several sites, followed by O_2 addition to form a

distribution of alkylperoxy radicals (RO_2, not shown). In the presence of NO these will form

organonitrate ($RONO_2$) species or alkoxy (RO) radicals. The RO radicals are important branch

points in oxidation reactions, and for large species will either fragment into two smaller products

or undergo an intramolecular H-rearrangement (isomerization). If the resulting products are

sufficiently low in volatility, they will partition into the aerosol phase; otherwise they will

continue to react in the gas-phase and form additional products that may themselves condense.[5]

Every subsequent reaction with an oxidant yields a new oxidation "generation" product (e.g.

first-, second-, third-, etc. generation). The resulting aerosol thus contains many product species,

formed by numerous pathways over several generations of oxidation.
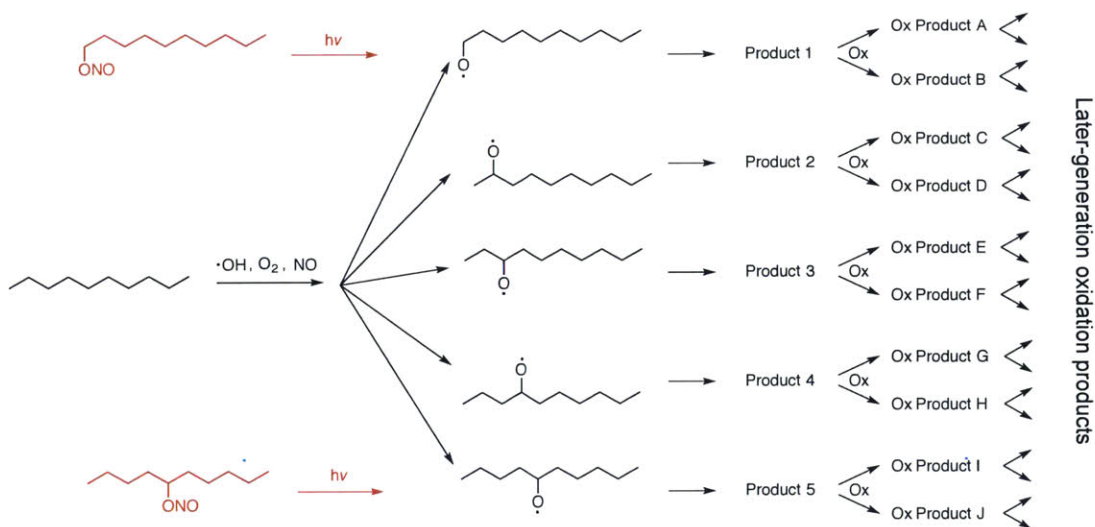
Figure 1. Formation of alkoxy radical isomers from *n*-decane. The OH radical can abstract any available H, yielding a distribution of five different radical isomers that then react to form a wide range of fragmentation or isomerization products; these then can oxidize further to form new products. Alkyl nitrite photolysis, shown in red, yields one specific alkoxy radical, with little secondary oxidation, greatly limiting the number of products formed.

In order to simplify this complex chemistry, we recently demonstrated the utility of

forming SOA by the direct photolytic generation of a single organic radical species.[6] This

approach limits both the number of reactive pathways available (since only one radical species is

22

formed) and the number of oxidation generations (since no oxidant is added). In that initial work, alkyl iodides (RI) were photolyzed at 254 nm in the presence of oxygen to give an alkylperoxy radical (RO_2). Here we expand this approach to a second key intermediate, the alkoxy radical, by the photolysis of alkyl nitrites (RONO):

$$RONO + h\nu \rightarrow RO + NO \hspace{3cm} (1)$$

Reaction 1 generally occurs in the 300-400 nm range, and therefore involves much lower-energy photons than required for RI photolysis.[7,8] RO radicals may still be initially formed vibrationally[9] or electronically[7] excited, but for the large (C_{10}) species considered here, collisional deactivation by bath gas molecules[8] is likely to remove this excess energy prior to reaction. In addition, because the NO photofragment is far less reactive than I atoms formed from RI photolysis, any undesired (and uncertain) secondary chemistry is less likely than in our previous work.

In studies of OH + alkanes under high-NO conditions, Ziemann and coworkers have shown that the chemistry of alkoxy radicals is crucial in determining the yields and composition of SOA.[5,10,11] Such chemical systems can involve a complex mixture of several RO isomers. Here, using the photolysis of a series of C_{10} RONO isomers, we are able to examine RO radical chemistry in even more detail, by isolating the role of individual alkoxy radical species in SOA formation. Furthermore, in the absence of an added oxidant, the effects of multigenerational oxidative chemistry are minimized. The study of aerosol formation from individual alkoxy radical isomers thus allows for a highly detailed examination of the role of chemical structure (position and degree of substitution of the radical center) on SOA yields and composition.

23

2.2 Experimental

Selection and Synthesis of Alkyl Nitrite Species. RONO species are not commercially available, and so were synthesized in the laboratory. This synthesis, described below, requires the corresponding alcohol as the starting material; a series of C_{10} RONO isomers (formula $C_{10}H_{21}ONO$) was chosen based on the large number of precursor alcohols available. The C_{10} alcohols used are 1-decanol and 2-decanol (Sigma Aldrich), 3-decanol, 4-decanol, 5-decanol, 2-methyl-5-nonanol, 2-methyl-4-nonanol, 4-methyl-5-nonanol, 2-methyl-2-nonanol, 5-methyl-5-nonanol, and 3,4-diethyl-5-hexanol (Chemsampco). The alkoxy radicals formed from the eleven C_{10} nitrite isomers synthesized are listed in Figure 2. These radicals are grouped by degree of substitution: primary (straight-chain molecules with the radical center at the terminal carbon atom), secondary (straight-chain molecules with the radical center at one of the secondary/internal carbon atoms), and branched (molecules with at least one methyl or ethyl group branching off the carbon chain).

Synthesis of the nitrites was carried out via O-nitrosation of the alcohol.[12] In this procedure, all glassware, laboratory utensils, and aluminum foil were combusted at 550°C for ten hours to remove all organic contaminants. Sodium nitrite (Sigma Aldrich) and the alcohol were combined in a 1.1:1.0 molar ratio and stirred with a magnetic stirrer at 10°C. To this mixture, chilled 6M sulfuric acid (Sigma Aldrich) was added drop-wise until a 0.5:1.0 acid:alcohol molar ratio was achieved. The resulting clear yellow liquid was dried over sodium sulfate (Sigma Aldrich), and neutralized with excess sodium bicarbonate (Sigma Aldrich). Purity was confirmed by analysis with GC-FID and UV-VIS. For GC analysis, 1 μL of nitrite solution (1 μg RONO/ 1 mL hexane) was injected into an Agilent 7890 GC-FID (50 m, 0.25 mm i.d. DB-5 column; held at 40°C for 3 minutes, then ramped to 250°C at 20°C/minute), which provided sufficient

separation of the RONO (10-12 minute retention time) from the precursor alcohol (12-14 minute retention time). For all syntheses, the ratio of FID signals for the RONO compound to the unreacted alcohol was > 95:1, indicating a conversion of at least 95% of the starting material to the nitrite. Confirmation of conversion to RONO was also made by UV-Vis spectroscopy of the same RONO mixture, with measured spectra similar to those reported by Heicklen.[8] Note that the RONO precursor was stored in the dark and used within 1-2 hours of synthesis to maintain its integrity.
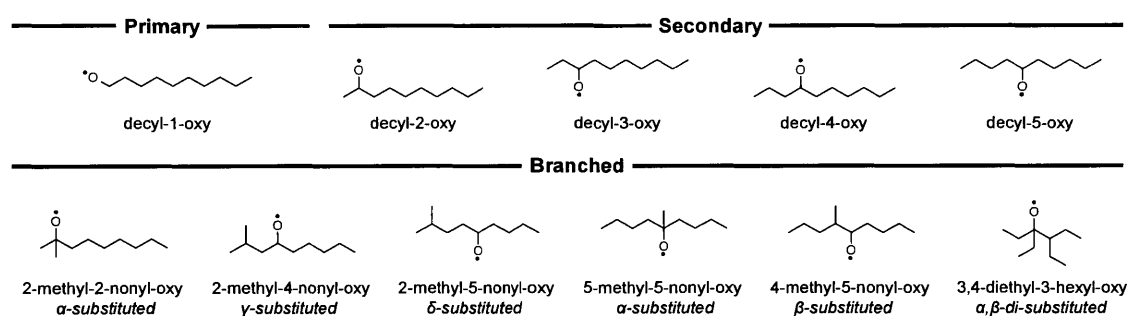
Figure 2. Alkoxy radical isomers examined in this study, listed according to their structural characterization (primary, secondary, or branched).

Chamber Studies. Experiments were conducted in a 1 m^3 Teflon PFA (40 mil) chamber (Ingeniven) surrounded by four 40W black lights (Sylvania BL350). The spectral output of these lamps (300 - 400 nm, centered at ~350 nm) overlaps well with the absorption spectrum of RONO species,[8] allowing for efficient photolysis. The chamber was operated at a constant volume such that the air sampled was balanced with dry (RH < 7%) makeup air from a clean air generator (Aadco, < 5 ppb$_v$ hydrocarbons). Gas phase RONO concentration was monitored with a GC-FID (SRI 8610C) equipped with a Tenax trap and a 30 m 0.53 mm DB-5 column. Prior to

each experiment, the chamber was flushed with clean air for a minimum of ten hours, giving a background particle concentration of < 10 particles/cm^3.

The RONO species (stored in the dark and synthesized within the previous 1-2 hours to maintain its integrity) and a dilution tracer hexafluorobenzene (C$_6$F$_6$, Sigma-Aldrich) were injected into the chamber via a stream of air to attain initial chamber concentrations of 200 ppb$_v$ and 40 ppb$_v$, respectively. For the experiments described here, high levels of NO (~1 ppm) were added to the chamber. While greater than ambient levels (typically < 100 ppb) this concentration serves both to ensure that RO$_2$ + NO reactions dominate the RO$_2$ chemistry across all experiments and to inhibit the formation of O$_3$ and NO$_3$.

Ammonium sulfate ((NH$_4$)$_2$SO$_4$) seed particles were added to promote condensation of low-volatility species onto particles, and also to correct for losses of particles to dilution or wall loss (as described below). Gas-phase products can interact with aerosol particles by two mechanisms: heterogeneous nucleation/adsorption and absorptive/Raoultian partitioning. Initially, association with the inorganic seed surface will occur by heterogeneous nucleation or adsorption processes until a critical amount of particulate organic material has formed, and then absorptive partitioning into this new phase will dominate. The role of seed composition has been identified as an important factor in aerosol growth[13] and is likely due to two features, the sorption coefficients and surface acidities for different materials. For example, partitioning will likely be more favorable for organic than inorganic media. As the polarity of inorganic seed can vary depending on the particular composition, it seems reasonable that the extent of sorption will vary as well. In addition, surface acidity of seed particles can also impact the chemistry of gas-particle partitioning by catalyzing chemical transformations.

Polydisperse $(NH_4)_2SO_4$ seed was generated by atomizing a 1 g/L aqueous solution with a constant output atomizer (TSI Instruments), dried by a drierite denuder, and neutralized using two ^{210}Po static eliminators (Nuclecel, 10 mCi) in series. To minimize the contribution of organic background from the seed, the aqueous $(NH_4)_2SO_4$ solution was extracted five times with high-purity dichloromethane (Omnisolv, VWR) and boiled for four hours to remove any residual solvent. Seed surface area concentrations were high enough ($1000 - 1800$ $\mu m^2/cm^3$ at ~30 $\mu g/m^3$) to inhibit new particle formation within the chamber. RONO, C_6F_6, NO, and seed particles were allowed to mix in the dark chamber for 30 minutes before the blacklights were turned on, initiating photochemistry. Data collection continued until particle growth finished. To account for any background contamination, several identical control experiments were conducted in the absence of precursor RONO.

Aerosol Composition. Particle composition was measured in real time using an Aerodyne high-resolution aerosol time of flight mass spectrometer (AMS),[14] run in "V mode" (resolving power of ~3000) to maximize sensitivity. Time series for the major aerosol families (sulfate, organic, nitrate) were generated from high-resolution fitting of individual mass spectra, and elemental ratios of the organics (O/C, H/C, N/C) were determined using the approach described in Aiken et al.[15,16] Filter blanks were taken for 10 minutes at the start and end of every experiment to measure and correct for the gas-phase CO_2^+ signal within the AMS. All N from NO^+ and NO_2^+ were included in the calculation of N/C, since any nitrate formed is likely to be from organonitrates; however only O atoms directly bonded to the carbon were included in the determination of O/C.

Yield Calculations The time-dependent SOA yield (Y) is given by equation (2):

$$Y(\%) = \frac{c_{OA}(t)}{\Delta RONO(t) \cdot 0.840} \cdot 100\%$$

(2)

where $\Delta c_{OA}(t)$ is the increase in organic aerosol concentration ($\mu g/m^3$) and $\Delta RONO(t)$ is the mass concentration of nitrite photolyzed (the multiplicative factor 0.840 is to exclude the mass of the NO photofragment from the yield calculation). $\Delta RONO(t)$ is calculated as the difference between the initial amount present, $RONO(t_0)$, and the amount remaining at time t, corrected for flushing using measured C_6F_6 concentrations. For all RONO measurements the FID calibration factor was determined by averaging the GC-FID response across all experiments at t_0 and equating this to 200 ppb$_v$.

The AMS and an SMPS (TSI model 3080) were used to determine organic aerosol formation (Δc_{OA}). Aerosol growth was corrected for wall loss and dilution using the method of Hildebrandt et al. (2009),[17] in which the organic-to-sulfate mass ratio (as measured by the AMS) is scaled by the initial sulfate mass (calculated from the SMPS volume and a density of 1.77 g/cm^3). Since sulfate mass concentration will change only by physical loss processes (deposition to the walls and flushing), this approach corrects for losses of organic particle mass to walls and dilution, losses of organic vapors to OA deposited on the chamber walls, and any changes to the AMS collection efficiency or sensitivity over the course of the experiment. Note that any partitioning of semi-volatile species to the chamber walls is not accounted for and while the absolute yields reported here represent a lower limit, the observed trends are unlikely to be affected.

Estimation of first-generation product branching ratios. The relative abundances of each first-generation product were estimated from the relative rates of reactions available to each alkoxy

radical. Alkoxy radicals were assumed to either fragment (k_{frag}) into smaller products, or isomerize "forward" ($k_{isom-forward}$) to form an alkylperoxy species or "backwards" ($k_{isom-back}$) to form the hydroxycarbonyl (Figure 3). Reactions of alkoxy radicals with O_2 to form carbonyls were negligible for the straight-chain species and are not shown in Figure 3; however, they were significant particularly for the alpha-substituted branched species and were considered there. Reactions of peroxy radicals with NO were assumed to produce either alkoxy radicals or organonitrates in a fixed ratio of 80:20, based on measurements and model predictions of alkylnitrate yields from alkane + OH experiments in the presence of NO_x.[18]

Estimates for k_{isom} are from Atkinson[19] (Table 1); all isomerization reactions involve H atoms at the δ-position. Values of k_{frag} were estimated using the enthalpy-based parameterization developed by Atkinson[18] (Table 2), This approach provides an estimate of reaction activation energies, E_d from:

$$E_d = a + \Delta_{frag}H*b \qquad (r1)$$

where a is a parameter based on the structure of the leaving radical species, b is a constant (0.4), and $\Delta_{frag}H$ is the reaction enthalpy which was estimated from smaller structurally similar species (Table 2).[1] These E_d values are then used to calculate k_{frag} values using the Arrhenius equation:

$$k_{frag} = A*exp(-E_d/RT) \qquad (r2)$$

where the recommended[19] pre-exponential factor A is 5.0×10^{11} s^{-1}, R is the ideal gas constant (1.987×10^{-3} kcal K^{-1} mol^{-1}), and T is the absolute temperature, 298 K. Finally, branching ratios were calculated from the rates of each channel available to all the alkoxy radicals within a given reaction sequence.
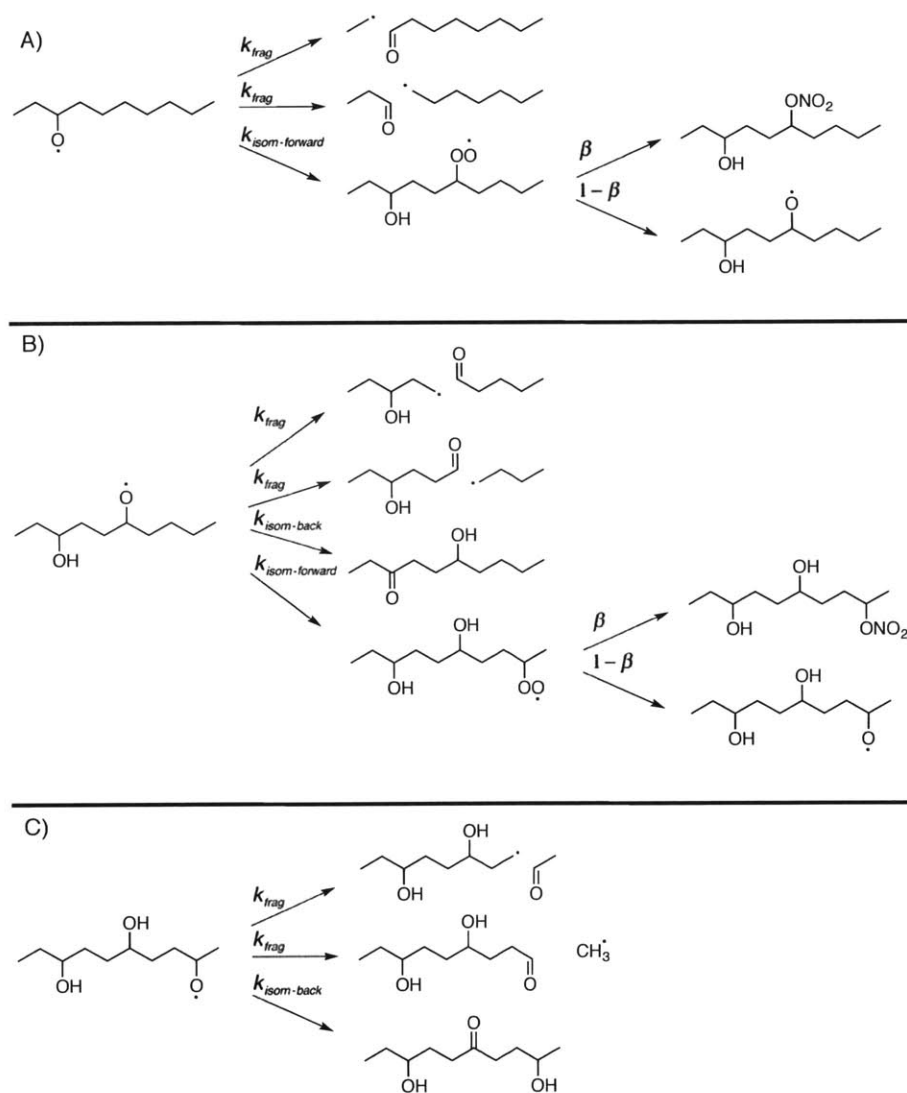
Figure 3. Branching of (A) alkoxy, (B) hydroxyalkoxy, and (C) dihydroxyalkoxy radicals for a representative alkoxy radical system (decyl-3-oxy). Each alkoxy radical pathway is denoted by its absolute rate constant (k_{frag} for fragmentation, $k_{isom-forward}$ for "forward isomerization", and $k_{isom-back}$ for "backward isomerization"); peroxy radical + NO reactions give the organic nitrate with a yield of β, taken to be 0.2 in all cases.

Fragmentation rates (Table 3) were also estimated using an alternative SAR, based upon the degree of α- and β-substitution of the alkoxy radical.[20] In that case, E_d is calculated from the following formula:

$$E_d = 17.5 - 2.1*N_\alpha - 3.1*N_\beta \qquad (r3)$$

where N_α and N_β are the number of alkyl substituents located on the carbon atom α and β to the alkoxy radical center, respectively.[20]

Table 1. Isomerization rate constants (from Atkinson[19]).

δ-Carbon Identity	k_{isom} (s^{-1})
RCH_3	3.2×10^5
$R_1CH_2R_2$	3.3×10^6
$R_1CH(R_2)R_3$	1.1×10^7
$R_1CH(OH)R_2$	2.4×10^7

Table 2. Fragmentation rate constants (based on Atkinson[19]).

Fragment	a	$\Delta_{frag}H$ (kcal/mole K)	E_d (kcal/mole)	k_{frag} (s^{-1})
$R + CH_3$ *Methyl radical*	12.9^a	5.30^a	15.00	4.69×10^2
$R + CH_2CH_3$ *Ethyl Radical*	9.8^a	7.60^a	12.80	1.87×10^4
$R + R'CH_2CH_3$ *Propyl, Butyl, Pentyl, Hexyl Radical*	9.5^a	8.73^b	13.00	1.45×10^4
$R + R'R''CH_2CH_3$ *Secondary Radical*	8.2^a	7.95^b	11.40	2.21×10^5

a. Atkinson[19]
b. Calvert[21]

Table 3. Fragmentation rate constants (based on Peeters[20]).

Fragment[a]	E_d (kcal/mole)	k (s^{-1})
Primary		
RCH_3	14.10	1.3×10^3
Secondary		
CH_3	10.20	2.5×10^2
RCH_2CH_3	13.30	4.7×10^4
$R'R''CH_2CH_3$	9.20	8.8×10^6
Tertiary		
RCH_3	10.20	1.6×10^6
CH_3	13.30	8.6×10^3

a. Primary, Secondary, and Tertiary headings refer to the substitution at the radical center (at the α-carbon)

2.3 Results

Aerosol formation and yields. Results for a representative experiment, the photolysis of 200 ppb$_v$ of decyl-3-nitrite, are shown in Figure 4. When the lights are turned on, RONO decays exponentially, with a decay constant of 2.1 x 10^{-4} s^{-1}. Photolysis rates for all nitrites are similar, with an average decay constant of 2.5 x 10^{-4} s^{-1} for all species studied. Significant GC interferences from gas-phase products with similar retention times to RONO preclude the direct measurement of RONO concentration after three to five hours, so fitted values (dotted line in Figure 4) were used for all values of ΔRONO. Roughly 25 minutes after irradiation is initiated, OA mass concentration (c_{OA}) begins increasing. A significant amount of SOA is formed, with corrected loadings reaching a plateau of ~25 μg/m^3 after 4-5 hours, indicating that reaction has reached completion. Also shown in Figure 4 are the elemental ratios of the SOA formed; these vary little over the course of the experiment, and are discussed in detail in a later section. Background organic concentrations from seed particles (in the dark) were < 1 μg/m^3, and in control experiments, the organic loading did not increase, even after 4-5 hours.
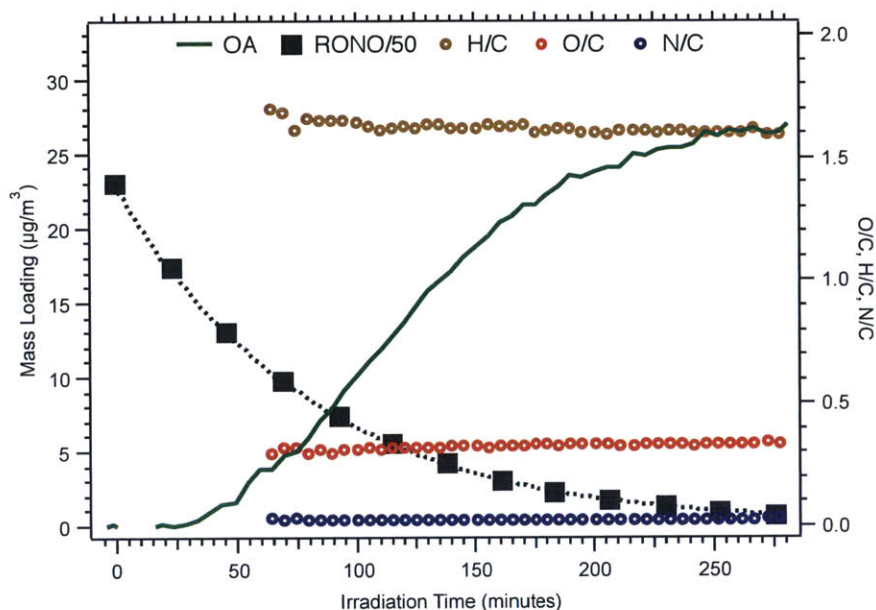
Figure 4. Time-dependent results from a representative alkoxy radical experiment, using decyl-3-nitrite as the precursor RONO species. GC-FID measurements of RONO concentrations (scaled by 1/50) are shown as black squares, with the exponential fit to the data as a dashed line. The organic aerosol mass concentration (c_{OA}), corrected for wall loss and dilution, is shown in green. Elemental ratios (O/C, H/C, and N/C) exhibit low signal-to-noise at low mass loadings and so are shown only after ~4 $\mu g/m^3$ of OA is formed.

SOA formation was observed for all alkoxy radical species studied, with the exception of 3,4-diethyl-3-hexyl-oxy. Yield curves (plots of aerosol yield as a function of c_{OA}) for all alkoxy radicals that formed SOA are shown in Figure 5. Any organic mass associated with the seed aerosol (<1 $\mu g/m^3$ in all cases) was subtracted prior to the calculation of yields. Yields (Y) from the three groups of alkoxy radicals decreased from $Y_{primary} > Y_{secondary} > Y_{branched}$. SOA yields for the straight-chain species generally decreased as the radical center was located closer to the center of the carbon skeleton ($Y_{decyl-1-oxy} > Y_{decyl-2-oxy} > Y_{decyl-4-oxy} > Y_{decyl-3-oxy} > Y_{decyl-5-oxy}$). The branched alkoxy radicals exhibited lower yields than the straight-chain isomers, with yields showing no obvious trend with the location of the branching methyl group relative to the radical center (α, β, γ, δ). No aerosol formation was observed from the α β-disubstituted isomer (3,4-diethyl-3-hexyl-oxy). These results are examined in detail in the Discussion section. The lower-

33

limit for the amount of SOA formed was from the 4-methyl-5-nonyl-oxy radical, which increased the aerosol diameter by ~85 nm. Given the size of the C_{10} precursor, this would imply the presence of greater than 2000 monolayers and hence the physical mechanism for particle growth is similar across all isomers.
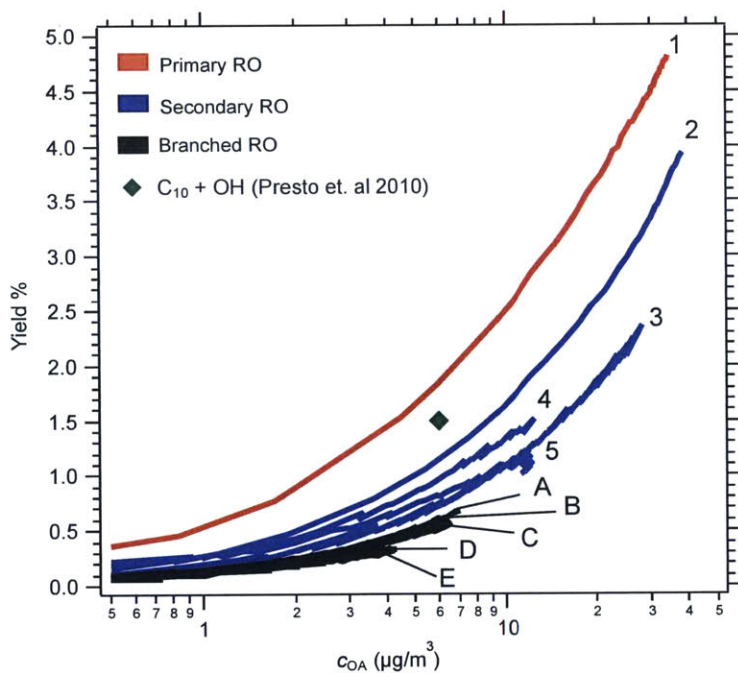
Figure 5. Yield % curves as a function of c_{OA} ($\mu g/m^3$) for the C_{10} alkoxy radical species studied. Curves are colored by structural type: red indicates the primary radical (1: decyl-1-oxy); blue the secondary radicals (2: decyl-2-oxy, 3: decyl-3-oxy, 4: decyl-4-oxy, and 5: decyl-5-oxy); and black the branched radicals (A: 2-methyl-2-nonyl-oxy, B: 2-methyl-4-nonyl-oxy, C: 2-methyl-5-nonyl-oxy, D: 5-methyl-5-nonyl-oxy, and E: 4-methyl-5-nonyl-oxy). No aerosol formation was observed from the 3,4-diethyl-3-hexyl-oxy radical. The SOA yield of the analogous reaction, *n*-decane + OH, as by Presto et al.[22] is shown as the green diamond. Yields from additional studies[23–25] are not shown here as they were conducted at higher c_{OA} levels.

Product saturation vapor pressure distributions were derived from yield curves using the volatility basis set approach,[26] with fixed saturation vapor concentration (c^*) bins of 1, 10, and 100 $\mu g/m^3$. These bins span the range of c_{OA} accessed in this study, and thus including additional bins did not improve the fits significantly. The mass-based yields for each bin (α_1, α_{10}, and α_{100})

are listed in Table 4, both for the individual alkoxy radicals and for averages of all secondary and

branched radicals.

Table 4. Summary of SOA yield parameters and elemental ratio measurements.[a]

RO isomer	O/C	H/C	N/C	α_1 ($c^* = 1$ μg/m³)	α_2 ($c^* = 10$ μg/m³)	α_3 ($c^* = 100$ μg/m³)
decyl-1-oxy *primary*	**0.19**	**1.62**	**0.05**	**0.33**	**2.15**	**7.95**
decyl-2-oxy *secondary*	0.23	1.60	0.05	0.23	0.47	9.55
decyl-4-oxy *secondary*	0.32	1.61	0.03	0.27	0.58	6.25
decyl-3-oxy *secondary*	0.32	1.61	0.03	0.22	0.00	7.89
decyl-5-oxy *secondary*	0.23	1.70	0.04	0.20	0.90	3.07
Secondary Average	**0.28 ± 0.05**	**1.63 ± 0.07**	**0.04 ± 0.01**	**0.23 ± 0.03**	**0.49 ± 0.37**	**6.69 ± 2.77**
2-methyl-2-nonyl-oxy *α-substituted*	0.23	1.64	0.04	0.09	0.13	6.67
2-methyl-4-nonyl-oxy *γ-substituted*	0.28	1.61	0.03	0.11	0.00	5.99
2-methyl-5-nonyl-oxy *δ-substituted*	0.25	1.66	0.03	0.11	0.00	5.99
5-methyl-5-nonyl-oxy *α-substituted*	0.21	1.66	0.03	0.14	0.00	4.76
4-methyl-5-nonyl-oxy *β-substituted*	0.25	1.64	0.03	0.06	0.39	2.68
3,4-diethyl-3-hexyl-oxy[b] *α,β-disubstituted*	-	-	-	-	-	-
Branched Average[c]	**0.24 ± 0.03**	**1.64 ± 0.02**	**0.03 ± 5 x 10⁻³**	**0.10 ± 0.03**	**0.10 ± 0.17**	**5.22 ± 1.58**

a. Species are listed in order of decreasing yields. Mass-based yields (α) were derived using a three-product fitting with the volatility basis set for c^* (μg/m³) = {1, 10, 100}. Averages are reported as ± 1σ.
b. SOA formation not observed.
c. Average of values for all branched alkoxy radicals except 3,4-diethyl-3-hexyl-oxy.

Aerosol composition. Elemental ratios (O/C, H/C, and N/C) of the SOA generated from all alkoxy radical species (averaged over the last two hours of each experiment) are also given in Table 4. Since our determination of N/C is dominated by the NO^+ and NO_2^+ ions, here N/C is a measure of organonitrate abundance. Similarly, since reported O/C ratios do not include the two terminal O atoms bonded to the nitrate-N,[27] they account only for oxygen atoms directly bonded to the carbon skeleton, and thus represent a measure of the degree of carbon oxidation. To correct for any contribution of background organic mass to the measured bulk properties, the total mass of C, O, H, and N present in the dark (seed aerosol) was subtracted from all subsequent runs. The low organic mass loading did not change the measured O/C or H/C by more than 5%. N/C of background organics was < 0.001, indicating a negligible contribution of organonitrates.

As illustrated in Figure 4, elemental ratios do not vary dramatically over the course of an experiment; on average O/C and N/C values increased slightly (by < 10% and ~5% respectively) while H/C decreased (by ~3-5%) over 2-3 hours of irradiation. This absence of "aging" is expected for the present system, whose chemistry is dominated by a single rate-limiting reaction step (the photolysis of the RONO species); the subsequent drift toward slightly more oxidized products may result from secondary oxidation reactions (described below) or slow repartitioning effects that result from dilution of the chamber.

SOA formed from the primary alkoxy radical is less oxidized (O/C = 0.19, H/C = 1.62) than SOA formed from secondary and branched alkoxy radicals (average values: O/C = 0.25, H/C = 1.63). This corresponds to differences in the degree of functionalization of the carbon skeleton: assuming that condensed species retain their C_{10} carbon skeleton (i.e., that the SOA includes no fragmentation products), SOA from the primary alkoxy radical contains on average

36

two oxygen-containing moieties per molecule, whereas for the SOA from secondary and branched alkoxy radicals have up to three such moieties per molecule. At the same time, the SOA formed from isomers with their radical centers closest to the terminus of the molecules tended to have the highest abundances of organonitrates (N/C of 0.05 for decyl-1-oxy and decyl-2-oxy vs. ~0.03 for all others). Since SOA from these isomers also had the lowest O/C values, nitrates appear to account for a relatively large fraction of the functional groups in the less-oxidized SOA.

2.4 Discussion

Reaction mechanism. Reaction pathways available to the alkoxy radicals studied in these experiments are shown in Figure 6. The top panel in Figure 6 shows the initial gas-phase reactions possible: the two key channels are (i) isomerization (green arrows), which forms a hydroxylalkyl radical, and fragmentation (red arrows), which forms a carbonyl and an alkyl radical. A third channel, the reaction with O_2 to form a carbonyl and HO_2, is expected to be negligible for straight-chain species but significant for some of the branched isomers.[28] The isomerization pathway tends to form multifunctional, lower-volatility products (generally promoting SOA formation), while fragmentation forms two smaller, relatively volatile species (generally inhibiting SOA formation).[10] Isomerization (including the initial H-atom transfer and immediate addition of O_2 to the alkyl radical) forms a peroxy radical, which will react with NO to form either an alkyl nitrate (blue arrow) or another alkoxy radical. This newly-formed alkoxy radical will mostly "back-isomerize" to form a hydroxycarbonyl, though some fraction (~10%) will instead "forward-isomerize", ultimately leading to the formation of a dihydroxycarbonyl or dihydroxynitrate.[23,28]

37
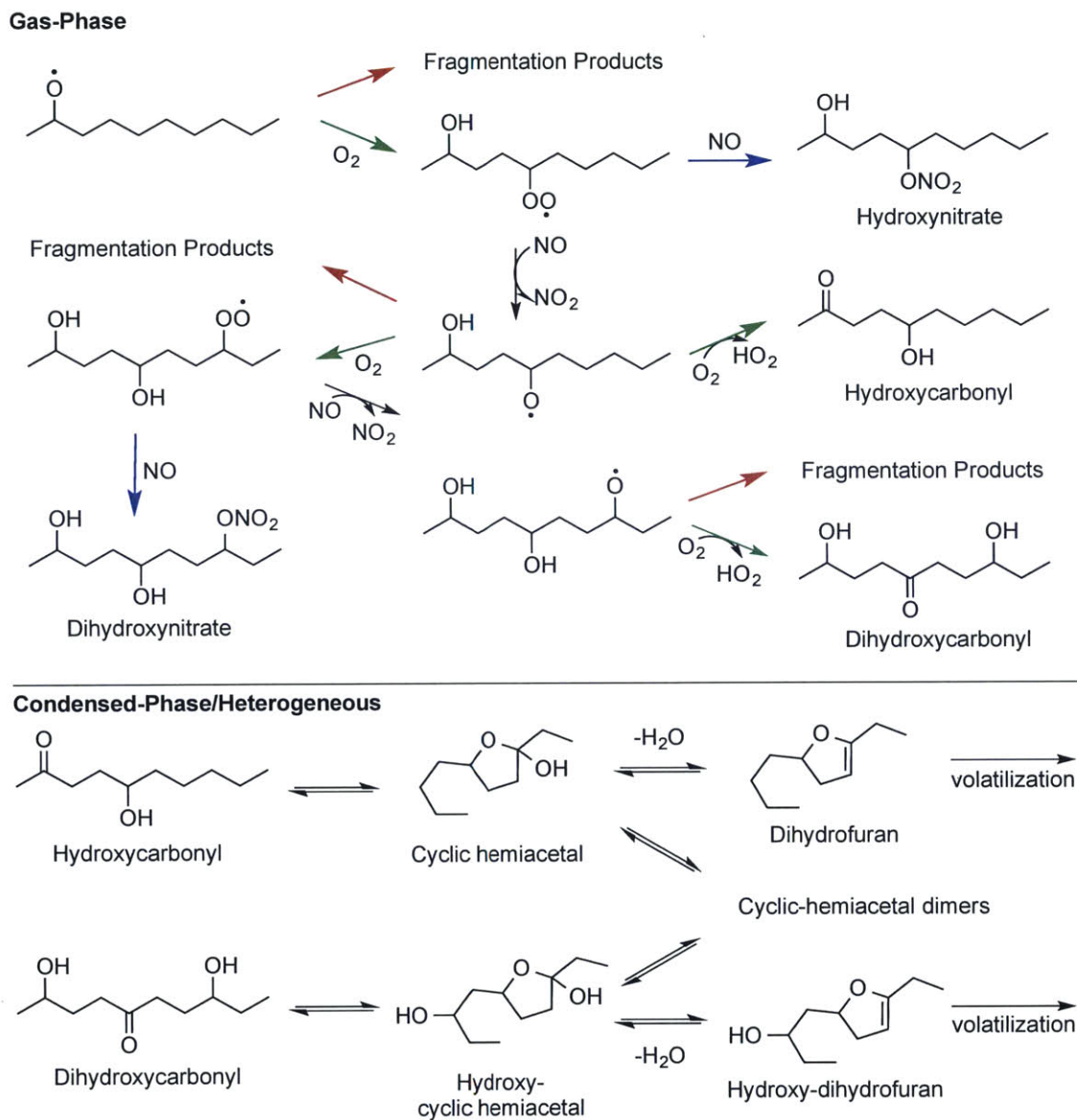
Figure 6. Formation of first-generation products from a single alkoxy radical species. Shown are the major gas-phase (top panel) and condensed phase/heterogeneous (bottom panel) reactions and products formed from a representative alkoxy radical, decyl-2-oxy. Alkoxy radicals will fragment (red arrow) or isomerize (green arrow); isomerization leads to the formation of a peroxy radical, which in the presence of NO can form an organonitrate (blue arrow) or a new alkoxy radical, opening up additional isomerization and fragmentation channels.

The lower panel of Figure 6 shows the subsequent heterogeneous and condensed-phase reactions available to (di)hydroxycarbonyls, which can undergo heterogeneous cyclization to form (hydroxy)cyclic hemiacetals.[10,11,23] Such compounds can dimerize to form hemiacetal

dimers, or dehydrate to form a (hydroxy)dihydrofuran. This latter compound is volatile and will likely partition into the gas-phase, where (if oxidants are present) it will rapidly react to form second-generation oxidation products.[29]

High molecular weight (m/z > 150 Da) ion fragments were observed in all mass spectra, and the chemical formulae of major ions were determined by high-resolution analysis (Figure 7). All such ions have 10 carbon atoms, and most are the C_{10} analogs of ions previously observed in alkane + OH experiments by Lim and Ziemann[23]; the high-resolution identification of these ions confirm the assignments of that study. Three of the most abundant fragments correspond to species with 10 carbon atoms and 1-2 oxygen atoms, m/z 155.143 ($C_{10}H_{19}O^+$), 169.122 ($C_{10}H_{17}O_2^+$) and 171.138 ($C_{10}H_{19}O_2^+$). The time series of each fragment from representative primary, secondary, and branched nitrite photolysis experiments are shown in Figure 8. Fragment abundances (shown as the fraction of the organic signal) increase immediately following irradiation and level off after 1.5 – 3 hours, with the exception of $C_{10}H_{19}O_2^+$, which peaks and then decreases slightly.

Following the molecular assignments of Lim and Ziemann,[23] we can tentatively assign observed ions to major products from alkane oxidation experiments, however, further study with softer ionization techniques (relative to electron impact) is necessary for definitive assignments. The $C_{10}H_{19}O^+$ and $C_{10}H_{19}O_2^+$ ions may correspond to two major first generation products, the cyclic hemiacetal (m/z 155.143) and the hydroxy-cyclic hemiacetal or hemiacetal dimer (m/z 171.138), respectively. The $C_{10}H_{17}O_2^+$ ion (m/z 169.122) has previously been identified as the cyclichemiacetal nitrate. This is a second-generation product, which as described may be formed in the present experiments; thus the molecular assignment of this species is uncertain and requires further study. Furthermore, several prominent N-containing ions of m/z > 200 are

present, pointing to the presence of organonitrate species; the detailed molecular assignments for such species are unclear. The absence of abundant ions corresponding to the hydroxycarbonyl, hydroxynitrate, and dihydrofuran (which would be found at m/z 154, 138, and 140 respectively)[23] is likely due to their high volatilities. Unfortunately, low ion intensities and unknown ionization efficiencies preclude the detailed interpretation of the high-mass ions in the AMS spectra, and in particular their relative intensities in different alkoxy radical experiments. Nonetheless, the observation of ions similar to those observed by Lim and Ziemann[23] provides strong confirmation that the present experiments access the chemistry important in the early-generation oxidation of alkanes.
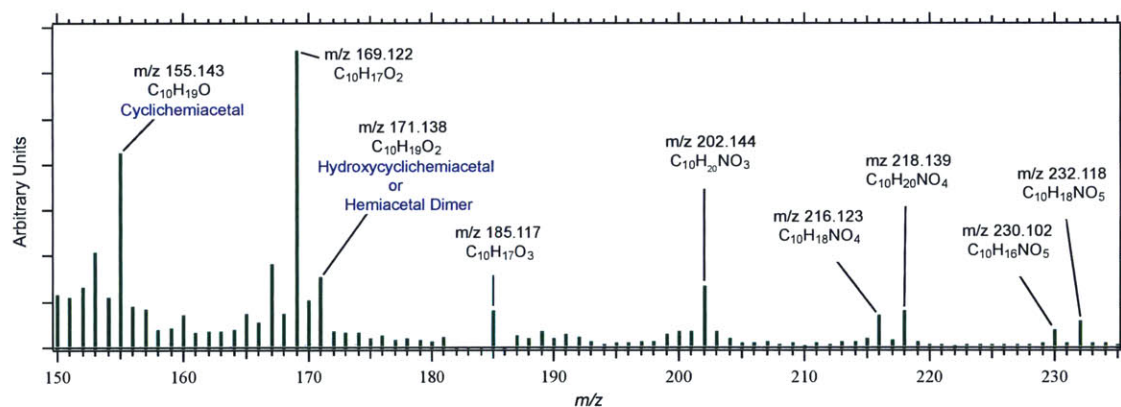
Figure 7. High-mass ions (m/z 150-235) in the AMS spectrum of SOA formed from decyl-1-nitrite photolysis. Ion formulae given were confirmed by high-resolution analysis; tentative molecular assignments are from Lim and Ziemann.[23]
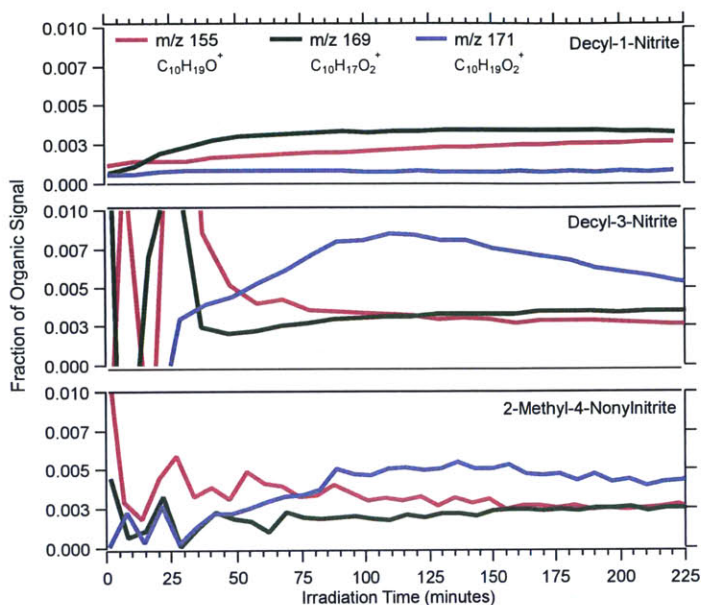
Figure 8. Ion time series for three of the major ions, *m/z* 155.143, 169.122, and 171.138 for a representative primary (decy-1-nitrite), secondary (decyl-3-nitrite), and branched (2-methyl-4-nonylnitrite) experiment. Traces are shown as a fraction of the total organic mass.

Role of multigenerational oxidation. The mechanism shown in Figure 6 includes no oxidation of the reaction products; in standard (oxidant-initiated) studies of SOA, reaction products will react further with oxidants, leading to a complex mixture of multigenerational products. By contrast, in the present chemical system (the photolytic generation of radicals), all chemistry is initiated without oxidants, allowing for individual oxidation steps to be studied in greater detail than in oxidant-initiated studies. Nonetheless, some additional oxidation may occur in the present studies via the secondary generation of oxidants. Oxidation by NO_3 and O_3 is unlikely, due to the high (ppm) levels of NO present. However, since HO_2 can be formed via secondary isomerization reactions (Figure 6), some OH formation may occur via the $HO_2 + NO$ reaction. While of the OH formed will react with NO_2 to form HNO_3, the rest may potentially react with the products formed. The importance of OH-initiated secondary chemistry can be estimated from the behavior of the cyclic hemiacetal species (*m/z* 155.143 in Figures 7 and 8). Since this

41

compound is in equilibrium with the highly reactive dihydrofuran (Figure 6), the presence of oxidants will lead to a rapid depletion of that ion. However, as shown in Figure 8 no such depletion is observed, in stark contrast to results from alkane oxidation studies.[11,29] It is possible that the depletion is not observed due to the absence of sufficient HNO$_3$ which is necessary to catalyze the cyclization of hydroxycarbonyls. Furthermore, the assignment of m/z 155 to the cyclichemiacetal is tentative, and thus this ion may correspond to an additional product. The influence of multigenerational chemistry thus remains not entirely clear. While the ion at *m/z* 171.138 does indeed decrease to some extent, this may be a result of non-oxidative chemistry of the hemiacetal dimer rather than oxidation of the hydroxy-cyclic hemiacetal.

Differences in SOA yields and properties measured in the present study and those in the analogous *n*-decane + OH reaction[22,24,25,30] are also consistent with the lack of multigenerational oxidation in our experiments. In particular, SOA yields from OH + *n*-decane are substantially higher than those from the RONO photolysis. Shown in Figure 5 is the SOA yield measured by Presto et al.[22] (green diamond). This yield falls between those measured in this study from decyl-1-oxy and decyl-2-oxy radicals, and thus is substantially higher than the yields inferred from the RONO experiments (since these two radicals together account for only ~24% of the first alkoxy radical isomers formed in the *n*-decane + OH reaction[31]). The difference between aerosol formation between these two studies is even more pronounced than is implied from these yield differences, given that decyl nitrate, a volatile first-generation product from OH + *n*-decane, is not formed from RONO photolysis. Studies of OH + *n*-decane carried out at higher OH exposures than accessed by Presto et al. found even higher SOA yields (> 10%),[24,25] consistent with additional OH oxidation leading to more SOA formation (the experiments from Lim and Ziemann[23] were carried out at much higher c_{OA}, preventing a direct comparison with our results

here). The primary and secondary RO radicals generated are those that would form from the reaction of OH with n-decane. The approximate contribution of first-generation products to the overall SOA yield from the OH initiated reaction is estimated from the sum of the weighted SOA yields from each isomer. Weighting our measured yields based on the fraction of each positional isomer expected to form results in a yield of 0.94 at $C_{OA}= 6$ $\mu g/m^3$, compared to 1.5 from decane + OH. Thus for a first approximation, neglecting heterogeneous oxidation processes and assuming that second-generation oxidation products are minor in our experiment (discussed below) , ~60% of SOA from decane + OH may be from first-generation products.

Similar differences are seen in the degree of oxidation of SOA; O/C ratios measured in this work are lower (0.19 – 0.32) on average than those from OH + n-decane (0.33-0.35),[25,30] whereas H/C ratios are higher (1.6-1.7 versus 1.5-1.6).[25,30] These results all suggest that multigenerational oxidation chemistry is suppressed in the present experiments, and that the SOA formed is predominantly made up of first-generation oxidation products.

Effect of alkoxy radical structure on SOA formation. The large variability in yields and chemical composition of SOA formed from various C_{10} alkoxy radical isomers (Figure 5 and Table 4) underscores the high degree of sensitivity of SOA formation to the exact chemical structure of the precursor species. The location and degree of substitution of the alkoxy radical center appears to have a governing effect on observed yields; this is particularly evident in the large differences in yields among the various radicals with straight-chain carbon skeletons, and between the structurally similar 2-methyl-2-nonyl-oxy and 5-methyl-5-nonyl-oxy radicals. As described below, differences in the yield and composition of SOA from the different isomeric alkoxy radicals can be explained in terms of two general factors, the branching between

43

fragmentation and isomerization of the alkoxy radicals (including those formed subsequent to isomerization), and the relative volatilities of the different isomeric products formed from each radical.

*Alkoxy Radical Products.* The exact chemical structure of each alkoxy radical has a governing influence on the reactive pathways available to it, which in turn can affect the amount and composition of SOA formed.[5,10,11] Using a structure-activity relationship (SAR) to describe alkoxy radical reactivity,[28] and in particular the branching between isomerization (functionalization) and C-C bond scission (fragmentation), we calculated the distribution of first-generation products from each alkoxy radical studied. Such calculations take into account the fate of not only the original alkoxy radical but also any alkoxy formed later in the reaction sequence (see Figures 3 and 6); calculation details are given below.

The calculated product distributions for the major first generation products of each alkoxy radical isomer are shown in Figure 9. For most of the alkoxy radicals studied, hydroxynitrates and hydroxycarbonyls are the major products. The predicted product distributions from decyl-1-oxy, decyl-2-oxy, and decyl-3-oxy are identical. For these species, the formation of fragmentation products is negligible (< 3%), whereas products arising from multiple isomerization reactions (dihydroxycarbonyls and dihydroxynitrates) represent a small but significant (~10%) fraction of the total products. Note that the rate for H-abstraction was assumed to be the same for all secondary carbons. The predicted products from the other two straight-chain radicals (decyl-4-oxy and decyl-5-oxy) are similar, though they do not include the dihydroxy species, since "forward-isomerization" reactions either cannot occur (due to the lack of H atoms in the δ -position) or are highly unfavorable (due to the δ-H atoms residing on methyl

Figure 9. Distribution of major first-generation products from each alkoxy radical isomer. Isomers are listed in order of decreasing yields; the identifiers in parentheses correspond to those used in Figure 5.
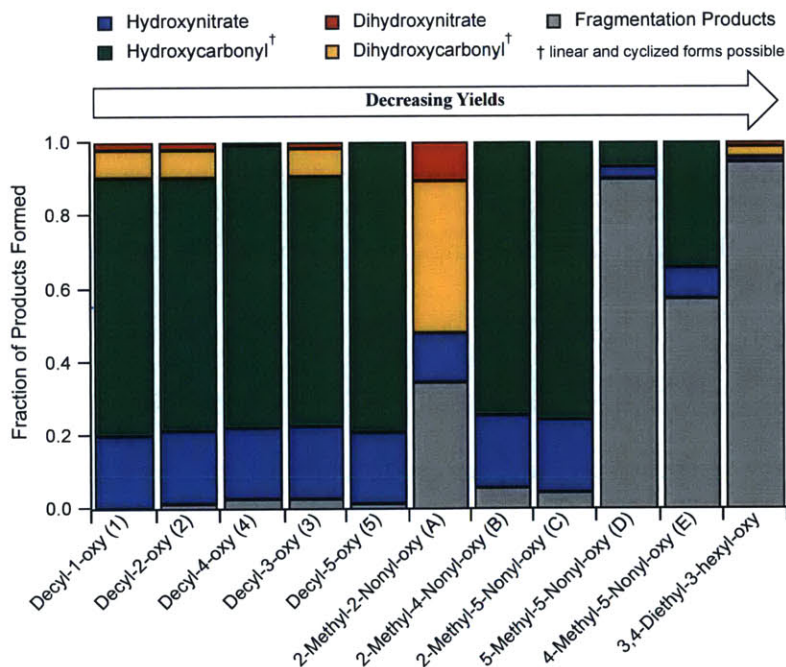
Figure 10. Distribution of major first-generation products from each alkoxy radical isomer using the substituent-based parameterization for fragmentation rates. Isomers are listed in order of decreasing yields; the identifiers in parentheses correspond to those used in Figure 5.

groups). The lack of formation of these low-volatility products may contribute somewhat to their lower SOA yields. However, since the SOA yield from the decyl-4-oxy radical is somewhat greater than that from the decyl-3-oxy radical, this appears to be a minor effect.

The calculated product distributions for the major first generation products of each alkoxy radical isomer are shown in Figure 9. For most of the alkoxy radicals studied, hydroxynitrates and hydroxycarbonyls are the major products. The predicted product distributions from decyl-1-oxy, decyl-2-oxy, and decyl-3-oxy are identical. For these species, the formation of fragmentation products is negligible ($<$ 3%), whereas products arising from multiple isomerization reactions (dihydroxycarbonyls and dihydroxynitrates) represent a small but significant (~10%) fraction of the total products. Note that the rate for H-abstraction was assumed to be the same for all secondary carbons. The predicted products from the other two straight-chain radicals (decyl-4-oxy and decyl-5-oxy) are similar, though they do not include the dihydroxy species, since "forward-isomerization" reactions either cannot occur (due to the lack of H atoms in the δ -position) or are highly unfavorable (due to the δ-H atoms residing on methyl groups). The lack of formation of these low-volatility products may contribute somewhat to their lower SOA yields. However, since the SOA yield from the decyl-4-oxy radical is somewhat greater than that from the decyl-3-oxy radical, this appears to be a minor effect.

Estimated product distributions from the δ- and γ-substituted branched species (2-methyl-5-nonyl-oxy and 2-methyl-4-nonyl-oxy, respectively) are similar to those of the straight-chain species, since the branch points are located relatively far from the alkoxy radical center and thus have little influence on the chemistry. The other branched alkoxy radicals, however, are predicted to form very different sets of products; these can include fragmentation products, which can at least partly explain their lower SOA yields. Three of the RO species studied have

46

tertiary (α-substituted) radical centers, the mono-substituted 2-methyl-2-nonyl-oxy, 5-methyl-5-nonyl-oxy and the di-substituted 3,4-diethyl-3-hexyl-oxy radical. The two mono-substituted branched species (2-methyl-2-nonyl-oxy and 5-methyl-5-nonyl-oxy), despite being quite similar structurally, have dramatically different product distributions, due to the number of isomerization reactions available to each. 2-Methyl-2-nonyl-oxy is unable to form a hydroxycarbonyl, since the α-substituted methyl group prevents "back-isomerization", however, it is able to undergo a second "forward-isomerization" that 5-methyl-5-nonyl-oxy cannot. Instead, the second alkoxy radical formed from 5-methyl-5-nonly-oxy will react with O_2 to form a significant amount of hydroxycarbonyl species (~50%). The result is that the products of the 2-methyl-2-nonyl-oxy radical are dominated by the low-volatility dihydroxy species (~80%), whereas those from 5-methyl-5-nonyl-oxy are either fragmentation products (25%) or hydroxycarbonyls (~50%) formed from the RO + O_2 pathway. This is consistent with 2-methyl-2-nonyl-oxy having the highest yields among the branched isomers, and 5-methyl-5-nonyl-oxy among the lowest. For these two tertiary RO isomers, the additional methyl group has only a minimal impact on the extent of fragmentation because in all cases scission results in a primary radical which is less favorable than corresponding isomerization reactions. However, fragmentation of the other tertiary isomer, 3,4-diethyl-3-hexyl-oxy, results in the formation of a secondary radical which is discussed below.

The lowest SOA yields measured were from the β-substituted species, 4-methyl-5-nonyl-oxy (mono- β -substituted) and 3,4-diethyl-3-hexyl-oxy (α, β-di-substituted, for which no SOA formation was observed). This suggests a high degree of radical fragmentation in those cases, however the amount of fragmentation predicted by the SAR is relatively modest: 4% from 4-methyl-5-nonyl-oxy and 30% from 3,4-diethyl-3-hexyl-oxy. This difference suggests that

fragmentation of β-substituted alkoxy radicals may be underestimated using the SAR, which estimates fragmentation based upon reaction enthalpy[28]; this may result from the lack of accurate values of reaction enthalpies of secondary β -substituted alkoxy radicals. An alternate SAR (Figure 10) for describing alkoxy radical fragmentation, based on the degree of substitution of the α - and β- carbon atoms,[20] predicts substantially more fragmentation (57% and 94% from 4-methyl-5-nonyl-oxy and 3.0% from 3,4-diethyl-3-hexyl-oxy, respectively). This generally agrees with the SOA trends observed; however that SAR also predicts increased fragmentation of α-substituted radicals, which is not consistent with the SOA yields from those species. Both SARs are based upon measurements of fragmentation rates of relatively small alkoxy radicals; the direct study of the fate of larger, more substituted radicals would be useful for better constraining these SARs. The results from this work alone, unfortunately, are not sufficient to improve these SARs as the detailed product yields and branching ratios not measured here are necessary.

Saturation Vapor Pressure of SOA components. As described above, the extent of alkoxy radical fragmentation and isomerization are in good qualitative agreement with many of the observed differences in yields, particularly for the branched species. However, the differences in yields among the straight-chain species (which are predicted to have very similar product distributions) and the relatively low O/C values for decyl-1-oxy and decyl-2-oxy, are not captured by this explanation alone, pointing to additional factors controlling SOA formation. These appear to be related to differences in the volatilities of the (isomeric) products formed. As shown in Table 4, SOA from the secondary and branched radicals exhibit saturation vapor pressure distributions that are skewed towards higher c^* bins relative to the SOA from primary radicals, as reflected in differences in both α_1/α_{100} and α_{10}/α_{100} ratios. This effect can also be seen in Figure 5, which

shows that the relative differences among yields from different radical types are most pronounced at low values of c_{OA}.

Such differences in SOA c*, even when formation occurs via similar chemistry (i.e., from straight-chain isomers), likely arise from differences in saturation vapor pressures of the isomeric product species. While the various precursor alkoxy radicals and their products (hydroxycarbonyls, hydroxynitrates, etc.) have the same chemical formulae, their spatial arrangement can lead to large differences in their relative volatilities. Among the straight-chain radicals, yields tend to increase as the alkoxy radical center is located closer to the terminus of the molecule. (The one exception is decyl-3-oxy, which has lower yields than decyl-4-oxy; however such a difference is small.) This effect likely arises from the fact that functional groups located closer to the terminus of molecules generally have larger influences on vapor pressure, since the molecules can "stack" more efficiently. For example, for straight-chain C_9 alcohols, the vapor pressure of 1-nonanol is 5 times lower than that of 2-nonanol, which in turn is 1.4 times lower than the vapor pressures of the remaining isomers (the differences among 3-nonanol, 4-nonanol, and 5-nonanol are much smaller, under 5%).[32] The relative ordering of SOA yields among the straight-chain alkoxy radicals, is broadly consistent with this trend, pointing to the role of the volatilities of product isomers on SOA formation. In addition, the presence of aldehydes (terminal carbonyls), which have slightly lower volatilities than ketones formed by secondary alkoxy radicals,[1] and are also more susceptible to oligomerization reactions (such as hemiacetal formation),[33] further decreases c*. Since the primary decyl-1-oxy species is the only isomer capable of forming aldehydes, its products have a lower c*, explaining its higher values of α_1/α_{100} relative to those from the secondary and branched isomers. Similarly, the structure of the carbon skeleton may play a role, since branched species generally have higher volatilities

49

than straight-chain isomers. This "P_{25} effect"[10] may contribute to the low yields from branched alkoxy radicals; however differences in alkoxy radical fragmentation (as described above) are likely the dominant factor for most of the isomers studied.

Such differences in volatilities of different product isomers may also explain some of the trends in O/C ratios, particularly among the straight-chain radicals, since products from the decyl-1-oxy and decyl-2-oxy have a lower c* relative to corresponding isomers from the other alkoxy radicals. This enhances the gas-to-particle partitioning of less oxidized (less functionalized) products, resulting in lower O/C of the aerosol.[34] It may also explain the increased abundance of organonitrate species, evident by higher N/C, in SOA that is the least oxidized (lowest O/C).

2.5 Conclusions

In the present work we highlight several important structural features of alkoxy radical structure that influence the SOA-forming potential of straight-chain and branched alkanes. The use of photolytically generated alkoxy radicals allows for the isolation of individual reaction pathways and oxidation generations, permitting the examination of the role of chemical structure in more detail than is typically possible in oxidant-initiated SOA studies. Measurements of SOA yields and composition broadly agree with previous work on the OH initiated oxidation of alkanes, indicating the relevance of this work to that important chemical system. However, both SOA yields and chemical composition are found to vary dramatically with alkoxy radical structure, even for those sharing the same carbon skeleton (e.g., the five unbranched isomers, decyl-1-oxy through decyl-5-oxy). Such differences can largely be explained in terms of (1) the complex branching between reaction pathways available to the alkoxy radical and (2) the role of

functional group position and carbon skeleton on the c* of the oxidation products. These SOA measurements also provide some insight into the role of structure on alkoxy radical reactivity; in particular, the very low SOA yields from the β-substituted alkoxy radicals suggests substantially more fragmentation than is predicted by commonly-used structure-activity relationships.[19,20]

More generally, the study of aerosol formation from single radical species enables the importance of individual reaction pathways and products in SOA formation to be examined in detail. For systems whose yields of condensable species are low (such as the first-generation oxidation of C_{10} hydrocarbons, studied here), products that are formed in small yields may still play a major role in SOA formation. For example, for the straight-chain structures studied, the primary radical (decyl-1-oxy) was found to form more SOA than any of the secondary ones. In the analogous OH + n-decane reaction, the formation of this radical (via abstraction at the terminal carbon) accounts for only ~4% of the total reaction[31]; however, the fractional contribution of this channel to the total SOA formed is likely to be substantially higher than this. Ultimately, the identification of these key channels and their products is necessary for relating the amounts and properties of SOA to the structure of a given precursor compound.

2.6 References

(1)   Kroll, J. H.; Seinfeld, J. H. Chemistry of Secondary Organic Aerosol: Formation and Evolution of Low-Volatility Organics in the Atmosphere. *Atmos. Environ.* **2008**, *42*, 3593–3624.

(2)   Hallquist, M.; Wenger, J. C.; Baltensperger, U.; Rudich, Y.; Simpson, D.; Claeys, M.; Dommen, J.; Donahue, N. M.; George, C.; Goldstein, A. H.; et al. The Formation, Properties and Impact of Secondary Organic Aerosol: Current and Emerging Issues. *Atmos. Chem. Phys.* **2009**, *9*, 5155–5236.

(3)   Kroll, J. H.; Donahue, N. M.; Jimenez, J. L.; Kessler, S. H.; Canagaratna, M. R.; Wilson, K. R.; Altieri, K. E.; Mazzoleni, L. R.; Wozniak, A. S.; Bluhm, H.; et al. Carbon

Oxidation State as a Metric for Describing the Chemistry of Atmospheric Organic Aerosol. *Nat. Chem.* **2011**, *3*, 133–139.

(4)   Goldstein, A. H.; Galbally, I. E. Known and Unexplored Organic Constituents in the Earth's Atmosphere. *Environ. Sci. Technol.* **2007**, *41*, 1514–1521.

(5)   Ziemann, P. J.; Atkinson, R. Kinetics, Products, and Mechanisms of Secondary Organic Aerosol Formation. *Chem. Soc. Rev.* **2012**, *41*, 6582–6605.

(6)   Kessler, S. H.; Nah, T.; Carrasquillo, A. J.; Jayne, J. T.; Worsnop, D. R.; Wilson, K. R.; Kroll, J. H. Formation of Secondary Organic Aerosol from the Direct Photolytic Generation of Organic Radicals. *J. Phys. Chem. Lett.* **2011**, *2*, 1295–1300.

(7)   Morabito, P.; Heicklen, J. Primary Photochemical Processes in the Photolysis of Alkyl Nitrites at 366nm and 23C in the Presence of 15NO. *Int. J. Chem. Kinet.* **1985**, *17*, 535–546.

(8)   Heicklen, J. The Decomposition of Alkyl Nitrites and the Reaction of Alkoxy Radicals. *Adv. Photochem.* **1988**, *14*, 177–272.

(9)   Orlando, J. J.; Tyndall, G. S.; Bilde, M.; Ferronato, C.; Wallington, T. J.; Vereecken, L.; Peeters, J. Laboratory and Theoretical Study of the Oxy Radicals in the OH- and Cl-Initiated Oxidation of Ethene. *J. Phys. Chem. A* **1998**, *102*, 8116–8123.

(10)   Lim, Y. B.; Ziemann, P. J. Effects of Molecular Structure on Aerosol Yields from OH Radical-Initiated Reactions of Linear, Branched, and Cyclic Alkanes in the Presence of NOx. *Environ. Sci. Technol.* **2009**, *43*, 2328–2334.

(11)   Lim, Y. Bin; Ziemann, P. J. Products and Mechanism of Secondary Organic Aerosol Formation from Reactions of N -Alkanes with OH Radicals in the Presence of NOx. *Environ. Sci. Technol.* **2005**, *39*, 9229–9236.

(12)   Noyes, W. A. Explanation of the Formation of Alkyl Nitrites in Dilute Solutions; Butyl and Amyl Nitrites. *J. Am. Chem. Soc.* **1933**, *55*, 3888–3889.

(13)   Cocker, D. R.; Mader, B. T.; Kalberer, M.; Flagan, R. C.; Seinfeld, J. H. The Effect of Water on Gas-Particle Partitioning of Secondary Organic Aerosol: II. M-Xylene and 1,3,5-Trimethylbenzene Photooxidation Systems. *Atmos. Environ.* **2001**, *35*, 6073–6085.

(14)   DeCarlo, P. F.; Kimmel, J. R.; Trimborn, A.; Northway, M. J.; Jayne, J. T.; Aiken, A. C.; Gonin, M.; Fuhrer, K.; Horvath, T.; Docherty, K. S.; et al. Field-Deployable, High-Resolution, Time-of-Flight Aerosol Mass Spectrometer. *Anal. Chem.* **2006**, *78*, 8281–8289.

(15) Aiken, A. C.; DeCarlo, P. F.; Jimenez, J. L. Elemental Analysis of Organic Species with Electron Ionization High-Resolution Mass Spectrometry. *Anal. Chem.* **2007**, *79*, 8350–8358.

(16) Aiken, A. C.; Decarlo, P. F.; Kroll, J. H.; Worsnop, D. R.; Huffman, J. A.; Docherty, K. S.; Ulbrich, I. M.; Mohr, C.; Kimmel, J. R.; Sueper, D.; et al. O/C and OM/OC Ratios of Primary, Secondary, and Ambient Organic Aerosols with High-Resolution Time-of-Flight Aerosol Mass Spectrometry. *Environ. Sci. Technol.* **2008**, *42*, 4478–4485.

(17) Hildebrandt, L.; Donahue, N. M.; Pandis, S. N. High Formation of Secondary Organic Aerosol from the Photo-Oxidation of Toluene. *Atmos. Chem. Phys.* **2009**, *9*, 2973–2986.

(18) Ziemann, P. J. Effects of Molecular Structure on the Chemistry of Aerosol Formation from the OH-Radical-Initiated Oxidation of Alkanes and Alkenes. *Int. Rev. Phys. Chem.* **2011**, *30*, 161–195.

(19) Atkinson, R. Rate Constants for the Atmospheric Reactions of Alkoxy Radicals: An Updated Estimation Method. *Atmos. Environ.* **2007**, *41*, 8468–8485.

(20) Peeters, J.; Fantechi, G.; Vereecken, L. A Generalized Structure-Activity Relationship for the Decomposition of (Substituted) Alkoxy Radicals. *J. Atmos. Chem.* **2004**, *48*, 59–80.

(21) Calvert, J. G.; Derwent, R. G.; Orlando, J. J.; Tyndall, G. S.; Wallington, T. J. *Mechanisms of the Atmospheric Oxidation of the Alkanes*; Oxford University Press, USA: New York, 2008; p. 992.

(22) Presto, A. A.; Miracolo, M. A.; Donahue, N. M.; Robinson, A. L. Secondary Organic Aerosol Formation from High-NO(x) Photo-Oxidation of Low Volatility Precursors: N-Alkanes. *Environ. Sci. Technol.* **2010**, *44*, 2029–2034.

(23) Lim, Y. Bin; Ziemann, P. J. Chemistry of Secondary Organic Aerosol Formation from OH Radical-Initiated Reactions of Linear, Branched, and Cyclic Alkanes in the Presence of NOx. *Aerosol Sci. Technol.* **2009**, *43*, 604–619.

(24) Lambe, A. T.; Onasch, T. B.; Croasdale, D. R.; Wright, J. P.; Martin, A. T.; Franklin, J. P.; Massoli, P.; Kroll, J. H.; Canagaratna, M. R.; Brune, W. H.; et al. Transitions from Functionalization to Fragmentation Reactions of Laboratory Secondary Organic Aerosol (SOA) Generated from the OH Oxidation of Alkane Precursors. *Environ. Sci. Technol.* **2012**, *46*, 5430–5437.

(25) Hunter, J. F.; Carrasquillo, A. J.; Daumit, K. E.; Kroll, J. H. Secondary Organic Aerosol Formation from Acyclic, Monocyclic, and Polycyclic Alkanes. *Submitt. to Environ. Sci. Technol.*

(26) Donahue, N. M.; Robinson, A. L.; Stanier, C. O.; Pandis, S. N. Coupled Partitioning, Dilution, and Chemical Aging of Semivolatile Organics. *Environ. Sci. Technol.* **2006**, *40*, 2635–2643.

(27) Farmer, D. K.; Matsunaga, A.; Docherty, K. S.; Surratt, J. D.; Seinfeld, J. H.; Ziemann, P. J.; Jimenez, J. L. Response of an Aerosol Mass Spectrometer to Organonitrates and Organosulfates and Implications for Atmospheric Chemistry. *Proc. Natl. Acad. Sci. U. S. A.* **2010**, *107*, 6670–6675.

(28) Atkinson, R. Rate Constants for the Atmospheric Reactions of Alkoxy Radicals: An Updated Estimation Method. *Atmos. Environ.* **2007**, *41*, 8468–8485.

(29) Lim, Y. Bin; Ziemann, P. J. Kinetics of the Heterogeneous Conversion of 1,4-Hydroxycarbonyls to Cyclic Hemiacetals and Dihydrofurans on Organic Aerosol Particles. *Phys. Chem. Chem. Phys.* **2009**, *11*, 8029–8039.

(30) Tkacik, D. S.; Presto, A. A.; Donahue, N. M.; Robinson, A. L. Secondary Organic Aerosol Formation from Intermediate-Volatility Organic Compounds: Cyclic, Linear, and Branched Alkanes. *Environ. Sci. Technol.* **2012**, *46*, 8773–8781.

(31) Atkinson, R. A Structure-Activity Relationship for the Estimation of Rate Constants for the Gas-Phase Reactions of OH Radicals with Organic Compounds. *Int. J. Chem. Kinet.* **1987**, *19*, 799–828.

(32) Verevkin, S. P.; Schick, C. Vapour Pressures and Heat Capacity Measurements on the C7–C9 Secondary Aliphatic Alcohols. *J. Chem. Thermodyn.* **2007**, *39*, 758–766.

(33) Jang, M.; Czoschke, N. M.; Lee, S.; Kamens, R. M. Heterogeneous Atmospheric Aerosol Production by Acid-Catalyzed Particle-Phase Reactions. *Science* **2002**, *298*, 814–817.

(34) Shilling, J. E.; Chen, Q.; King, S. M.; Rosenoern, T.; Kroll, J. H.; Worsnop, D. R.; DeCarlo, P. F.; Aiken, A. C.; Sueper, D.; Jimenez, J. L.; et al. Loading-Dependent Elemental Composition of A-Pinene SOA Particles. *Atmos. Chem. Phys.* **2009**, *9*, 771–782.

Chapter 3

Alkoxy radical reactivity in the condensed phase: Probing the relative roles of intermolecular and intramolecular reactions

3.1 Introduction. In Chapter 2 we considered the major reaction pathways for alkoxy radicals in the gas-phase using the photolysis of alkyl nitrites. Here we extend this work to examine the reactivity of alkoxy radicals in the condensed-phase. Condensed-phase organic radicals are ubiquitous in both natural and engineered chemical systems, and play central roles in key processes such as the degradation of pollutants,[1] weathering of materials,[2] combustion reactions,[3] and the oxidative evolution of atmospheric organic aerosol particles.[4] Such organic radicals, which include alkyl (R), alkoxy (RO) and alkylperoxy (RO_2) species, are highly reactive and often have many reactive pathways possible. Most mechanistic studies of radical reactions have focused on the gas phase, which (under most conditions) limits the available reactions to unimolecular processes, or bimolecular reactions with major inorganic species (O_2, NO_x, etc.).[5–7] However, the condensed phase represents a more complex molecular environment since the high concentrations may facilitate bimolecular reactions with other organic species (molecules or radicals).[8–13] Furthermore, solvent or cage effects may modify the reactivity and dynamics of individual radical species. Condensed-phase radicals can therefore exhibit fundamentally different reactivity than gas-phase radicals; however in general these have received far less study, particularly within the context of atmospheric condensed phase (reactions in aerosol and cloud droplets).

55

Here, we use a new technique (nebulization followed by aerosol mass spectrometry) to examine the reactions of organic radicals in the condensed phase. Our specific focus is the chemistry of alkoxy radicals (RO), key intermediates in combustion processes and the atmospheric oxidation of organic compounds in both the gas and condensed phases.[14–17] RO radicals can form within the condensed phase (e.g., fuel mixtures or in atmospheric particles or droplets by several channels): self- and cross-reactions of peroxy radicals, the reaction of RO_2 with NO, and the direct photolysis of hydroperoxide (ROOH) species. In the gas phase, RO radicals react via one of three channels (Scheme 1): (r_1) isomerization, a 1,5-intramolecular H-atom abstraction reaction that increases the degree of functionalization; (r_2) reaction with O_2 to form a carbonyl and HO_2; or (r_3) C-C bond scission (fragmentation) to form two smaller species (a carbonyl and an alkyl radical).[18] In the condensed organic phase, an additional channel (r_4) is available, the intermolecular (bimolecular) abstraction of H atoms from other organic species (RO + RH), forming an alcohol and an alkyl radical. Recently, such chemistry has been invoked to explain observations of alcohol formation in heterogeneous oxidation experiments of organic aerosol particles.[9–11,19–21] However, the relative importance of unimolecular and bimolecular reactions of RO radicals is not well-constrained, and to our knowledge has not been investigated directly.
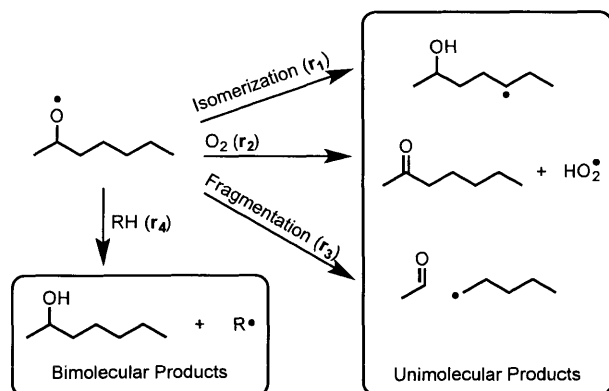
Scheme 1. Possible reactions of condensed-phase alkoxy radicals.

56

In our previous work, we examined the gas-phase unimolecular chemistry of alkoxy radicals, specifically the branching between isomerization (r_1) and fragmentation (r_3), using the photolysis of a series of gas-phase C_{10} alkyl nitrites (RONO) to generate RO radicals.[22] Here we extend this technique to study the chemistry of RO radicals in the condensed phase. A large alkyl nitrite (octyl-2-dodecyl-1-nitrite, $C_{20}H_{41}ONO$) was photolyzed in hexanes to generate condensed-phase RO radicals (octyl-2-dodecyl-1-oxy, $C_{20}H_{41}O$) and the reactivity of this this species was monitored via nebulization and aerosol mass spectrometry (AMS).[23] The reactions of alkoxy radicals generated from other large alkyl nitrites (eicosanyl-1-nitrite, $C_{20}H_{41}ONO$, hexacosanyl-2-nitrite, $C_{26}H_{53}ONO$, and octacosanyl-10-nitrite, $C_{28}H_{57}ONO$) was also studied; these were found to be similar to that of octyl-2-dodecyl-1-oxy and so are not discussed here.

3.2 Experimental. RONO species were synthesized in the laboratory by O-nitrosation of the corresponding alcohol (octyl-2-dodecanol, Sigma Aldrich, 98% purity). The alcohol and sodium nitrite (Sigma Aldrich, > 99.99% trace) were combined in a 1.1:1.0 molar ratio and stirred with a magnetic stirrer at 25 °C while 2.5 M sulfuric acid (Sigma Aldrich, 99%) was added drop-wise until a 0.5:1.0 acid:alcohol molar ratio was obtained. For solid alcohols (1-octacosanol, Sigma Aldrich, > 99%;10-hexacosanol, ChemSampco), this synthesis was modified by dissolving the precursor alcohol in hexanes prior to the addition of sodium nitrite and sulfuric acid. Finally, additional (excess) sodium nitrite was added to neutralize any remaining acid in solution. The resulting clear yellow liquid (or hexane + RONO solution for the solid nitrites) was dried over sodium sulfate (Sigma Aldrich, 99%), dissolved in hexanes, and analyzed by UV-VIS absorption spectroscopy to confirm the presence of the nitrite group, by comparison with previously published spectra of smaller RONO.[24]

RONO photolysis experiments were conducted by adding 0.01 – 0.1% (v/v) $C_{20}H_{41}ONO$ in hexanes (Sigma Aldrich, 99% anhydrous) or CCl_4 (Sigma Aldrich, 99%) to a borosilicate bottle attached to a constant output atomizer (TSI, Inc.). To attain particle volumes centered around 250 nm, the atomizer was connected to clean, dry air (Aadco clean air generator) at 10 psi. The output from the atomizer was passed through a charcoal denuder to remove hexane solvent, and the flow was split to a scanning mobility particle sizer (TSI, Inc.) to measure particle size and an Aerodyne High-Resolution Aerosol Mass Spectrometer (AMS) to measure particle composition. The AMS was run in high-resolution "W-mode" for exact mass confirmation, and time series for individual ions were constructed using the lower-resolution "V-mode" which affords a greater sensitivity to these high molecular weight ions. After ~10 minutes of atomization of the unreacted mixture in the dark, a single blacklight (40 W, centered at 350 nm) positioned 2-3 cm adjacent to the reactor was illuminated. The reaction was run until the major high molecular weight signals stopped changing (typically within one hour). For several experiments, perfluoroheptacosane (PFH, $C_{27}F_{56}$) was used as an internal standard for accurate mass calibration at $m/z > 250$, enabling high-resolution analysis at those high masses. In order to add PFH (which is insoluble in hexane), air was passed over a heated (~80 °C) PFH reservoir, and then into a cooling area, allowing for the formation of pure PFH particles), before being added to the atomizer aerosol stream and sent into the AMS.

For offline GC analysis, the reaction mixture (10 μL) was injected into an Agilent 9575C GC-MS inlet (280 °C) and loaded onto a column (50 m, 0.25 mm i.d. DB-5MS) held at 50°C for two minutes and ramped to 220°C at 35°C/minute. Substantial decomposition of the precursor RONO was observed due to the elevated GC temperatures, the products of which co-eluted with the alcohol. Prior to analysis, the aliquots were derivatized with BSTFA with 1% TCMS (in

10:1 molar excess of the ROH initially added) which provided adequate separation of the alcohol. The abundance of the derivatized alcohol (RO + Si(CH$_3$)$_3$), m/z 355) was monitored for all samples.

3.3 Results and Discussion. No aerosol growth was observed from the irradiation of hexanes or the C$_{20}$ alcohol (the precursor used to synthesize the nitrite, as discussed in the Experimental section) in a solution of hexanes (0.1 - 0.01%). Upon UV irradiation of the RONO mixture, there is a dramatic change in the chemical composition of the solution mixture as measured by the AMS, as discussed below. The output of the atomizer, measured as the aerosol loading by the AMS, immediately began to increase by as much as a factor of 10 over the course of an hour. While the exact reason for this remains unclear, this growth likely reflects changes in the behavior of the atomizer as a result of the changing chemical composition of the mixture.

Figure 1 shows the aerosol mass spectra (m/z 260 – 320) of the C$_{20}$-ONO/hexane mixture before and after irradiation. The major ion associated with the precursor RONO molecule (C$_{20}$H$_{41}$ONO) is C$_{19}$H$_{39}$$^+$ [M – CH$_2$ONO]$^+$ at m/z 267.305. A second tracer ion for RONO may be C$_{20}$H$_{40}$$^+$ [M – HONO]$^+$ at m/z 280.313. However as shown in Figure 3, this is also a major ion ([M – H$_2$O]$^+$) in the mass spectrum of the corresponding alcohol, ROH (C$_{20}$H$_{41}$OH). ROH which may be formed photochemically (r$_4$, Scheme 1) though it may instead simply be unreacted precursor from RONO synthesis. The major high-MW ions that appeared during photolysis are m/z 294.292 (C$_{20}$H$_{38}$O$^+$), 295.300 (C$_{20}$H$_{39}$O$^+$), 311.295 (C$_{20}$H$_{39}$O$_2$$^+$), and a C$_{19}$ N-containing fragment at m/z 277.276 (C$_{19}$H$_{35}$N).

Typical time series of the C$_{20}$ ions, normalized to the total organic signal (to account for changes in atomizer output), are shown in Figure 3. Repeat experiments gave very similar results,

though with small variations (0 – 50%) in the relative abundances of the large oxygen-containing ions ($C_{20}H_{38}O^+$ and $C_{20}H_{39}O^+$); this is potentially due to small differences in the AMS response for high-MW ions arising from variations in the vaporizer temperature. Also reported are the traces for NO^+ and NO_2^+, fragments of the RONO reactant as well as organic nitrate ($RONO_2$) products. Upon initiation of photolysis the abundance of $C_{19}H_{39}^+$ decays exponentially (k_{photo} = 3.6 x 10^{-4} s^{-1}), as expected for the nitrite reactant. By contrast, $C_{20}H_{40}^+$ drops slightly and then remains fairly constant; the difference between these two traces suggests contributions by the ROH, which is discussed in detail below. The NO^+ ion (a minor fragment in the RONO spectrum) also decreases, though not as rapidly as the RONO marker peak ($C_{19}H_{39}^+$), whereas the NO_2^+ ion rapidly increases. After 60 minutes the NO^+/NO_2^+ ratio levels off at ~15, strongly suggesting the formation of organic nitrates.[25–27]
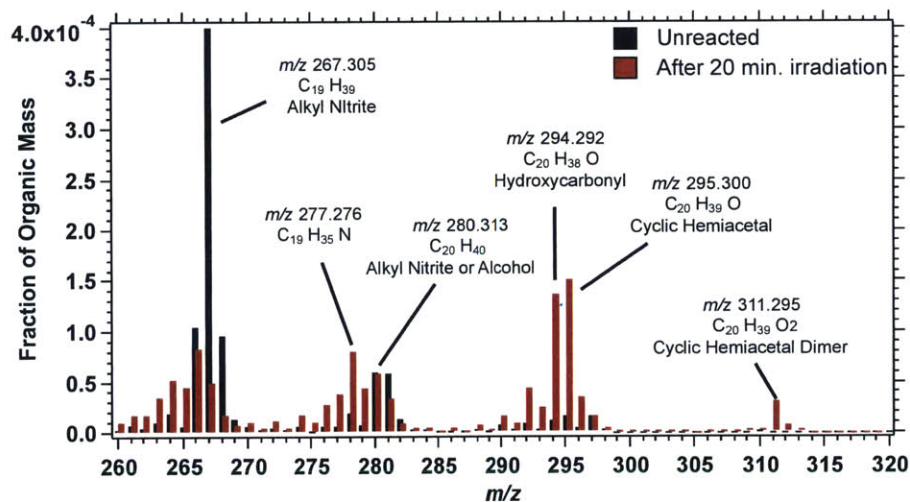

Figure 1. Unit mass resolution AMS spectrum (*m/z* 260 – 320) of $C_{20}H_{41}ONO$ in hexanes in the dark (black) and after 20 min irradiation (red, positive x-axis offset). Exact masses were identified by high-resolution analysis, and molecular assignments are based on Lim and Ziemann.[16]

60

In addition, several large oxygen-containing ions ($C_{20}H_{38}O^+$, $C_{20}H_{39}O^+$, and $C_{20}H_{39}O_2^+$) increase upon UV exposure, indicating they are reaction products. Similar product ions have been previously observed in studies of alkane oxidation by Lim and Ziemann[16] and in our earlier work on SOA from gas-phase RONO photolysis.[22]; based on that work, the $C_{20}H_{38}O^+$, $C_{20}H_{39}O^+$, and $C_{20}H_{39}O_2^+$ ions likely correspond to the hydroxycarbonyl, cyclic hemiacetal, and the acetal or cyclic hemiacetal dimer, all first-generation products of alkane oxidation. The identity of the single N-containing fragment at m/z 277.276 ($C_{19}H_{35}N^+$) is unknown, and may result from fragmentation of a nitrate species on the heater or during ionization; thus further study with a softer ionization technique is needed.
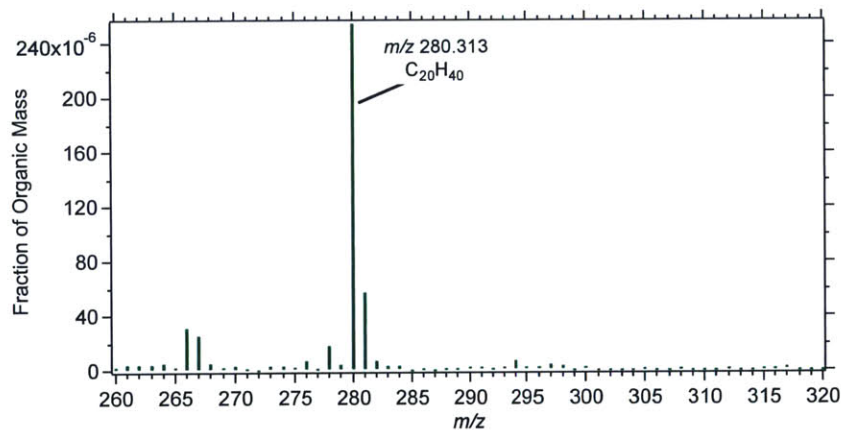

Figure 2. High mass ions (m/z 260 – 320) in the AMS mass spectrum of $C_{20}H_{41}OH$ in hexanes. The major ion in the spectrum at m/z 280.303 corresponds to the dehydrated product $[M - H_2O]^+$.
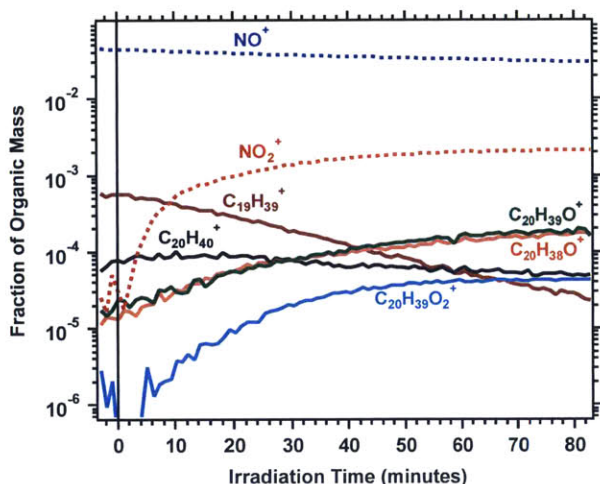
Figure 3. Ion time series for a typical $C_{20}H_{41}ONO$ photolysis experiment in hexanes. All ions are normalized to total organic loading to account for changes in the atomizer output. UV lights were turned on at t=0 (vertical black line), after which point there is a decrease in the abundance of NO^+ and the major RONO ion ($C_{19}H_{39}^+$), and an increase in NO_2^+ and oxygenated ions ($C_{20}H_{38}O^+$, $C_{20}H_{39}O^+$, and $C_{20}H_{39}O_2^+$). There is a slight decrease in $C_{20}H_{40}^+$ which may be due to the normalization approach taken or by the formation of dimers with hydroxycarbonyl or cyclic hemiacetal species.

The observed ions and time traces (Figures 1 and 3) are broadly consistent with known features of alkoxy radical reactivity, shown in detail in Scheme 2. Following its formation, the RO radical will either fragment (r_3) to two smaller molecules or isomerize (r_1) and react with O_2 to form a hydroxylated RO_2 radical (Reaction r_2, reaction with O_2, is expected to be negligible).[18] Products from fragmentation reactions will include a number of species with 19 or fewer carbon atoms; these may be too volatile to be measured with the current setup or difficult to distinguish from the decomposition of C_{20} products on the heater or during EI ionization. RO_2 can react with either NO or another RO_2 to form an additional RO radical. The newly formed RO radical will "back-isomerize" and form the hydroxycarbonyl (*m/z* 294.292, $[M - H_2O]^+$), its cyclization product the cyclic hemiacetal (*m/z* 295.300, $[M - OH]^+$), and acetal or hemiacetal dimers ($[M - C_{20}H_{41}O_2]^+$).[28] Products from multiple "forward isomerization" reactions (i.e. dihydroxycarbonyl and hydroxyl cyclic hemiacetal) were not observed, which s consistent with
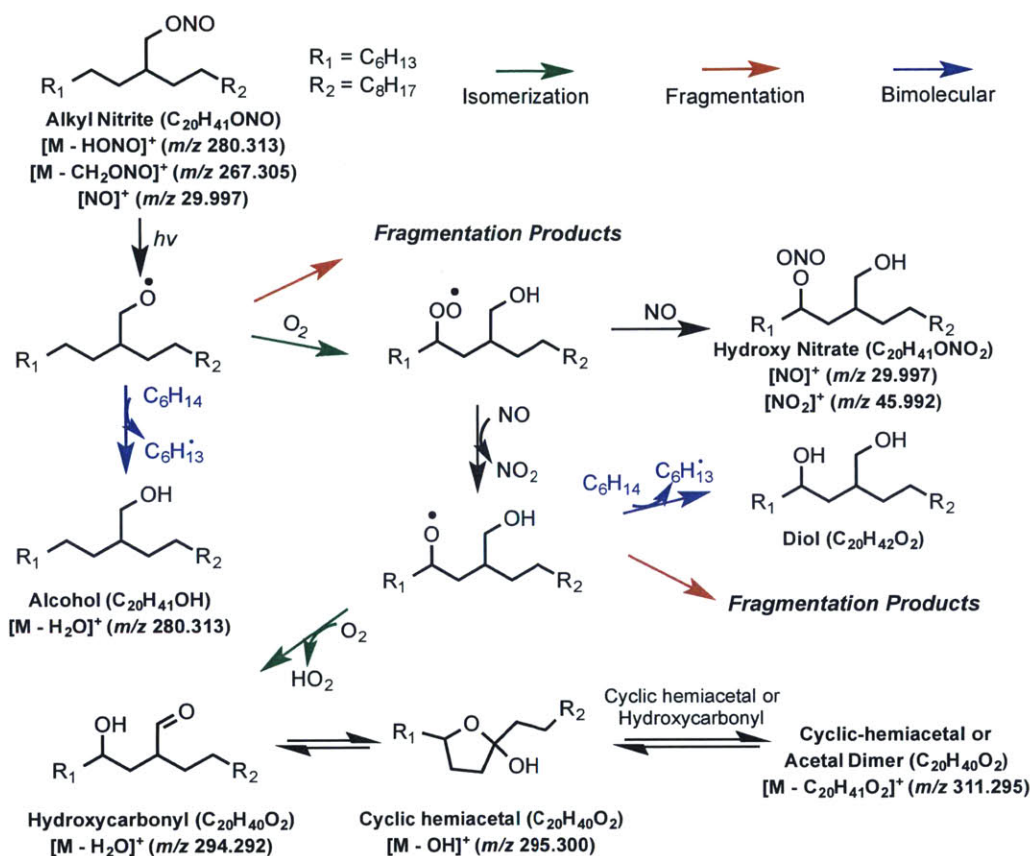
Scheme 2. Mechanism and reaction products for a single C_{20} alkoxy radical in the condensed phase.

our previous results of β-substituted RO radicals.[22] The observation of ions corresponding to the expected products of RO isomerization (nitrates, hydroxycarbonyls, and (cyclic) hemiacetals) provides strong evidence that unimolecular (intramolecular H-atom abstraction) reactions are an important reaction pathway for condensed-phase $C_{20}H_{41}O$ radicals.

The evidence for bimolecular reactions (intermolecular H-atom abstraction reactions) with hexane solvent molecules (r_4) is less clear. This reaction yields ROH and a hexyl radical (C_6H_{13}); however, only ROH is likely to be of low enough volatility to be measured by the AMS. AMS measurements of a pure ROH standard confirm that the dominant high molecular weight ion is $C_{20}H_{40}^+$ ([M − H_2O]$^+$), formed from dehydration (on the vaporizer or within the ionizer)

63

(Figure 3). As shown in Figures 1 and 3, this ion is also present prior to photolysis, suggesting that it is either a tracer ion for the RONO, and/or that some residual ROH from the RONO synthesis was present in the reaction mixture. The fact that the $C_{20}H_{40}^+$ ion abundance decreases more slowly than that of $C_{19}H_{37}^+$ (the other RONO tracer ion) indicates that some ROH is present in the product mixture as well. However, from this time dependence it is unclear whether this is a result of ROH formation from $\mathbf{r_4}$ (which counterbalances the drop in $C_{19}H_{37}^+$ from loss of RONO) or whether it arises from residual, relatively unreactive ROH in the mixture. In order to distinguish these two cases, the experiment was repeated using CCl_4 as a solvent instead of hexanes, in order to prevent any possible bimolecular RO + RH reactions. Results were similar to those in hexanes (Figure 4), with only a slight drop in $C_{20}H_{40}^+$ ion signal upon photolysis, implying that the precursor RONO contributes to this signal. Furthermore, these results are consistent with preliminary GC-MS analysis of aliquots of the reaction mixture taken throughout the course of thee experiments. No significant increase in the total abundance of the derivatized ROH was observed (Figure 5). Both results strongly suggest that any ROH present in the reaction mixture was an artifact from RONO synthesis rather than a product of the bimolecular reactions ($\mathbf{r_4}$). The lack of formation of the ROH in these experiments indicates that bimolecular H-atom abstraction reactions, RO + RH, are not competitive with the available unimolecular (isomerization) pathways.
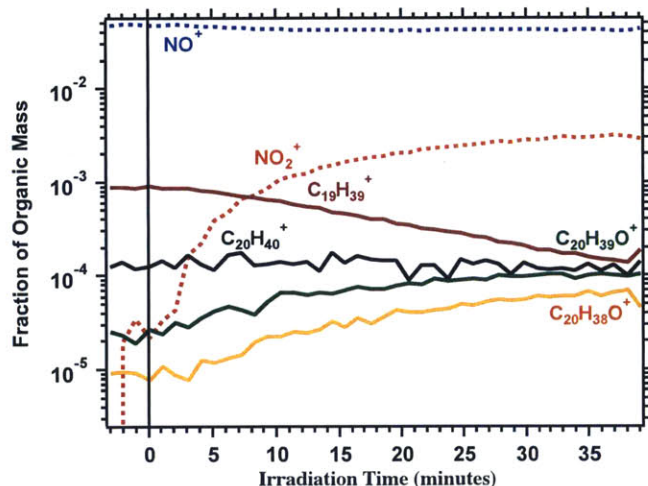
Figure 4. Ion time series for a typical C_{20}-ONO photolysis in CCl_4 normalized to total organic loading for the major high molecular weight (> m/z 250) organic ions in addition to NO^+ and NO_2^+ ions. The vertical black line indicates when the lights were turned on.
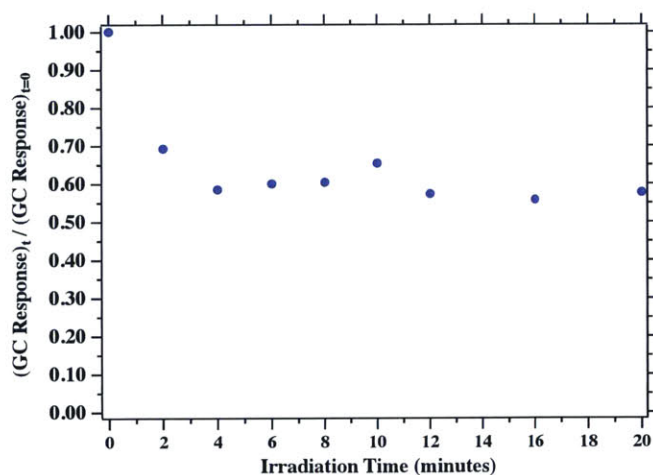
Figure 5. GC-MS response to derivatized reaction mixtures taken at two-minute intervals, normalized to the initial response at t=0. There is an initial drop in the amount of derivatized ROH once the lights are turned on. This may be due to the formation of hemiacetal/acetal species with newly produced hydroxycarbonyl/cyclic hemiacetals. Responses are raw integrated counts from extracted ion chromatograms of m/z 355 ($C_{20}H_{40}O$ + $Si(CH_3)_2$).

The absence of observed intermolecular abstraction reactions is consistent with the fact that bimolecular reactions involve higher entropic penalties than the corresponding unimolecular ones, since they involve the loss of translational rather than vibrational degrees of freedom.[29] The present results are also consistent with previous studies of chemistry of large alkoxy radicals in

the condensed phase.[30,31] While many earlier studies showed that ROH could be formed from condensed-phase RO radicals, most of these focused on small radicals ($C_1 - C_4$), for which the 1,5-isomerization cannot occur, and for which fragmentation is known to be slow.[32] In addition, most previous studies were conducted under high concentrations (1 – 10%) of radical precursors, which may promote alkoxy disproportionation (RO + RO) reactions that form ROH and carbonyl species. Indeed, such reactions likely explain the roughly equal observed yields of carbonyls and ketones,[30] which would not be expected from the RO + RH reaction. In one of the few studies examining the room-temperature chemistry of larger alkoxy radicals, Kabasakalian and co-workers found that once alkoxy radicals reach the size at which unimolecular isomerization is facile (i.e., in which a 1,5 H-atom shift from a secondary or tertiary carbon can occur), the yields of the ROH (and carbonyl) drop dramatically and the yields of isomerization products greatly increase, indicating the dominance of intramolecular abstraction reactions.[30,31] While some minor reaction products from H-atom abstraction from solvent molecules were also reported,[31] their formation may have been influenced by the oxygen-free conditions of that study, which may have impacted the lifetime of RO radicals. Thus the results of the present study are consistent with previous work on long-chain RO radicals, and indicate that in the liquid phase, unimolecular 1,5-H-abstraction reactions are generally more favorable than the corresponding bimolecular RO + RH reactions. Furthermore, estimates of bimolecular H-abstraction rates by structure-activity relationships developed with small RO radicals suggest that reaction with hydrocarbons are not competitive with unimolecular isomerization.[33] Even for the most readily abstractable H-atoms on aromatic (i.e. benzene or toluene) or branched (i.e. squalane), the rates are estimated to be less than 50 s^{-1} which are on the order of 10^4 slower than the corresponding unimolecular reactions. This dominance of unimolecular reactions over bimolecular ones likely

also holds for autoxidation chemistry associated with RO_2 radicals, which was recently suggested as a potentially important oxidation channel within organic aerosol.[34]

3.4 Summary and Implications. The reactions of condensed phase alkoxy radicals were probed by photolyzing and nebulizing large $C_{20}H_{41}ONO$ species into an aerosol mass spectrometer for analysis. Products from intramolecular isomerization and bimolecular reactions with inorganic species were observed, however, the major product, an alcohol, formed from a bimolecular H-abstraction with the surrounding organic matrix was not observed. We note that this work focuses on one specific chemical system, the reactions of unfunctionalized RO radicals within a simple liquid alkane solvent, and our results do not necessarily imply that bimolecular reactions never happen in ambient atmospheric aerosol. In particular, when diffusion is slow (e.g., solid matrices or "glassy" organic aerosol)[10], or in which the surrounding molecules have readily abstractable hydrogen atoms (e.g., oxygenates), bimolecular H-atom abstractions may be of increased importance. This is an important area of future research, and may help explain why recent laboratory studies have observed alcohols that were attributed to bimolecular reactions,[9–11,19–21] in contrast to the present results. However, alcohol species can also be formed by reactions other than RO + RH, such as RO_2 + RO_2 and RO + RO disproportionation reactions. Moreover, in many cases (such as in most atmospheric organic aerosol) a given condensed-phase radical will likely be chemically similar to its surrounding molecules. There, any enhancement in bimolecular rates (for example from more readily abstractable H atoms) will also involve a coincident enhancement in unimolecular rates. In such systems, the reactivity of alkoxy radicals in the condensed (liquid) phase is likely to be dominated by unimolecular chemistry, similar to alkoxy radical reactivity in the gas phase.

3.5 References

(1)   Schwarzenbach, R.; Gschwend, P.; Imboden, D. *Environmental Organic Chemistry*; 2nd ed.; John Wiley & Sons, Inc.: Hoboken, NJ, USA, 2003.

(2)   Kutz, M. *Handbook of Environmental Degradation of Materials, 2nd Edition | Myer Kutz | ISBN 9781437734553*; 2nd ed.; Elsevier Inc.: Waltham, Massachusetts, 2012; p. 936.

(3)   Curran, H. J.; Gaffuri, P.; Pitz, W. J.; Westbrook, C. K. A Comprehensive Modeling Study of N-Heptane Oxidation. *Combust. Flame* **1998**, *114*, 149–177.

(4)   Kroll, J. H.; Seinfeld, J. H. Chemistry of Secondary Organic Aerosol: Formation and Evolution of Low-Volatility Organics in the Atmosphere. *Atmos. Environ.* **2008**, *42*, 3593–3624.

(5)   Atkinson, R. Atmospheric Chemistry of VOCs and NOx. *Atmos. Environ.* **2000**, *34*, 2063–2101.

(6)   Ziemann, P. J.; Atkinson, R. Kinetics, Products, and Mechanisms of Secondary Organic Aerosol Formation. *Chem. Soc. Rev.* **2012**, *41*, 6582–6605.

(7)   Calvert, J. G.; Derwent, R. G.; Orlando, J. J.; Tyndall, G. S.; Wallington, T. J. *Mechanisms of the Atmospheric Oxidation of the Alkanes*; Oxford University Press, USA: New York, 2008; p. 992.

(8)   Smith, J. D.; Kroll, J. H.; Cappa, C. D.; Che, D. L.; Liu, C. L.; Ahmed, M.; Leone, S. R.; Worsnop, D. R.; Wilson, K. R. The Heterogeneous Reaction of Hydroxyl Radicals with Sub-Micron Squalane Particles: A Model System for Understanding the Oxidative Aging of Ambient Aerosols. *Atmos. Chem. Phys.* **2009**, *9*, 3209–3222.

(9)   Liu, C.-L.; Smith, J. D.; Che, D. L.; Ahmed, M.; Leone, S. R.; Wilson, K. R. The Direct Observation of Secondary Radical Chain Chemistry in the Heterogeneous Reaction of Chlorine Atoms with Submicron Squalane Droplets. *Phys. Chem. Chem. Phys.* **2011**, *13*, 8993–9007.

(10)   Ruehl, C. R.; Nah, T.; Isaacman, G.; Worton, D. R.; Chan, A. W. H.; Kolesar, K. R.; Cappa, C. D.; Goldstein, A. H.; Wilson, K. R. The Influence of Molecular Structure and Aerosol Phase on the Heterogeneous Oxidation of Normal and Branched Alkanes by OH. *J. Phys. Chem. A* **2013**, *117*, 3990–4000.

(11)   Nah, T.; Zhang, H.; Worton, D. R.; Ruehl, C. R.; Kirk, B. B.; Goldstein, A. H.; Leone, S. R.; Wilson, K. R. Isomeric Product Detection in the Heterogeneous Reaction of Hydroxyl Radicals with Aerosol Composed of Branched and Linear Unsaturated Organic Molecules. *J. Phys. Chem. A* **2014**, *118*, 11555–11571.

(12)   George, I. J.; Vlasenko, A.; Slowik, J. G.; Broekhuizen, K.; Abbatt, J. P. D. Heterogeneous Oxidation of Saturated Organic Aerosols by Hydroxyl Radicals: Uptake Kinetics, Condensed-Phase Products, and Particle Size Change. *Atmos. Chem. Phys.* **2007**, *7*, 4187–4201.

(13)   George, I. J.; Abbatt, J. P. D. Heterogeneous Oxidation of Atmospheric Aerosol Particles by Gas-Phase Radicals. *Nat. Chem.* **2010**, *2*, 713–722.

(14)   Atkinson, R. Rate Constants for the Atmospheric Reactions of Alkoxy Radicals: An Updated Estimation Method. *Atmos. Environ.* **2007**, *41*, 8468–8485.

(15)   Lim, Y. Bin; Ziemann, P. J. Products and Mechanism of Secondary Organic Aerosol Formation from Reactions of N -Alkanes with OH Radicals in the Presence of NOx. *Environ. Sci. Technol.* **2005**, *39*, 9229–9236.

(16)   Lim, Y. Bin; Ziemann, P. J. Chemistry of Secondary Organic Aerosol Formation from OH Radical-Initiated Reactions of Linear, Branched, and Cyclic Alkanes in the Presence of NOx. *Aerosol Sci. Technol.* **2009**, *43*, 604–619.

(17)   Lim, Y. B.; Ziemann, P. J. Effects of Molecular Structure on Aerosol Yields from OH Radical-Initiated Reactions of Linear, Branched, and Cyclic Alkanes in the Presence of NOx. *Environ. Sci. Technol.* **2009**, *43*, 2328–2334.

(18)   Atkinson, R. Rate Constants for the Atmospheric Reactions of Alkoxy Radicals: An Updated Estimation Method. *Atmos. Environ.* **2007**, *41*, 8468–8485.

(19)   Kolesar, K. R.; Buffaloe, G.; Wilson, K. R.; Cappa, C. D. OH-Initiated Heterogeneous Oxidation of Internally-Mixed Squalane and Secondary Organic Aerosol. *Environ. Sci. Technol.* **2014**, *48*, 3196–3202.

(20)   Zhang, H.; Ruehl, C. R.; Chan, A. W. H.; Nah, T.; Worton, D. R.; Isaacman, G.; Goldstein, A. H.; Wilson, K. R. OH-Initiated Heterogeneous Oxidation of Cholestane: A Model System for Understanding the Photochemical Aging of Cyclic Alkane Aerosols. *J. Phys. Chem. A* **2013**, *117*, 12449–12458.

(21)   Chan, M. N.; Zhang, H.; Goldstein, A. H.; Wilson, K. R. Role of Water and Phase in the Heterogeneous Oxidation of Solid and Aqueous Succinic Acid Aerosol by Hydroxyl Radicals. *J. Phys. Chem. C* **2014**, 140314152232002.

(22)   Carrasquillo, A. J.; Hunter, J. F.; Daumit, K. E.; Kroll, J. H. Secondary Organic Aerosol Formation via the Isolation of Individual Reactive Intermediates: Role of Alkoxy Radical Structure. *J. Phys. Chem. A* **2014**, *118*, 8807–8816.

(23)   DeCarlo, P. F.; Kimmel, J. R.; Trimborn, A.; Northway, M. J.; Jayne, J. T.; Aiken, A. C.; Gonin, M.; Fuhrer, K.; Horvath, T.; Docherty, K. S.; et al. Field-Deployable, High-

Resolution, Time-of-Flight Aerosol Mass Spectrometer. *Anal. Chem.* **2006**, *78*, 8281–8289.

(24) Heicklen, J. The Decomposition of Alkyl Nitrites and the Reaction of Alkoxy Radicals. *Adv. Photochem.* **1988**, *14*, 177–272.

(25) Bruns, E. A.; Perraud, V.; Zelenyuk, A.; Ezell, M. J.; Johnson, S. N.; Yu, Y.; Imre, D.; Finlayson-Pitts, B. J.; Alexander, M. L. Comparison of FTIR and Particle Mass Spectrometry for the Measurement of Particulate Organic Nitrates. *Environ. Sci. Technol.* **2010**, *44*, 1056–1061.

(26) Fry, J. L.; Kiendler-Scharr, A.; Rollins, A. W.; Wooldridge, P. J.; Brown, S. S.; Fuchs, H.; Dubé, W.; Mensah, A.; dal Maso, M.; Tillmann, R.; et al. Organic Nitrate and Secondary Organic Aerosol Yield from NO_3 Oxidation of B-Pinene Evaluated Using a Gas-Phase Kinetics/aerosol Partitioning Model. *Atmos. Chem. Phys.* **2009**, *9*, 1431–1449.

(27) Rollins, A. W.; Kiendler-Scharr, A.; Fry, J. L.; Brauers, T.; Brown, S. S.; Dorn, H.-P.; Dubé, W. P.; Fuchs, H.; Mensah, A.; Mentel, T. F.; et al. Isoprene Oxidation by Nitrate Radical: Alkyl Nitrate and Secondary Organic Aerosol Yields. *Atmos. Chem. Phys.* **2009**, *9*, 6685–6703.

(28) Aimanant, S.; Ziemann, P. J. Chemical Mechanisms of Aging of Aerosol Formed from the Reaction of N -Pentadecane with OH Radicals in the Presence of NO X. *Aerosol Sci. Technol.* **2013**, *47*, 979–990.

(29) Page, M. I. The Energetics of Neighbouring Group Participation. *Chem. Soc. Rev.* **1973**, *2*, 295.

(30) Kabasakalian, P.; Townley, E. R.; Yudis, M. D. Photolysis of Nitrite Esters in Solution. III. Photochemistry of Primary, Secondary and Tertiary Alkyl Nitrites. *J. Am. Chem. Soc.* **1962**, *84*, 2718–2722.

(31) Kabasakalian, P.; Townley, E. R. Photolysis of Nitrite Esters in Solution. I. Photochemistry of N -Octyl Nitrite. *J. Am. Chem. Soc.* **1962**, *84*, 2711–2716.

(32) Gray, P.; Williams, A. The Thermochemistry And Reactivity Of Alkoxyl Radicals. *Chem. Rev.* **1959**, *59*, 239–328.

(33) Hendry, D. G.; Mill, T.; Piszkiewicz, L.; Howard, J. A.; Eigenmann, H. K. A Critical Review of H-Atom Transfer in the Liquid Phase: Chlorine Atom, Alkyl, Trichloromethyl, Alkoxy, and Alkylperoxy Radicals. *J. Phys. Chem. Ref. Data* **1974**, *3*, 937.

(34) Crounse, J. D.; Nielsen, L. B.; Jørgensen, S.; Kjaergaard, H. G.; Wennberg, P. O. Autoxidation of Organic Compounds in the Atmosphere. *J. Phys. Chem. Lett.* **2013**, *4*, 3513–3520.

Chapter 4

Reactivity of condensed-phase radicals: A molecular-level study of RO and RO_2 products and pathways

4.1. Introduction. Chapter 2 highlighted how alkoxy (RO) radical structure can influence its reactivity in the gas-phase and in Chapter 3, a new method to monitor its reactions in the organic condensed phase was described. There, bimolecular RO reaction with surrounding aerosol, a pathway previously hypothesized to occur in the condensed phase, was found to be slow at best, relative to unimolecular isomerization reactions. The Aerosol Mass Spectrometer (AMS), used in these experiments, provided a measurement of bulk properties (O/C, H/C, and N/C), and to some extent molecular information from high molecular weight ions. A major drawback to this approach is that assignments were only tentative due of the hard ionization scheme used in the AMS. In this chapter, data taken with a different ionization technique, Direct Analysis in Real Time (DART), which is well-suited for measuring the molecular ions of large organic species with little to no fragmentation, will be applied to the study of the same condensed phase system measured in Chapter 3 (C_{20} nitrites).

An assessment of the impacts of organic aerosol (OA) on climate change, human health, and air quality, must include estimates of its atmospheric lifetime, which in turn requires an explicit description of how it evolves chemically (e.g. with exposure to gas-phase oxidants). This requires knowledge of the important reactions and corresponding products formed within the particle, however, much less is known about these processes relative to analogous gas-phase. As

discussed in Chapter 3, much of what we know about condensed-phase chemistry is derived from analogous gas-phase reactions; however, aerosol particles represent fundamentally different molecular environments due to the higher concentrations of molecules. Observations from Chapter 3, for example, suggest that the pathways for alkoxy radical reactions in the condensed phase are similar to those in the gas phase, in stark contrast to previous heterogeneous oxidation studies.[1-6]

The mechanism leading to the formation of first-generation oxidation products for a simple alkane is given in Figure 1. The heterogeneous reaction of gas-phase OH with an aerosol phase organic compound will yield the corresponding alkyl radical. Addition of O_2 produces an alkylperoxy (RO_2) radical, which in the gas-phase under high-NO_x conditions will form an RO radical or an alkyl nitrate ($RONO_2$). Under conditions where NO concentrations are low (i.e. pristine environments) or RO_2 concentrations are relatively high (i.e. within aerosol particles), RO_2 can react by a number of other pathways: (i) with HO_2 to form a hydroperoxide, (ii) with another RO_2 radical to form **either** two alkoxy radicals similar to RO_2 + NO, an organic peroxide (ROOR), or a ketone and alcohol. Recently, the role of autoxidation, or unimolecular RO_2 isomerization, was identified as an important channel for SOA formation, and hence represents another potential pathway.[7-9] RO radicals will either fragment into smaller molecules or isomerize and form a second RO_2 species. This new RO_2 molecule is subject to the same branching discussed above: reaction by unimolecular isomerization or by bimolecular reactions with RO_2, HO_2, or NO. The relative role of each channel in the overall RO_2 branching will thus be strongly dependent on the specific oxidation regime that a radical exists in (high or low NO_x or RO_2).
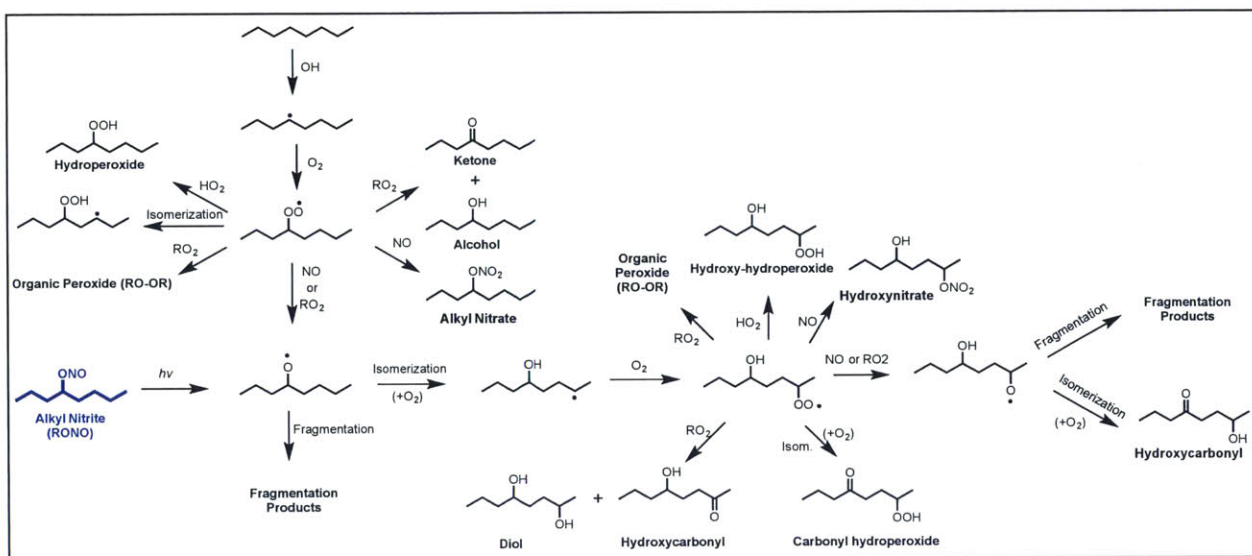
Figure 1. Chemical mechanism for the formation of first generation oxidation products from reaction with OH and alkyl nitrite photolysis (blue).

Most of the previous heterogeneous oxidation studies of OA were conducted in flow tubes under high concentrations of OH ($1 \times 10^{10} - 1 \times 10^{12}$ molecules cm^{-3} s^{-1}) such that several days to weeks of oxidation can be accessed over the residence time of the reactor (seconds – several minutes).[e.g.10,11] Such high concentrations are often achieved through the photolysis of high levels of O_3 in the presence of water vapor- conditions that do not allow for the addition of NO (since the reaction of $NO + O_3 \rightarrow NO_2$ is fast). Under these conditions, self- reactions are expected to be the dominant fate of RO_2 (with minor contributions from reaction with HO_2 and isomerization), and hence the system is an oxidation regime that may not be atmospherically relevant, particularly to polluted environments. To our knowledge, two studies have examined heterogeneous oxidation in the presence of NO_x, one by the O_3 oxidation of a squalene thin-film, and another by oxidation with Cl of super-cooled brassidic acid aerosol particles.[12,13] In both cases, yields of organonitrates were observed to be lower than in the gas-phase, implying that $RO_2 + NO$ reactions were of minor importance. It is unclear if this was due to the slow diffusion

of NO into the particle, or if the relative branching between the formation of RO and $RONO_2$ formation may favor the former in the condensed phase. The use of alkyl nitrites (RONO), however, initiates radical oxidation chemistry without added OH, and generates NO within the particle thereby facilitating the reactions of RO_2 + NO and allowing for this potentially important chemical regime to be directly probed. The goal of the work presented in this chapter is to identify the molecular species formed from the reactions of the RO and RO_2 radicals using a new approach (DART, described below). The identities of individual species measured will then be used to identify the major pathways responsible for their formation.

4.2 Experimental.

4.2.1 Preparation of RONO

The condensed phase reactivity of two $C_{20}H_{41}ONO$ alkyl nitrite isomers, a β-substituted (β-C_{20}) and straight chain (n-C_{20}) were measured in hexane solution (Figure 2). Preparation of the nitrites was accomplished by O-nitrosation of the corresponding alcohol[14] (octyl-2-dodecanol and 1-eicosanol, both Sigma Aldrich, 98%). The alcohol and sodium nitrite (Sigma Aldrich, > 99.99% trace) were combined in a 1.1:1.0 molar ratio and stirred with a magnetic stirrer at 25 °C while 2.5 M sulfuric acid (Sigma Aldrich, 99%) was added dropwise until a 0.5:1.0 acid:alcohol molar ratio was obtained. For n-C_{20} (a solid), this synthesis was modified by dissolving the precursor alcohol in hexanes prior to the addition of sodium nitrite and sulfuric acid. Finally, additional (excess) sodium nitrite was added to neutralize any remaining acid in solution. The resulting clear yellow liquid (or hexane + RONO solution for the solid nitrites) was dried over sodium sulfate (Sigma Aldrich, 99%) and stored at 20 °C in the dark until it was used (within 10-12 hours).

74
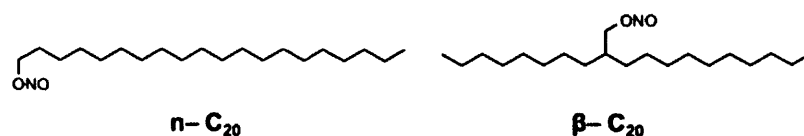
Figure 2. Molecular structures of the straight chain (n-C_{20}) and β-substituted (β-C_{20}) $C_{20}H_{41}ONO$ isomers used in this study.

4.2.2 Experimental Setup

All experiments were conducted at the Lawrence Berkeley National Laboratory Advanced Light Source in Berkeley, Ca. Experimental conditions and the overall setup were similar to those described in Chapter 3. Briefly, the solution (0.05%) was photolyzed and then atomized through a charcoal denuder to remove the hexane solvent and the flow was split for on-line measurement of particle size (SMPS) and composition. In these experiments, in place of the AMS we used a soft chemical ionization technique, *Direct Analysis in Real Time (DART, IonSense)* coupled to a high resolution Orbitrap (Thermo Finigan, LTQ XL) mass spectrometer, to obtain chemical information on the system.

DART is a real-time atmospheric pressure chemical ionization technique that provides molecular ions with little to no fragmentation of the parent species.[15,16] Briefly, N_2 or He gas flows past a corona discharge needle operated at 3600 – 5000 V, producing electrons and metastable (N_2* or He*) species. This gas flows through a grounded perforated electrode and then into a heated (80 – 450 °C) reservoir before exiting the ion source at 2 L/min. Heated N_2* or He* flows out of the ion source and is directed at the opening of the Orbitrap which is located at a 45° angle 0.3 cm away (Figure 3). Positive mode ionization (used in this study) occurs by means of Penning ionization when, for example, N_2* interacts with atmospheric water molecules by:

$$N_2{}^*(g) + nH_2O\ (g) \rightarrow N_2(g) + [(H_2O)_{n-1}H]^+(g) + OH\text{-}(g) \qquad (1)$$

75

The experimental setup is such that the outlet from the atomizer is directed at the space between the DART ionization source and the inlet to the Orbitrap. The heated N_2^* thermally desorbs analyte molecules (M) from the surface of the aerosol particles where they then react with the protonated water clusters, $[(H_2O)_{n-1}H]^+(g)$, generated in Equation (1) to form protonated molecular ions $[M+H]^+$ by:

$$[(H_2O)_{n-1}H]^+(g) + M(g) \rightarrow [M + H]^+(g) + nH_2O(g) \tag{2}$$
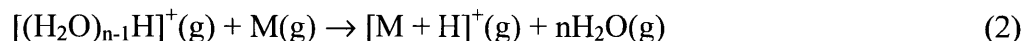
These ions are sampled into an Orbitrap Mass Spectrometer that was operated in ultra high-resolution mode (resolution of 140,000 at m/z 400 and mass accuracy to < 1 ppm) over the range of 110 – 600 Da. The particle flow rate out of the atomizer was ~ 0.7 liters/minute to allow sufficient time for aerosols to interact with the DART gas stream, and is based on previous observations which provided the the greatest sensitivity to desorbed molecules.[17] While it is currently unknown exactly how sample flow rate can impact the sensitivity of this technique, maintaining a constant flow to the DART source will likely limit any variability. Unlike electron impact ionization (the ionization technique commonly used in the AMS), which ionizes all molecules with roughly the same efficiency, the chemical ionization of DART is dependent on the structure of the analyte molecule and on the nature of ion-molecule interactions. Specifically, DART is selective towards molecules containing functional groups with polar heteroatoms (i.e. O, N, and S) or double bonds, due to the electron-rich nature of these moieties. As this proton affinity is dependent on the structure of the functional group and the identity of the heteroatom, ionization efficiencies are thus non-constant. Furthermore, the presence of multiple functionalities can enhance the probability of ionization. Little is known about the ionization potentials for a wide-range of M molecular structures, however, they are hypothesized to be similar to those from atmospheric pressure photoionization (APPI).[16] Hence, unlike electron

impact ionization, quantification with DART requires the use of standards for individual molecules. Additionally, DART ionization efficiency can be susceptible to matrix effects,[18] how the composition of the aerosol particles can influence sensitivity must be considered and hence a series of "control" runs with the appropriate standards are necessary. Data analysis was completed with mzMine (3.13).[19]
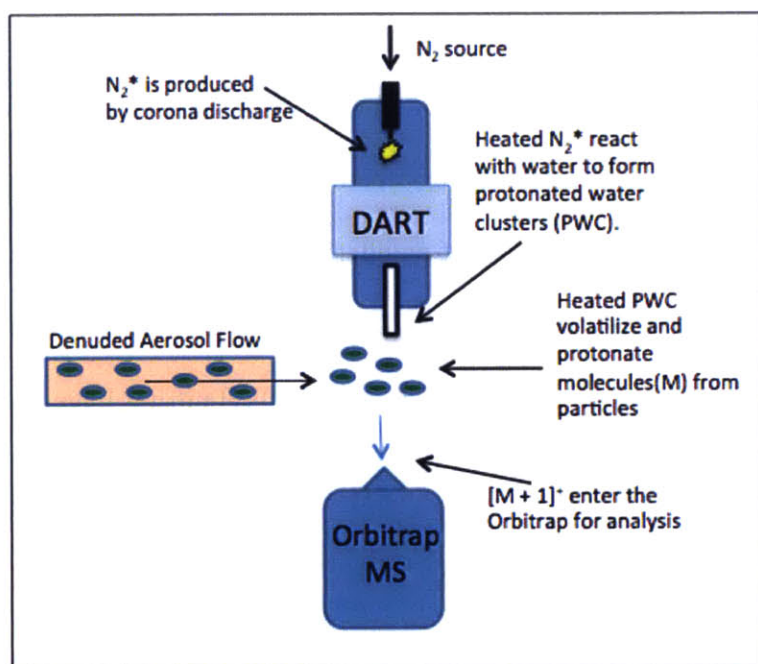
Figure 3. Schematic of the DART-Orbitrap setup. Metastable N_2^* is produced by corona discharge in a heated (~450 °C) stream of nitrogen and react with atmospheric water to produce protonated water clusters (PWC). These heated PWC then interact with aerosol particles to volatilize and ionize individual molecules prior to entering the Orbitrap inlet. The distance between the outlet of the DART source and Orbitrap inlet was ~0.3 cm and held at a 45° angle.

4.3 Results

Aerosol particles were generated from the reaction mixture of either $n\text{-}C_{20}$ or $\beta\text{-}C_{20}$ in hexanes, ionized by the DART source (using He and N_2) and measured with the Orbitrap (in

both positive and negative ion modes). Ion intensities and diversity was highest with N_2 gas in positive mode, and thus the following discussion is limited to that dataset. An example mass spectrum from a β-C_{20} photolysis experiment in hexanes, taken 35 minutes after turning the lights on, is shown in Figure 4 (bottom panel). For comparison with data previously collected with the AMS, a mass spectrum of the same system is given in the top panel of Figure 4 (Chapter 3). The two most striking differences between spectra are the number of individual product ions formed at a particular m/z, which is substantially larger in the AMS spectrum, and the presence of more high-molecular weight ($m/z > 280$) ions in the DART spectrum. These features result from increased fragmentation of parent molecules by electron impact ionization relative to the much softer chemical ionization used by DART. Neither the alcohol nor nitrite species were detectable by DART, as determined by use of standards. While polyols (molecules containing multiple –OH functionalities) are easily detected, simple alcohols are known to have low ionization efficiencies with DART,[20] and to our knowledge alkyl nitrites have not been explicitly tested with this setup.
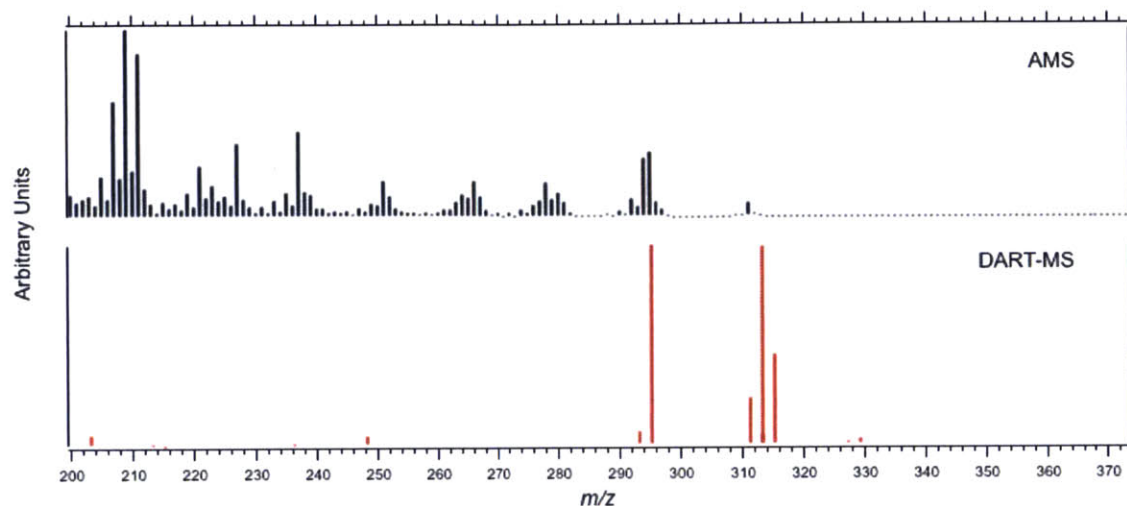
Figure 4. Comparison of mass spectra from β-C_{20} photolysis experiments with the AMS (top panel) and DART-Orbitrap-MS (bottom panel). The "hard" electron impact ionization used in the AMS results in substantial fragmentation and hence produces a large number of fragment ions, while the softer chemical ionization of the DART generates mostly protonated non-fragmented molecular ions (listed in Table 1).

Since DART ionization occurs in open air, these measurements are susceptible to interferences from the ambient atmosphere. The following criteria were applied to the dataset to prevent the identification of any transient or contaminant species as product ions: ion abundances must be greater than 0.01% of the largest ion in the spectrum (in both photolysis experiments this corresponded to the ion at *m/z 313.3106*), and be present for more than five consecutive minutes over the course of the experiment (~1 hour). Previous work has shown that for carbonyls, esters, and alcohols (polyols), molecules with functional groups similar to those expected to be present in this study, DART positive-mode molecular ions were observed as $[M+1]^+$ species.[17] Therefore, the mass of one H^+ was subtracted from each observed mass and the molecular formulae for each product ion was determined by constraining the exact mass to within 0.3 ppm and allowing for 0-100 C, H, and O and 0-5 N atoms to be present. The molecular formulae for all C_{20} products measured here are given in Table 1 for both β-C_{20} and n-C_{20}. Many of the ions are similar in the two samples, corresponding to species with 0-1 nitrogen atoms, 36-42

hydrogen atoms, and 0-7 oxygen atoms. In general these ions contain higher abundances of oxygen and nitrogen than those that were measured with the AMS (see Chapter 3). The major difference observed in the mass spectra of the two nitrites studied is the presence of C_{18} and C_{19} products that were formed only from the photolysis of n- and β-C_{20} respectively (Table 2), a feature that is discussed below. Several ions were observed for species at *m/z* < 220, and corresponded to C_6 – C_{11} species with varying levels of oxidation. For the purposes of the following discussion, these are assumed to be either contaminants or, for the C_6 molecules, result from the oxidation of the hexane solvent by secondary oxidants (see discussion).

The time series for the major product ions formed from the photolysis of both nitrites are shown in Figure 5 (as the time series for both isomers are similar, we confine our discussion to the β-C_{20} species). The intensity of the major product ions increases sharply immediately upon irradiation, consistent with the production of products from β-C_{20} photolysis, and slows down after approximately 10-15 minutes. There is a slight lag in the initial growth for some species, potentially due to the formation of later-generation products, discussed below. Again, caution is needed in the interpretation of the relative magnitudes of ion intensities, as they are not directly proportional to relative concentrations due to differences in ionization efficiencies.

.   .

m/z (M + 1)	Molecular Formula	n-C_{20}	β-C_{20}	1st Generation?
277.28188	$C_{20}H_{36}$		✓	
291.26113	$C_{20}H_{34}O$		✓	
293.27679	$C_{20}H_{36}O$		✓	
293.27679	$C_{20}H_{36}O$	✓		
295.29245	$C_{20}H_{38}O$	✓	✓	✓
307.25604	$C_{20}H_{34}O_2$	✓	✓	
309.2717	$C_{20}H_{36}O_2$	✓	✓	
311.28736	$C_{20}H_{38}O_2$	✓	✓	✓
313.30302	$C_{20}H_{40}O_2$	✓	✓	✓
323.25095	$C_{20}H_{34}O_3$	✓		
324.2826	$C_{20}H_{37}NO_2$		✓	
325.26661	$C_{20}H_{36}O_3$	✓	✓	
327.28227	$C_{20}H_{38}O_3$	✓	✓	
329.29793	$C_{20}H_{40}O_3$	✓	✓	
331.31359	$C_{20}H_{42}O_3$	✓	✓	✓
340.27751	$C_{20}H_{37}NO_3$	✓	✓	
343.27718	$C_{20}H_{38}O_4$	✓	✓	
347.3085	$C_{20}H_{42}O_4$	✓	✓	✓
356.27242	$C_{20}H_{37}NO_4$	✓	✓	
363.30341	$C_{20}H_{42}O_5$	✓	✓	
374.28299	$C_{20}H_{39}NO_5$	✓	✓	
390.2779	$C_{20}H_{39}NO_6$		✓	
392.29356	$C_{20}H_{41}NO_6$	✓	✓	
406.27281	$C_{20}H_{39}NO_7$		✓	
408.28847	$C_{20}H_{41}NO_7$	✓	✓	

Table 1. Ions, molecular formulae, and oxidation generation for the C_{20} species detected by DART-MS. Molecular formulae correspond to the measured m/z minus the mass of one H^+. Checkmarks in the appropriate column, n-C_{20} or β-C_{20} denotes the presence of individual ions in each experiment. A checkmark in the "First-generation" column indicates that the ion has been assigned to a first-generation product.

m/z (M + 1)	Molecular Formula	n-C_{20}	β-C_{20}
265.28188	$C_{19}H_{36}$		✔
267.26113	$C_{18}H_{34}O$	✔	
279.26113	$C_{19}H_{34}O$		✔
281.24038	$C_{18}H_{32}O_2$	✔	
281.27679	$C_{19}H_{36}O$		✔
283.25604	$C_{18}H_{34}O_2$	✔	
283.29245	$C_{19}H_{38}O$		✔
285.2717	$C_{18}H_{36}O_2$	✔	
295.25604	$C_{19}H_{34}O_2$		✔
297.23529	$C_{18}H_{32}O_3$	✔	
297.2717	$C_{19}H_{36}O_2$		✔
299.25095	$C_{18}H_{34}O_3$	✔	
299.28736	$C_{19}H_{38}O_2$		✔
315.24586	$C_{18}H_{34}O_4$	✔	
344.23601	$C_{18}H_{33}NO_5$	✔	

Table 2. Ions and molecular formula for the C_{18} and C_{19} products detected by DART-MS. Molecular formulae correspond to the measured m/z minus the mass of one H^+. Checkmarks in the appropriate column, n-C_{20} or β-C_{20} denotes the presence of individual ions in each experiment.
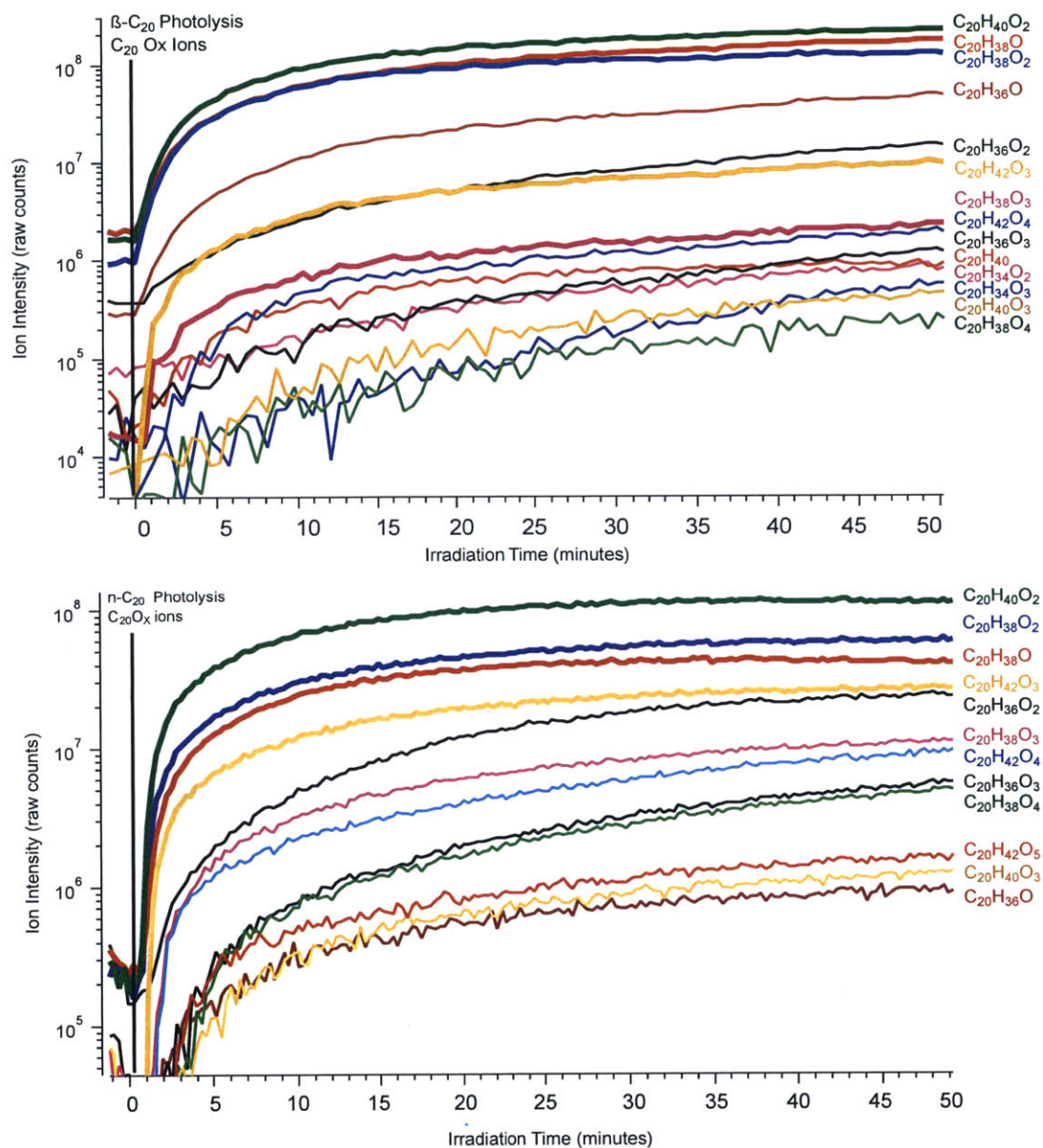
Figure 5. Time series of absolute ion abundance for the $C_{20}H_yO_x$ oxidation products (first-generation products are bolded) identified from β -C_{20} (top) and n-C_{20} (bottom) photolysis during the first 50 minutes of reaction. Vertical black line corresponds to the time when the lights were turned on.

4.4 Discussion

The ions listed in Table 1 correspond to molecular products and are unlikely to be that of

a radical intermediate (RO or RO_2) as their lifetimes are expected to be too short for detection.

83

Furthermore, the extent to which thermally labile molecules decompose from the elevated temperatures of the DART gas, are assumed to be a minor factor in the following interpretation of the data. The gas is heated to 450 °C inside the source; however, recent observations indicate that the gas temperature decreases precipitously once it enters the room air.[6,17] The temperature that aerosol particles are exposed to is hence significantly lower (< 100 - 150 °C). Decomposition, particularly dehydration of alcohols and hydroperoxides, may occur to some extent; however their dehydrated products should be present in the mass spectrum. As there is likely a steep temperature gradient along the radius of a given particle, resulting from external heating by the DART gas, we expect that some amount of the non-dehydrated molecule will be present. If dehydration does occur, these ions will appear less oxygenated and should have the same time dependence as their analogous non-dehydrated parent. The only products that were observed to have a similar time trend and had a chemical formula identical to a dehydration [M − H$_2$O]$^+$ product were at m/z 325.2666 (C$_{20}$H$_{36}$O$_3$) and 343.2771 (C$_{20}$H$_{38}$O$_4$) (Figure 5). The other ions are thus expected to be non-decomposed molecular ions.

The product ions formed from β-C$_{20}$ photolysis (Figure 5) increase in intensity immediately when the lights are turned on. There are several time dependences observed, with some ions growing in at much faster rates than others. The goal of the next section is to assign observed ions to specific products. For clarity, the section is broken up into several segments: first we compare **the molecular formulae of observed ions to those of products from likely first-generation mechanisms**, then we refine **this list of assignments based on their observed time dependences,** and finally **we consider other means for forming these species.** The results are then discussed **in the context of estimated branching ratios from a simple kinetic model that we developed.**

84

4.4.1 Comparison of observed ions to potential first-generation products. To this end, the products from each of the major radical intermediates formed from RONO photolysis will be considered following the general pathway outlined in Scheme 1. Each intermediate is colored so as to provide a guide for the reader, and, as several RO and RO_2 radicals will be formed, they are identified in the text by "first," "second," or "third."

Scheme 1. Major radical intermediates formed following alkyl nitrite photolysis.

The first alkoxy radical (blue) generated from RONO photolysis can either fragment and form a C_{19} radical (discussed in a later section) or undergo a 1,5-H isomerization ($+ O_2$) to yield the first RO_2 radical (Scheme 2). Note that the reaction of $RO + O_2$ to form an aldehyde is assumed to be a minor pathway here.[21]

Scheme 2: Reactions of the first alkoxy radical formed from RONO photolysis. Note that reaction with O_2 is expected to be slow here.

The first RO_2 radical (green) can react by a number of bimolecular channels (Scheme 3) with NO, HO_2, RO_2 (self-reaction), or unimolecularly (isomerization or "autoxidation"). For clarity,

the discussion of how the DART data compare with the expected products from each channel are bulleted below:
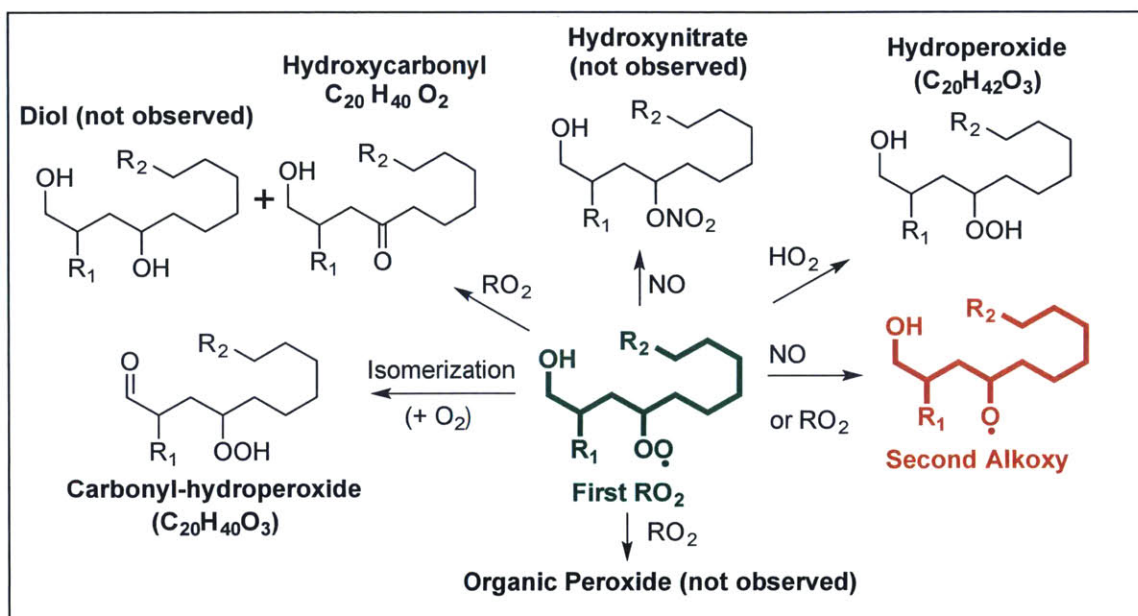
Scheme 3: Reactions of the first RO_2 radical (green).

NO: Reaction with NO will produce **either** the hydroxynitrate (not observed) or the *second* alkoxy radical (red). The absence of the hydroxynitrate may indicate that it is not observable with DART, which is consistent with our inability to ionize alcohol and nitrite standards. Furthermore, the branching ratios for products formed from the condensed-phase reaction of RO_2 + NO (forming RO vs. $RONO_2$) are unknown and thus it may be possible that the hydroxynitrate simply did not form.

RO_2: The self-reaction of this RO_2 species will result in a number of products: (i) two alkoxy radicals (identical to the one produced from RO_2 + NO, in red), (ii) a hydroxycarbonyl (observed, m/z 313.3030, $C_{20}H_{40}O_2$) and a diol (not observed), or (iii) an organic peroxide (not observed). For the hydroxycarbonyl to be generated by this channel, a diol would

86

also be produced. As the diol was not observed, but expected to be detectable with DART, the hydroxycarbonyl present is unlikely to have formed from this pathway.

HO$_2$: The major product of RO$_2$ + HO$_2$ is the hydroperoxide (observed, m/z 331.3135 C$_{20}$H$_{42}$O$_3$) species.

Isom.: Unimolecular isomerization (+ O$_2$) of the first RO$_2$ radical is most favored to occur by a 1,6-H transfer with the δ-carbon (shown in more detail in Scheme 4) to form the carbonyl hydroperoxide (observed, m/z 329.2979, C$_{20}$H$_{40}$O$_3$). Note that a 1,5-H isomerization with a secondary carbon atom is expected to be slow relative to isomerization with an –OH substituted carbon.[9]
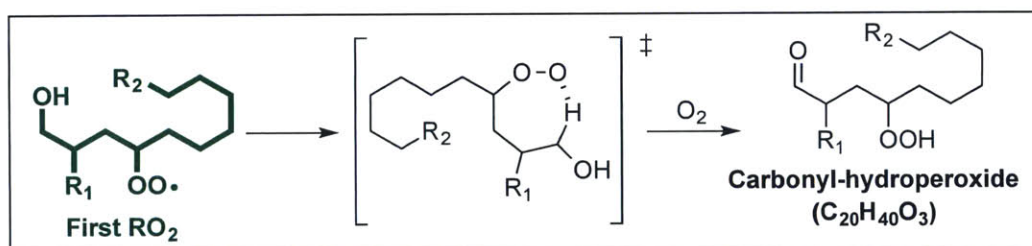
Scheme 4. Example of a 1,6-H unimolecular RO$_2$ isomerization.

The second RO radical formed (red) can either fragment into smaller species, back-isomerize (+ O$_2$) to form the hydroxycarbonyl (observed, m/z 313.3030, C$_{20}$H$_{40}$O$_2$), or forward-isomerize (+ O$_2$) and form the second RO$_2$ (orange) intermediate (Scheme 5). Based on the estimates reported in Chapter 2 for the gas-phase, the newly formed RO radicals (+O$_2$) will mostly back-isomerize to form the hydroxycarbonyl (m/z 313.3030, C$_{20}$H$_{40}$O$_2$), while ~10 – 15% will forward-isomerize to form the second RO$_2$ intermediate (orange). The hydroxycarbonyl will undergo (acid-catalyzed) cyclization to the cyclic hemiacetal, which can dehydrate to the dihydrofuran (observed, m/z 295.2924, C$_{20}$H$_{38}$O), all of which are major ions detected in the mass spectrum. Unlike in electron impact ionization where each has its own characteristic fragmentation

patterns, the cyclichemiacetal and hydroxycarbonyl are indistinguishable with the DART, as they have the same molecular formulae. The hydroxycarbonyl and cyclic hemiacetal can also form dimers with one another (not observed).
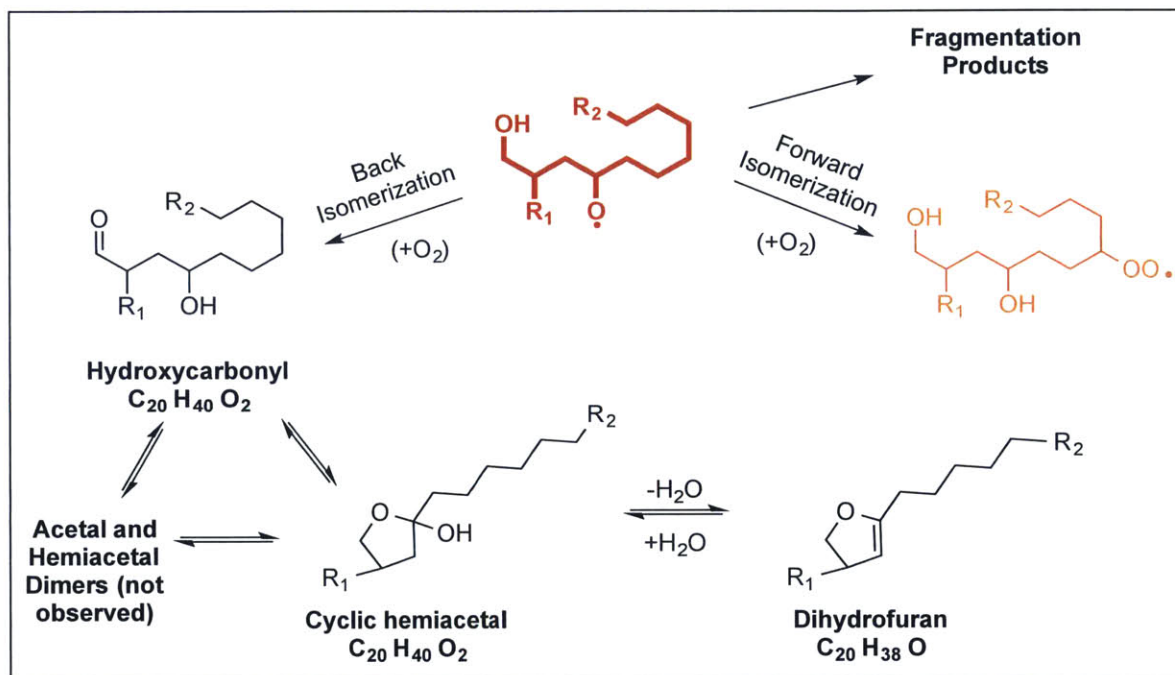
Scheme 5. Major reactions of the second alkoxy radical.

The second RO_2 species (orange) formed from the forward-isomerization pathway is subject to the same reactions discussed above, isomerization or reaction with NO, RO_2, or HO_2 (Scheme 6) and are bulleted below.
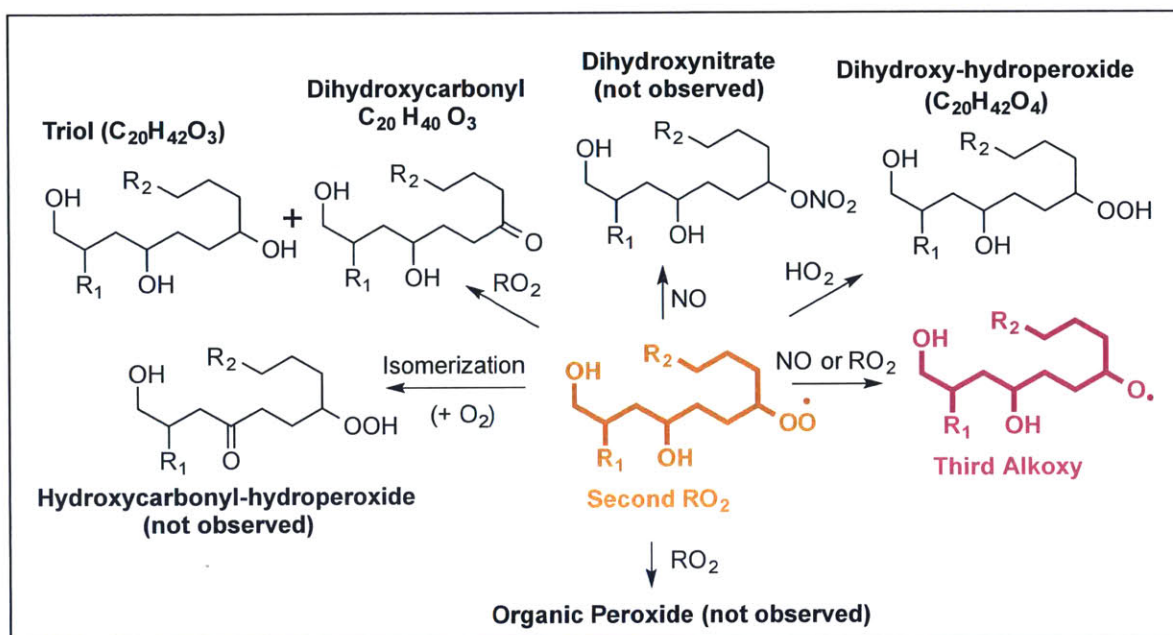
Scheme 6: Reactions of the second RO_2 intermediate.

NO: The reaction with NO will yield either a dihydroxynitrate (not observed) or a *third* alkoxy radical (pink).

RO_2: Reaction with RO_2 will produce a triol (observed, m/z 331.3135, $C_{20}H_{42}O_3$) and a dihydroxycarbonyl (observed, m/z 329.2979, $C_{20}H_{40}O_3$), an organic peroxide (not observed), or two alkoxy radicals (pink).

HO_2: The major product of $RO_2 + HO_2$ is the dihydroxy-hydroperoxide (observed, m/z 347.3085 $C_{20}H_{42}O_4$) species.

Isom.: The major product for unimolecular isomerization is the hydroxycarbonyl-hydroperoxide which was not observed.

The third RO (Scheme 7) radical can fragment into smaller species, forward isomerize to yield a new RO_2, or back-isomerize to form a dihydroxycarbonyl (observed, m/z 329.2979 $C_{20}H_{40}O_3$). The dihydroxycarbonyl will cyclize to the hydroxy-cyclic hemiacetal (observed, m/z 329.2979

$C_{20}H_{40}O_3$), which can dehydrate to the hydroxy dihydrofuran (observed, $C_{20}H_{38}O_2$, *m/z* 311.2873). Further forward-isomerization, while extremely unlikely in the gas-phase, would result in dihydroxy hydroperoxides, trihydroxycarbonyls, and trihydroxyhydrofurans, which are masses corresponding to additional ions measured by the DART (not shown in the schemes). However, in order for these first-generation product assignments to be correct, they should exhibit the appropriate corresponding chemistry, discussed below.
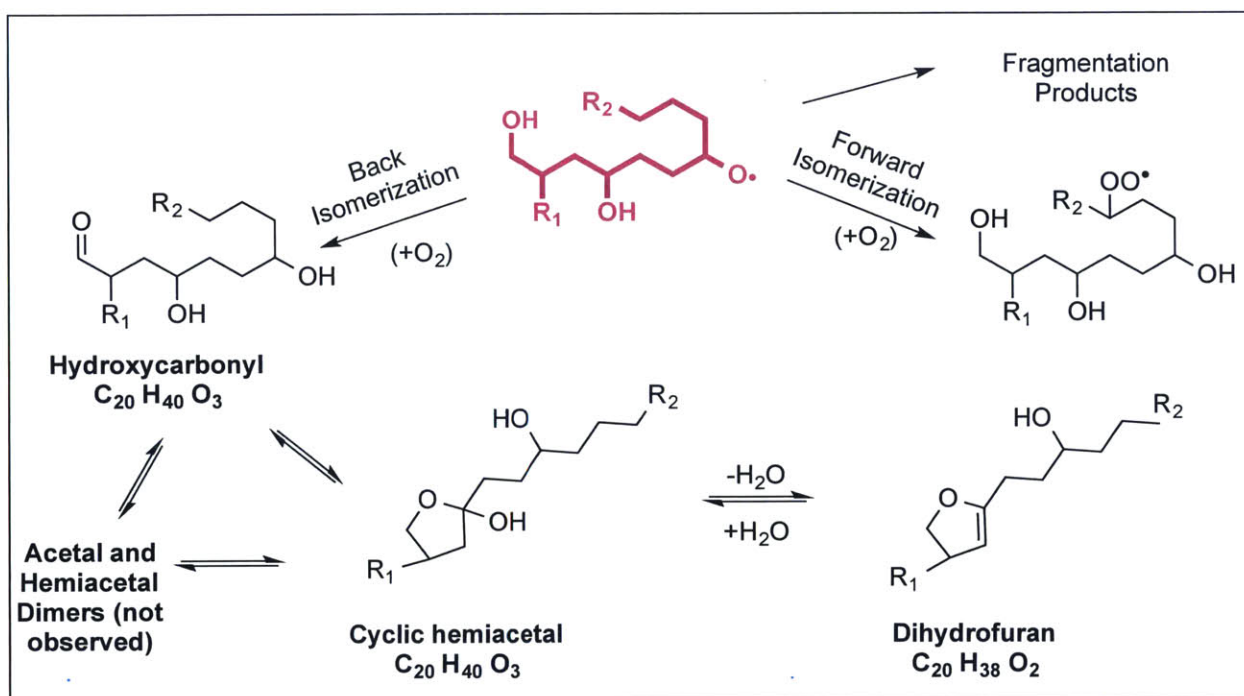
Scheme 7. Reactions of the third alkoxy intermediate.

4.4.2 Refinement of assignments based on time dependencies. All of the assignments in the previous section correspond to species that are first-generation products. The production rate of first-generation products will scale linearly with the depletion rate of RONO (for every RONO photolyzed, a certain fraction will form a particular first-generation product). If a product forms from other means (e.g. by reaction with OH or O_3), its rate of production will thus not scale

linearly with RONO depletion. The time series in Figure 5 thus provides information as to whether the observed ions correspond to first vs second (or later) generation products. Unfortunately in these experiments we are unable to track the evolution of RONO- however, if we assume that the assignment of m/z 313.3030 is indeed that of the major first generation product, the hydroxycarbonyl, then any product with the same formation rate is also of first-generation. This is assessed qualitatively by comparing the growth of this ion with the growth of all of the other ions in the time series. The period of growth for each ion is the greatest during the first 8 minutes of irradiation, and for clarity this region is enlarged and presented in three panels in Figure 6 for: (a) the identified first-generation products, (b) the second generation $C_{20}H_yO_x$ products, and (c) the $C_{20}H_yNO_x$ products. Based on this method, the only first-generation products are the dihydrofuran ($C_{20}H_{38}O$), hydroxydihydrofuran ($C_{20}H_{38}O_2$), dihydroxydihydrofuran ($C_{20}H_{38}O_3$), and hydroxyhydroperoxide ($C_{20}H_{42}O_3$). The following C_{20} ions that were previously assigned to first-generation products are thus likely to be later-generation: (i) the carbonyl-hydroperoxide from the first RO_2 isomerization ($C_{20}H_{40}O_3$), (ii) the triol ($C_{20}H_{42}O_3$) and dihydroxycarbonyl ($C_{20}H_{40}O_3$) from the self-reaction of the second RO_2, (iii) the hydroperoxide ($C_{20}H_{40}O_4$) from the second RO_2 + HO_2, and (iv) the dihydroxycarbonyl ($C_{20}H_{40}O_3$) formed from back isomerization of the third alkoxy radical. Note that the double bond on the dihydrofuran molecule will dramatically increase its sensitivity to DART ionization, so while the precursor dihydroxycarbonyl is not present as a first generation product, this may be because its abundance and efficiency are too low.
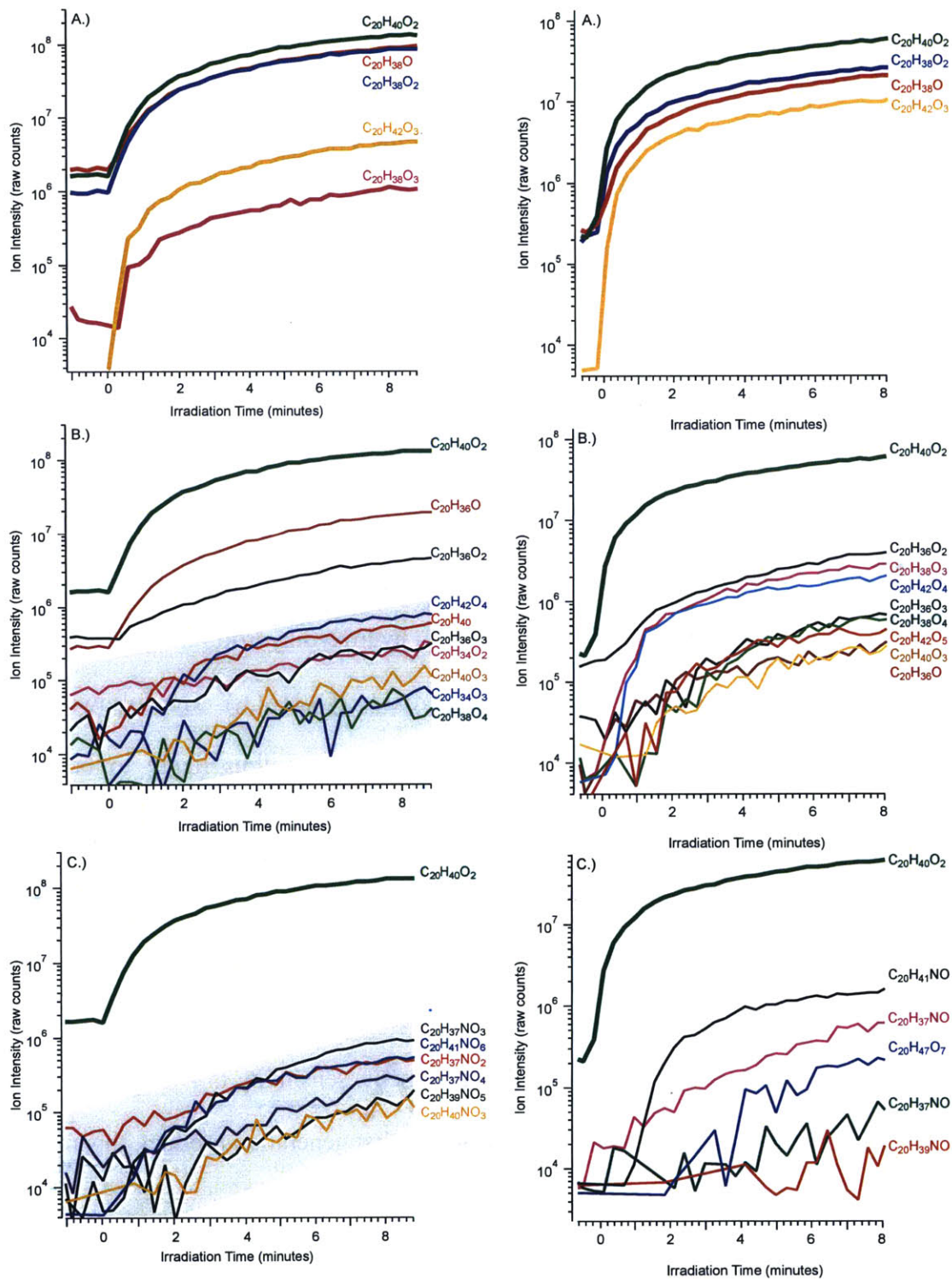
Figure 6. Time series for the first eight minutes of reaction for (A) identified first generation products, (B) second generation $C_{20}H_yO_x$ ions, and (C) $C_{20}H_yNO_x$ ions from β - C_{20} (left) and n-C_{20} (right) photolysis. Note that the shaded regions are used as a guide for the general trend observed for a given cluster of traces.

Interestingly, the products believed to form from multiple forward-isomerizations, by this method are not predicted to be first-generation. This is surprising as they are completely saturated – indicating that they contain only alkyl, hydroxyl or hydroperoxide functionalities (opposed to carbonyls, double bonds, rings, or nitrate groups). The dihydrofuran has two double bond equivalents (DBE) from the olefin and cyclic ether. Any later generation oxidation products will have at least two DBEs and thus it is unclear how these fully saturated products can form. Similarly, it is unclear how some of the most unsaturated species ($C_{20}H_{34-36}O_{0-3}$,) can form by means other than decomposition/dehydration reactions. If we assume that oxidation occurs via OH-addition to the dihydrofuran double bond, at most two carbonyl groups would form from ring opening products. Thus we cannot effectively rule out the possibility of dehydration reactions promoted by the heated DART gases, for first- and later-generation oxidation products. Furthermore, these results indicate that the ion previously assigned as the carbonyl hydroperoxide ($C_{20}H_{40}O_3$,), is not a first-generation product, and so is unlikely to arise from RO_2 isomerization. A number of ions remain unidentified, however, none of them appear to be first - generation products and are thus unlikely to have formed from RO_2 isomerization, but potentially by additional oxidation (see below)

4.4.3 Assessing the potential for later-generation oxidation chemistry. As discussed above, several of the observed ions believed to be first-generation products are likely to have formed by other means. An alternative formation pathway is by later-generation oxidation. While oxidants such as OH, O_3 or NO_3 are not intentionally added to the system, they can form from secondary reactions of the HO_x and NO_x cycles. Their production and subsequent reactions with the first-generation products, particularly the double-bond bearing dihydrofuran, must be considered in

the interpretation of this data. In the gas-phase work (Chapter 2), second-generation chemistry was not believed to be a major source of the measured SOA, as nitric acid concentrations were not sufficiently high to promote the formation of the dihydrofuran. However, in this system, we believe, based on its molecular formula and time dependence, that we observe formation of the dihydrofuran (in addition to the hydroxylated dihydrofurans). The addition of OH and O_2 across the dihydrofuran double bond initiates a new set of radical chemistry, shown in Scheme 8 but not discussed here in explicit detail. Instead, we focus on the tentative identification of three products from this pathway to highlight the potential for second-generation oxidation chemistry to form observed ions: the cyclic hemiacetal nitrate ($C_{20}H_{39}NO_5$) and two "ring-opening" products, ($C_{20}H_{38}O_3$ and $C_{20}H_{39}NO_6$). Furthermore, the photolysis of NO_2 will facilitate the formation of O_3 and NO_3; however, at this time we only note that their reaction with the dihydrofuran may contribute to observed second-generation products.
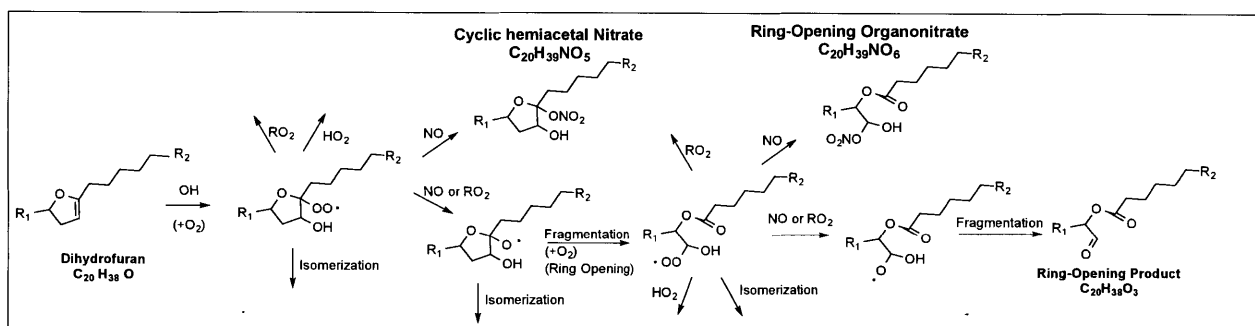
Scheme 8. Second-generation product generation from the reaction of OH with dihydrofuran

4.4.5 RO radical fragmentation Products

As discussed in Chapter 2, β-substituted RO radicals (such as 4-methyl-5-nonyl-oxy) are expected to undergo substantial fragmentation due to the enhanced stability of the secondary alkyl radical formed upon scission. Fragmentation is expected to be a minor pathway for n-C_{20} as the production of a primary alkyl radical is not as energetically favorable. This is consistent with

the presence of C_{19} products in the mass spectrum of β- C_{20} and their absence in n-C_{20}. The same reaction schemes described above for the C_{20} molecules will occur but the major products will have one less methylene (-CH_2-) group (Scheme 9). Note that for simplicity only the radical chain-propagating reactions are shown. The products observed are the C_{19} hydroxycarbonyl/cyclic hemiacetal (m/z 296.272, $C_{19}H_{38}O_2$), the dihydrofuran (280.277, $C_{19}H_{36}O$), and the hydroxy dihydrofuran (m/z $C_{19}H_{36}O_2$). The absence of the precursor to the hydroxylated furan species may be due to lower abundance or ionization efficiency than for the furan. The presence of C_{18} species from n-C_{20} photolysis is not entirely understood, however, there is a possibility that the alcohol standard (98% purity) may contain a C_{18} impurity, leading to the generation of $C_{18}H_{37}ONO$. If present, this nitrite could photolyzed along with n-C_{20}, yielding these products. This is currently under investigation.

Scheme 9. First generation products from C_{19} alkyl radical.

4.4.4 Estimates of RO₂ branching ratios. Observations of individual products with DART are essential for identifying the presence of a particular mechanism in the overall oxidation scheme; however, the absence of product concentrations hinders our ability to assess the relative importance of each pathway. As discussed in previous sections, the fate of RO_2 species formed will drive much of the observed chemistry. However, the number of different RO_2 intermediates that will each form and react by multiple pathways complicates the direct comparison of the chemical mechanism with the experimental data. To this end we developed a simple kinetic model to predict the integrated branching ratios for the major RO_2 reactions (isomerization and reaction with RO_2, NO, and HO_2). The model consists of a system of differential equations describing the formation and loss of each of the major inorganic (HO_x, NO_x and O_3) and organic species. Rate constants for many of the reactions have not been measured in the condensed organic phase, and when necessary either aqueous or gas-phase constants were used. For reaction channels that have a number of possible products (i.e. RO_2 + NO forming an RO **or** an $RONO_2$), the relative branching was assumed to be identical to the gas-phase. The species monitored and the rate constants used are given in Tables 3 and 4. The most uncertain rates correspond to those for the aqueous phase reaction of RO_2 + NO, with measurements spanning nine orders of magnitude ($3 \times 10^{-9} - 1 \times 10^{-18}$ molecule cm^{-3} s^{-1})[22,23]. In addition, to better assess the fate of the dihydrofuran species and specifically the likelihood that unidentified product ions correspond to second-generation products, the fraction that reacted with secondary oxidants was estimated from gas-phase kinetic data.

The bulk system examined in this work is treated as a pure phase organic solvent containing 0.05% (v/v) RONO. The system was solved in Matlab using a stiff ODE solver (ode15s). The integrated branching ratios for RO_2 isomerization and reaction with NO, HO_2,

RO$_2$, were then determined by considering all of the potential reactions shown in Schemes 1-8 (Table 3). The results for this scenario are extremely sensitive to the rate constant used for RO$_2$ + NO, and instead we use the gas-phase measurement (8 x 10^{-12} cm^3 molec^{-1} s^{-1})[24] as it has been studied extensively and is between those mentioned above. The estimates indicate that in this system the overwhelming majority of products will react with NO (> 65%), and isomerization (28%) and reaction with HO$_2$ (4%) will be a secondary and minor channels respectively. The estimates are consistent with our observations of many of the major first-generation products from RO$_2$ + NO and the absence of those from RO$_2$ + RO$_2$. The presence of the hydroxy-hydroperoxide (*m/z* 331.3155, C$_{20}$H$_{42}$O$_3$) from reaction with HO$_2$ implies the DART is sensitive enough for the detection of the products from minor pathways. However, products from RO$_2$ isomerization were not observed (Schemes 2,3, and 5). The major product, the carbonyl hydroperoxide, is structurally similar to other first generation products and should ionize with DART. Based on our observation of hydroxy hydroperoxide formation from RO$_2$ + HO$_2$, we expect to be sensitive enough to products formed with a 4% yield. We can thus constrain the rate of RO$_2$ isomerization in this (condensed-phase) system with an upper limit approaching that of 2.46 s^{-1}. This is an order of magnitude slower than the analogous gas-phase rate constant measured for smaller C$_5$ species. While the exact reason for this discrepancy is unclear at present, it may be due to the larger molecular size or phase (condensed vs. gas-phase).

Species	Abbreviation
Hydroxyl Radical	OH
Hydrogen Peroxide	H_2O_2
Ozone	O_3
Hydroperoxy Radical	HO_2
Nitrogen monoxide Radical	NO
Nitrite Radical	NO_2
Nitrate Radical	NO_3
Nitric Acid	HNO_3
Alkyl Nitrite	RONO
Alkyl Peroxy Radical	RO_2
Hydroxynitrate	HN
Alkoxy Radical (second generated)	RO
Alkyl Peroxy Radical (second generated)	RO_2_b
Hydroxycarbonyl	HC
Dihydrofuran	DHF
Dihydrofuran + O3 Products	DHF_O_3
Dihydrofuran + OH Products	DHF_OH
Alcohol and Carbonyl (from RO2 + RO2)	CTP
Hydroperoxide	ROOH
Squalane (OA surrogate)	Squalane
RO2 isomerization (1,5-H shift)	RO_2_15iso
RO2 isomerization (1,6-H shift)	RO_2_16iso

Table 3. List of species monitored in chemical kinetic model and their abbreviations used in Table 4.

Reaction	Rate	Ref
$OH + OH + M = H_2O_2$	2.20×10^{-11}	25
$H_2O_2 + hv = OH + OH$	[a]2.07×10^{-6}	c
$HO + HO_2 = H_2O + O_2$	1.10×10^{-10}	25
$HO + H_2O_2 = H_2O + HO_2$	1.81×10^{-12}	25
$HO + O_3 = HO_2 + O_2$	7.30×10^{-14}	25
$HO_2 + HO_2 + M = H_2O_2 + M + O_2$	2.90×10^{-12}	25
$HO_2 + O_3 = HO + 2O_2$	2.00×10^{-15}	25
$HO_2 + NO = NO_2 + OH$	8.50×10^{-12}	25
$NO + O_3 = NO_2 + O_2$	1.80×10^{-14}	25
$NO_2 + hv = NO + O_3$	[a]2.00×10^{-3}	24
$OH + NO_2 = HNO_3$	8.50×10^{-12}	25
$NO_2 + O_3 = NO_3 + O_2$	2.40×10^{-17}	25
$HO_2 + NO_3 = Prods$	3.50×10^{-12}	25
$NO + NO_3 = NO_2 + NO_2$	2.60×10^{-11}	25
$NO_3 + NO_3 = NO_2 + NO_2 + O_2$	2.30×10^{-16}	25
$OH + NO_3 = Products$	2.20×10^{-11}	25
$RONO + hv = RO_2 + NO$	[a]4.00×10^{-4}	26
$RO_2 + NO = HN$	$(0.4) \times 8 \times 10^{-12}$	24
$RO_2 + NO = RO + NO_2$	$(0.6) \times 8 \times 10^{-12}$	24
$RO + O_2 = HC + HO_2$	1.87×10^{-4}	21
Hydroxycarbonyl = Dihydrofuran	2×10^{-3}	27
Dihydrofuran + O_3 = DHF_O3	3.49×10^{-15}	27
Dihydrofuran + OH = DHF_OH	2.18×10^{-10}	27
$RO_2 + RO_2 = RO + RO$	$(0.6) \times 4.82 \times 10^{-15}$	28
$RO_2 + RO_2 = CTP$	$(0.4) \times 4.82 \times 10^{-15}$	28
$RO_2 + HO_2 = ROOH$.	1.50×10^{-11}	29
RO2 1,6-Isomerization Upper Limit	[a]2.46×10^{2}	9 b
RO2 1,6-Isomerization Upper Lower	[a]1×10^{-1}	9 b
RO2 1,5-isomerization	a2.76×10^{-3}	9 b

Table 4. Rate constants for kinetic model. All rates are cm^3 molecule^{-1} s^{-1} except those denoted with an [a] which are s^{-1}.

b. Rate constants for 1,6-isomerization were estimated to be equivalent to 1,5-isomerization based on their discussion.

c. Personal communication with J. Hunter, measured.

Species	K_{OA}	Flow Tube	Urban	Pristine
RO_2	NA	1×10^{17}	6×10^{14}	3×10^{14}
OH	NA	1×10^{11}	6×10^{6}	1×10^{6}
HO_2	7.03×10^{3} (refs [30,31])	0	1.38×10^{10}	1×10^{10}
O_3	NA	7.05×10^{13}	6.62×10^{7}	6.62×10^{8}
NO	3.13×10^{-2} (refs [32,31])	0	1.16×10^{8}	1.93×10^{4}

Table 5. Calculated octanol-air (K_{OA}) and condensed phase concentrations (molecules/cm^3) of OH, O_3, NO and HO_2 and RO_2 used to obtain integrated branching ratios (Table 6). Flow tube values were adapted from Smith et. al.[10] except for O_3, which is from observations by C. Lim (personal communication).

RO_2 Integrated Branching Ratio	This Study	Flow Tube	OA (Urban)	OA (Pristine)
RO_2	< 0.01	0.78 (0.77)	0.10 (0.50)	0.06 (0.39)
NO	0.68 (0.91)	< 0.01	< 0.01	< 0.01
Isomerization	0.28 (0.04)	0.01 (< 0.01)	0.88 (0.43)	0.93 (0.58)
HO_2	0.04 (0.05)	0.22	0.02 (0.07)	< 0.01 (0.03)

Table 6. Predicted branching ratios for all RO_2 reactions leading to the formation of first-generation products using the gas-phase (Crounse et. al)[9] and our constrained condensed phase isomerization rate in parentheses.

Many of the ions observed in the DART mass spectrum remain unidentified at the present, and are potentially second-generation products from the oxidation of dihydrofuran with secondary oxidants OH, O_3, or NO_3. We estimate that approximately half of the dihydrofuran formed will be oxidized by, ~35% by OH and 15% with O_3, consistent with this hypothesis. As mentioned above, the second-generation chemistry was predicted for reaction with OH, leading to the identification of several products, however, the products from ozonolysis must also be considered.

Implications for Condensed-Phase RO₂ chemistry

The model was run for additional scenarios with conditions that are representative of (i) urban and (ii) pristine atmospheres and (iii) traditional laboratory heterogeneous oxidation studies.[adapted from 24,33,34] The three scenarios differ by the concentrations of inorganic species, NO, HO_2, O_3 and OH input into the model (Table 3). Particle-phase concentrations of NO, HO_2 and O_3 were estimated from their corresponding octanol-air partition coefficients (K_{oa}), and typical gas-phase concentrations for each scenario (Tables 3 and 4).[31] In all scenarios, radical chemistry is initiated by heterogeneous reaction with gas-phase OH and addition of O_2 to form the first RO_2 species, that is then subject to the same chemistry described previously (Schemes 1 – 8). Note that this first RO_2 formed is not accessible by this RONO (Figure 1). Additionally, isomerization for this first RO_2 can only occur by 1,5-H rearrangement and hence this much slower rate constant was used $(2.76 \times 10^{-3}\ s^{-1})^9$. As OH is assumed to react only on the surface of the particles, gas-phase concentrations from each scenario were used. Furthermore, NO, HO_2, O_3, and OH are assumed to be in steady state with the gas-phase. Physically, this implies that gas-particle diffusion is instantaneous and always at equilibrium with the gas-phase. The results from model runs for each scenario are presented below.

Heterogeneous Oxidation Studies: The estimated branching ratios (Table 6) for typical heterogeneous oxidation studies[e.g. 10,11] imply that reaction with RO_2 dominates (0.77). Reaction with HO_2 is predicted to also be an important pathway (0.22). Even if the faster RO_2 isomerization rates are used, only ~1% of reactions are expected to go this route. Based on our observations that this is a minor pathway it is unlikely that products from RO_2 isomerization would be formed in these studies.

Ambient OA: The RO_2 branching ratios for reactions within ambient OA are not predicted to be dramatically different between pristine and urban environments (Table 6). Using the constrained isomerization rate constant derived here, RO_2 chemistry is expected to be dominated by reaction with RO_2 and isomerization, with minor contributions from HO_2 reactions on the order of < 10%. The difference in the branching ratios for reaction with RO_2 or HO_2 between the two systems is almost entirely due to the difference in RO_2 concentrations, resulting from different OH exposures (and hence uptake coefficients: $\gamma_{urban} = 2.78 \times 10^{-6} \ s^{-1}$ and , $\gamma_{pristine} = 9.28 \times 10^{-7}$ calculated for a 200 nm spherical squalane particle and the OH concentrations in Table 5). Surprisingly, the contribution of RO_2 + NO reactions is expected to be at best, minor. In the gas-phase, it has been well established that NO_x concentrations can have governing effects on the RO_2 chemistry,[e.g.24,35,36] in stark contrast to the estimates for the condensed phase. In our model NO is predicted to only enter the particle phase by equilibrium partitioning (opposed to other means: e.g. the in-particle production of NO_x from the photolysis of condensed phase organonitrates). As a result of both low gas-phase concentrations and solubility (low K_{oa}, Table 5) the overall rate of reaction with RO_2 is limited relative to other channels (particularly self-reaction). So, as our model assumes that the aerosol and NO are well mixed and therefore because it is not soluble, NO is unlikely to react with RO_2. However, the heterogeneous reaction of NO with RO_2 radicals on the surface of the particle is not explicitly considered, as these rates are currently unknown. Previous heterogeneous oxidation studies in the presence of NO_x[12,13] observed organonitrate yields that were significantly lower than in the gas-phase; however, it is not known if (gas-phase) NO concentrations were sufficiently high to outcompete self-reaction of RO_2 under elevated oxidant concentrations. This is an important point that requires further study in the future to better assess the role of NO in the chemical evolution of organic aerosol.

Without a complete description of the processes by which NO can interact with OA, and more certain condensed phase rate constants, our model output likely represents a lower-limit for RO_2 + NO branching.

4.5 Summary and Conclusions

Previously we used the photolysis of condensed-phase alkyl nitrites to identify the major reaction pathways for alkoxy radicals in an organic solvent. In this chapter we use the same approach, but instead focus on the reactions of condensed phase alkylperoxy (RO_2) radicals that form from alkoxy radical isomerization. Using a soft chemical ionization technique coupled to an ultra high-resolution mass spectrometer we were able to obtain molecular level information about the major products formed from this same system. The chemical composition of individual ions and their production kinetics were compared with likely mechanisms, leading to the identification of several key first-generation products. The formation of specific products from RO_2 reactions with NO and HO_2 were consistent with estimates of branching ratios from a kinetic model discussed above. Furthermore, we did not identify the major (first-generation) products expected to form from RO_2 isomerization reactions. This observation implies that the available rate constants for gas-phase reactions are likely upper limits for this reaction in the condensed phase.

The chemical system discussed here is distinct from others (i.e. heterogeneous oxidation studies) aimed at studying radical reactions in aerosol particles. Previous studies exposed aerosol particles to high oxidant concentrations, typically under NO_x free conditions, and the RO_2 chemistry is dominated by either self-reaction or with HO_2. While several studies have probed the role of RO_2 + NO reactions, their interpretations are complicated by uncertain gas-OA

transfer kinetics. In our work we expect that reaction with NO is the dominant pathway, thus providing new insight into condensed-phase processes in an entirely different RO_2 regime. For example, under high NO_x conditions, we expect a greater fraction of RO_2 conversion to RO, which as discussed in Chapter 2 will generally form the first-generation hydroxycarbonyl (from "back-isomerization). Whenever this particular reaction happens, an HO_2 radical is produced, providing a mechanism for the generation of secondary oxidants within particles. The presence of later generation oxidation products in our system provides strong evidence for the production of secondary oxidants in the condensed phase; potential pathways for additional oxidation to occur.

In the atmosphere, the fate of RO_2 radicals in aerosol particles is uncertain. We estimate for both urban and pristine environments that RO_2 isomerization or reactions with RO_2 will dominate. The differences in branching ratios between urban and pristine environments are driven by the relative concentrations of OH input into the model– which is directly proportional to the production rate of RO_2. In the gas phase, it is well established that NO_x concentrations can have governing effects on the observed chemistry, as RO_2 + NO reactions are quite fast. However, the difference in the concentrations of NO between the two systems does not appear to have much of an impact on the overall RO_2 branching in the particle phase. This is because of its low concentration and solubility in organic solvents we estimate that the concentrations of NO in atmospheric aerosol particles are likely too low to have much of an impact on the RO_2 chemistry. Instead, we estimate that reaction with HO_2, RO_2, or isomerization will dominate within particles. While we did not explicitly model other processes for interaction with NO, such as heterogeneous reactions of NO with RO_2 on aerosol surfaces, or from alkyl nitrate photolysis,

this is a potentially important pathway. Future work should consider these additional means by which NO_x as well as HO_2 can interact with OA.

As it is unclear how NO + particle-phase RO_2 radicals can react heterogeneously, it is difficult to comment on how relevant these particular results are to the atmosphere; however this study provides new and important information for a different RO_2 regime. Future RONO/DART studies with hexane and other organic matrices (e.g. aromatics or oxygenates) should consider ways to run under more atmospherically relevant NO_x conditions. This can be achieved by decreasing the initial concentration of RONO added to the reaction mixture. Furthermore, with the use of standards, both the rate constants and yields for individual products can be determined. This would be of particular value as many of the condensed-phase rate constants needed for the kinetic model were unavailable and gas-phase measurements were substituted. Additional work is needed to fully constrain condensed phase radical processes, particularly in organic-based media to best model condensed phase processes. The results from this work highlight the major pathways for RO_2 chemistry in the condensed phase and add to our ability to predict how the chemical composition of organic aerosol may change under different conditions.

4.6 References

(1)   Liu, C.-L.; Smith, J. D.; Che, D. L.; Ahmed, M.; Leone, S. R.; Wilson, K. R. The Direct Observation of Secondary Radical Chain Chemistry in the Heterogeneous Reaction of Chlorine Atoms with Submicron Squalane Droplets. *Phys. Chem. Chem. Phys.* **2011**, *13*, 8993–9007.

(2)   Ruehl, C. R.; Nah, T.; Isaacman, G.; Worton, D. R.; Chan, A. W. H.; Kolesar, K. R.; Cappa, C. D.; Goldstein, A. H.; Wilson, K. R. The Influence of Molecular Structure and Aerosol Phase on the Heterogeneous Oxidation of Normal and Branched Alkanes by OH. *J. Phys. Chem. A* **2013**, *117*, 3990–4000.

(3)   Nah, T.; Zhang, H.; Worton, D. R.; Ruehl, C. R.; Kirk, B. B.; Goldstein, A. H.; Leone, S. R.; Wilson, K. R. Isomeric Product Detection in the Heterogeneous Reaction of Hydroxyl Radicals with Aerosol Composed of Branched and Linear Unsaturated Organic Molecules. *J. Phys. Chem. A* **2014**, *118*, 11555–11571.

(4)   Kolesar, K. R.; Buffaloe, G.; Wilson, K. R.; Cappa, C. D. OH-Initiated Heterogeneous Oxidation of Internally-Mixed Squalane and Secondary Organic Aerosol. *Environ. Sci. Technol.* **2014**, *48*, 3196–3202.

(5)   Zhang, H.; Ruehl, C. R.; Chan, A. W. H.; Nah, T.; Worton, D. R.; Isaacman, G.; Goldstein, A. H.; Wilson, K. R. OH-Initiated Heterogeneous Oxidation of Cholestane: A Model System for Understanding the Photochemical Aging of Cyclic Alkane Aerosols. *J. Phys. Chem. A* **2013**, *117*, 12449–12458.

(6)   Chan, M. N.; Zhang, H.; Goldstein, A. H.; Wilson, K. R. Role of Water and Phase in the Heterogeneous Oxidation of Solid and Aqueous Succinic Acid Aerosol by Hydroxyl Radicals. *J. Phys. Chem. C* **2014**, 140314152232002.

(7)   Jokinen, T.; Sipilä, M.; Richters, S.; Kerminen, V.-M.; Paasonen, P.; Stratmann, F.; Worsnop, D.; Kulmala, M.; Ehn, M.; Herrmann, H.; et al. Rapid Autoxidation Forms Highly Oxidized RO_2 Radicals in the Atmosphere. *Angew. Chem. Int. Ed. Engl.* **2014**, *53*, 14596–14600.

(8)   Ehn, M.; Thornton, J. A.; Kleist, E.; Sipilä, M.; Junninen, H.; Pullinen, I.; Springer, M.; Rubach, F.; Tillmann, R.; Lee, B.; et al. A Large Source of Low-Volatility Secondary Organic Aerosol. *Nature* **2014**, *506*, 476–479.

(9)   Crounse, J. D.; Nielsen, L. B.; Jørgensen, S.; Kjaergaard, H. G.; Wennberg, P. O. Autoxidation of Organic Compounds in the Atmosphere. *J. Phys. Chem. Lett.* **2013**, *4*, 3513–3520.

(10)   Smith, J. D.; Kroll, J. H.; Cappa, C. D.; Che, D. L.; Liu, C. L.; Ahmed, M.; Leone, S. R.; Worsnop, D. R.; Wilson, K. R. The Heterogeneous Reaction of Hydroxyl Radicals with Sub-Micron Squalane Particles: A Model System for Understanding the Oxidative Aging of Ambient Aerosols. *Atmos. Chem. Phys.* **2009**, *9*, 3209–3222.

(11)   Kessler, S. H.; Smith, J. D.; Che, D. L.; Worsnop, D. R.; Wilson, K. R.; Kroll, J. H. Chemical Sinks of Organic Aerosol: Kinetics and Products of the Heterogeneous Oxidation of Erythritol and Levoglucosan. *Environ. Sci. Technol.* **2010**, *44*, 7005–7010.

(12)   Renbaum, L. H.; Smith, G. D. Organic Nitrate Formation in the Radical-Initiated Oxidation of Model Aerosol Particles in the Presence of NO_x. *Phys. Chem. Chem. Phys.* **2009**, *11*, 8040–8047.

(13)   Petrick, L.; Dubowski, Y. Heterogeneous Oxidation of Squalene Film by Ozone under Various Indoor Conditions. *Indoor Air* **2009**, *19*, 381–391.
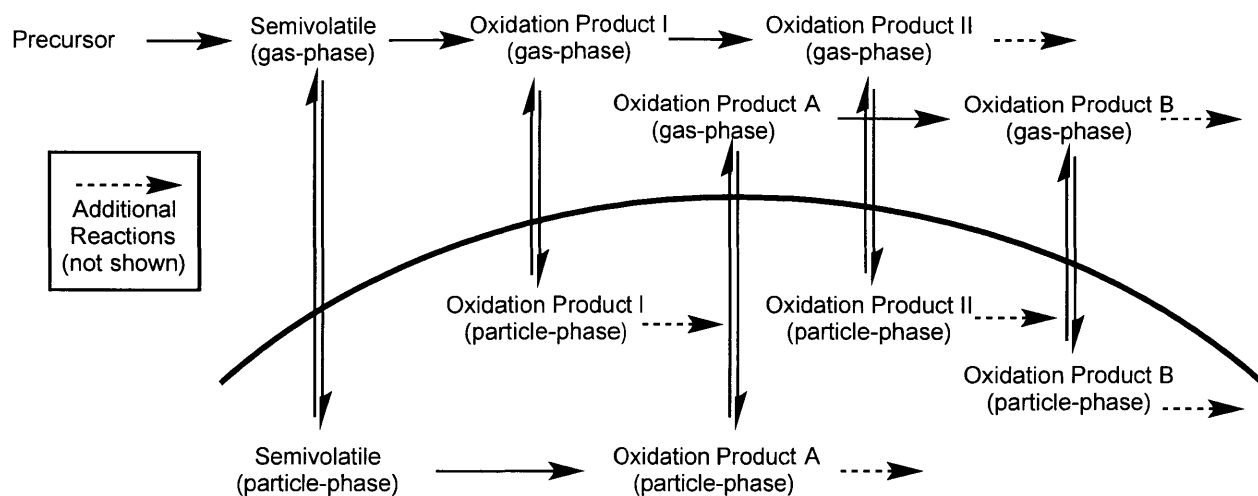
(14) Noyes, W. A. Explanation of the Formation of Alkyl Nitrites in Dilute Solutions; Butyl and Amyl Nitrites. *J. Am. Chem. Soc.* **1933**, *55*, 3888–3889.

(15) Cody, R. B.; Laramée, J. A.; Durst, H. D. Versatile New Ion Source for the Analysis of Materials in Open Air under Ambient Conditions. *Anal. Chem.* **2005**, *77*, 2297–2302.

(16) Cody, R. B. Observation of Molecular Ions and Analysis of Nonpolar Compounds with the Direct Analysis in Real Time Ion Source. *Anal. Chem.* **2009**, *81*, 1101–1107.

(17) Nah, T.; Chan, M.; Leone, S. R.; Wilson, K. R. Real Time in Situ Chemical Characterization of Submicrometer Organic Particles Using Direct Analysis in Real Time-Mass Spectrometry. *Anal. Chem.* **2013**, *85*, 2087–2095.

(18) Hajslova, J.; Cajka, T.; Vaclavik, L. Challenging Applications Offered by Direct Analysis in Real Time (DART) in Food-Quality and Safety Analysis. *TrAC Trends Anal. Chem.* **2011**, *30*, 204–218.

(19) Pluskal, T.; Castillo, S.; Villar-Briones, A.; Oresic, M. MZmine 2: Modular Framework for Processing, Visualizing, and Analyzing Mass Spectrometry-Based Molecular Profile Data. *BMC Bioinformatics* **2010**, *11*, 395.

(20) Cody, R. B.; Dane, A. J. Soft Ionization of Saturated Hydrocarbons, Alcohols and Nonpolar Compounds by Negative-Ion Direct Analysis in Real-Time Mass Spectrometry. *J. Am. Soc. Mass Spectrom.* **2013**, *24*, 329–334.

(21) Atkinson, R. Rate Constants for the Atmospheric Reactions of Alkoxy Radicals: An Updated Estimation Method. *Atmos. Environ.* **2007**, *41*, 8468–8485.

(22) Dahl, E. E. The Aqueous Phase Yield of Alkyl Nitrates from ROO + NO: Implications for Photochemical Production in Seawater. *Geophys. Res. Lett.* **2003**, *30*, 1271.

(23) Goldstein, S.; Lind, J.; Merenyi, G. Reaction of Organic Peroxyl Radicals with NO_2 and NO in Aqueous Solution: Intermediacy of Organic Peroxynitrate and Peroxynitrite Species. *J. Phys. Chem. A* **2004**, *108*, 1719–1725.

(24) Finlayson-Pitts, B.; Pitts, J. *Chemistry of the Upper and Lower Atmosphere*; Elsevier Academic Press: San Diego, Ca, USA, 2000; p. 969.

(25) Atkinson, R.; Baulch, R.; Cox, R.; Crowley, J.; Hampson, R.; Hynes, R.; Jenkin, M.; ROssi, M.; Troe, J. IUPAC Task Group on Atmospheric Chemical Kinetic Data Evaluation. *Atmos. Chem. Phys.* **2004**, *4*, 1461–1738.

(26) Carrasquillo, A. J.; Hunter, J. F.; Daumit, K. E.; Kroll, J. H. Secondary Organic Aerosol Formation via the Isolation of Individual Reactive Intermediates: Role of Alkoxy Radical Structure. *J. Phys. Chem. A* **2014**, *118*, 8807–8816.

(27) Lim, Y. Bin; Ziemann, P. J. Kinetics of the Heterogeneous Conversion of 1,4-Hydroxycarbonyls to Cyclic Hemiacetals and Dihydrofurans on Organic Aerosol Particles. *Phys. Chem. Chem. Phys.* **2009**, *11*, 8029–8039.

(28) Denisov, E.; Afanas'ev, I. *Oxidation and Antioxidants in Organic Chemistry and Biology*; Taylor & Francis: Boca Raton, Fl, USA, 2005; p. 981.

(29) Calvert, J. G.; Derwent, R. G.; Orlando, J. J.; Tyndall, G. S.; Wallington, T. J. *Mechanisms of the Atmospheric Oxidation of the Alkanes*; Oxford University Press, USA: New York, 2008; p. 992.

(30) Breithaupt, J. *Summary Review of Available Literature for Hydrogen Peroxie and Peroxyacetic Acid for New Use to Treat Wastewater*; 2007.

(31) Sanders, R. Compilation of Henry's law constants for inorganic and organic species of potential importance in environmental chemistry, (Version 3), http://www.henrys-law.org.

(32) Abraham, M.; Gola, J.; Cometto-Muniz, J.; Cain, W. The Solvation Properties of Nitric Oxide. *Journal of the Chemical Society, Perkin Transactions 2*, 2000.

(33) Jacob, D. *Introduction to Atmospheric Chemistry*; Princeton University Press: Princeton, New Jersey, USA, 1999; p. 264.

(34) Creasey, D. J.; Heard, D. E.; Lee, J. D. OH and HO_2 Measurements in a Forested Region of North-Western Greece. *Atmos. Environ.* **2001**, *35*, 4713–4724.

(35) Kroll, J. H.; Seinfeld, J. H. Chemistry of Secondary Organic Aerosol: Formation and Evolution of Low-Volatility Organics in the Atmosphere. *Atmos. Environ.* **2008**, *42*, 3593–3624.

(36) Hallquist, M.; Wenger, J. C.; Baltensperger, U.; Rudich, Y.; Simpson, D.; Claeys, M.; Dommen, J.; Donahue, N. M.; George, C.; Goldstein, A. H.; et al. The Formation, Properties and Impact of Secondary Organic Aerosol: Current and Emerging Issues. *Atmos. Chem. Phys.* **2009**, *9*, 5155–5236.

Chapter 5

Summary, Conclusions, and Implications

Summary and Conclusions. An understanding of the formation and fate of atmospheric particulate matter is necessary to assess its impacts on human health, climate change, air quality, and visibility. Much of the current uncertainty in this area exists in our ability to predict how the organic aerosol fraction forms and evolves over its lifetime in the atmosphere. To this end, an understanding of the underlying chemistry involved is necessary. The *goal* of this thesis research was to add to this understanding by conducting a series of experiments aimed at identifying the importance of the major oxidative pathways. As discussed in Chapter 1, the evolution of organic material in the atmosphere is highly complex owing to the number of potential reactions, radical intermediates, and products that can form from even a simple precursor molecule (Chapter 1, Figure 1, reproduced below). Here, we presented data using a novel approach to study the formation and chemical evolution of organic aerosol– the explicit consideration of individual reactive intermediates. A summary of the major results from each chapter are presented below:

Precursor → Semivolatile (gas-phase) → Oxidation Product I (gas-phase) → Oxidation Product II (gas-phase) ---→

Oxidation Product A (gas-phase) → Oxidation Product B (gas-phase) ---→

Additional Reactions (not shown) ------→

Oxidation Product I (particle-phase) ---→ Oxidation Product II (particle-phase) ---→

Oxidation Product B (particle-phase) ---→

Semivolatile (particle-phase) → Oxidation Product A (particle-phase) ---→

Figure 1. A highly generalized schematic of the complexity associated with VOC oxidation. The precursor VOC is oxidized with OH, followed by the subsequent gas/particle partitioning and chemical processing of individual oxidation products.

In *Chapter 2,* we highlighted the role of alkoxy radical structure on the formation of low-volatility products, probing the factors that influence the extent of the precursor → semivolatile (particle-phase) reaction in Figure 1. SOA yields and chemical composition from RO radicals with the same molecular formulae but different molecular structure were measured to identify the major features that influence the formation of low volatility species. The largest yields observed were from straight chain RO radicals with the radical center located near the terminus of the molecule. The primary RO radical, a species that would only form upon abstraction of a hydrogen at the terminus of a molecule and expected to occur only ~4% of the time. This observation highlights the potential role of minor pathways in the generation of SOA. Branched isomers were observed to have the lowest yields among those measured. The extent to which branching along the carbon chain, and specifically how the proximity of a branching group to the radical center enhances radical fragmentation reactions was probed. Notably, the enhanced fragmentation of β-substituted RO radicals, which occurred to a greater extent than was predicted by existing structure activity relationships, resulted in a substantial reduction in observed aerosol

110

yields. This result implies that existing structure activity relationships that were developed for small RO radicals (C_2 – C_5) should be applied to larger systems with caution. Lastly, we considered the volatility of SOA components through volatility basis set fittings and found that yields were intimately linked to the saturation vapor pressures of the expected products for each isomer. While all of the products measured have the same molecular formula, the presence of an aldehyde or a ketone or a branched methyl group will all influence volatility in different ways, and will thus impact yield. ***These results highlight how subtle differences in RO molecular structure can have major impact on product yields and SOA formation***. Future work in this area should focus on the reactivity of radical intermediates with more complex molecular structures, including rings, double bonds, and oxygenated functional groups, to examine the chemistry of gas-phase oxidation products I and II in Figure 1. Furthermore, the role of RH, seed composition, seed acidity, and temperature, should be examined to improve on our understanding of how different atmospheric conditions impact SOA formation.

In *Chapter 3*, a new method was developed to examine organic radical reactivity in the condensed phase, starting with the semi-volatile (particle-phase) species in Figure 1 and identifying its major reaction products. Photolysis of a $C_{20}H_{41}ONO$/hexane mixture, followed by nebulization and measurement with the AMS, permitted the real-time measurement of the chemical composition of this system. The goal of this work was to measure the branching ratio between unimolecular RO pathways analogous to those in the gas-phase and bimolecular reactions (i.e. H-abstraction) with the surrounding aerosol. Our observations, however, imply that ***the bimolecular H-abstraction pathways for alkoxy radicals were at best, minor relative to unimolecular ones***. This is consistent with previous observations in the physical organic chemistry literature, which found that when facile (i.e. when the delta-carbon is not primary),

unimolecular pathways of the alkoxy radical would dominate over bimolecular ones. These results come in stark contrast to those from previous heterogeneous oxidation studies, which implicated these reactions in the formation of alcohols. In those experiments, the likely mechanism for alcohol formation is by self-reaction of RO_2 radicals. These results imply that *condensed-phase mechanisms for RO radicals are likely similar to those in the gas-phase.*

In *Chapter 4*, we identified some of the major products formed from the condensed-phase photolysis of a large C_{20} nitrite, again starting with the semivolatile (particle-phase) species in Figure 1. The same system developed in Chapter 3 was used, however, the aerosol composition was measured with a new instrument suitable for the generation of molecular ions with little fragmentation, Direct Analysis in Real Time (DART). The goal of this work was to assign the ions observed by DART to the major products expected from traditional gas-phase mechanisms. This molecular level approach allowed for the identification of products that formed from specific RO_2 pathways. Notably, we did not observe the expected products of RO_2 isomerization reactions, implying that the currently available rate constants may not directly applicable to the condensed-phase. Furthermore, we observed many ions that we believe to have formed from second-generation oxidation chemistry, indicating that the in-particle generation of secondary oxidants (OH, HO_2, NO, O_3, etc.) may be an important pathway for continued condensed-phase oxidation. In the development of a simple kinetic model for predicting reaction branching we observed a large knowledge gap regarding the availability of condensed-phase radical rate constants that are necessary to better understand this important system. Future work should measure these, particularly in the condensed organic phase. This study is one of only a few that have used the DART technique for analyzing OA composition. The next set of experiments should aim to quantify product yields for the determination of branching ratios. This will require

the use of authentic standards for quantification. Furthermore, additional studies with more highly functionalized RONO and solvents are necessary to understand how the major condensed phase chemical reactions change as a function of the specific molecular environment. Finally, the direct application of our results to the atmosphere requires an improved understanding of the physical mechanism by which NO can interact with condensed-phase RO_2 radicals. As both gas-phase NO concentrations and solubility in organic and aqueous phases are low, condensed-phase reactions are unlikely, however, heterogeneous reaction with RO_2 on the surface of the particles represent a possible means by which this reaction can occur and warrants further study.

Implications. The data collected in this thesis provides an explicit, highly detailed, description of specific chemical reactions and how they relate to the formation and evolution of organic gases and aerosol. This information is essential for improving our predictive capabilities for both aerosol *loadings* and *composition*. In terms of how this work can be utilized, at the present time it is unrealistic to identify and track every individual organic radical intermediate in the atmosphere, whether it be experimentally or in a global chemical transport model. These results, however, provide a basis for identifying some criteria (general chemical features) that can be used to refine emissions inventories to include the species most relevant to SOA formation. In addition, while considering how best to translate flow-tube studies of heterogeneous oxidation processes to the atmosphere, our data implies that some of the previous reactions previously identified may not be relevant. To this end, the lifetime of particle-phase organics and, for example, their role in cloud or smog formation can be better predicted. *While the goal of this work was to constrain radical chemistry and simplify these systems were still immensely complicated- which speaks to just how complex the actual atmosphere is.*